General Disclaimer

One or more of the Following Statements may affect this Document

- This document has been reproduced from the best copy furnished by the organizational source. It is being released in the interest of making available as much information as possible.

- This document may contain data, which exceeds the sheet parameters. It was furnished in this condition by the organizational source and is the best copy available.

- This document may contain tone-on-tone or color graphs, charts and/or pictures, which have been reproduced in black and white.

- This document is paginated as submitted by the original source.

- Portions of this document are not fully legible due to the historical nature of some of the material. However, it is the best reproduction available from the original submission.

APPLICATION AND SENSITIVITY INVESTIGATION OF FOURIER

TRANSFORMS FOR MICROWAVE RADIOMETRIC INVERSIONS

by

John J. Holmes

Constantine A. Balanis

Prepared by

Department of Electrical Engineering
West Virginia University
Morgantown, West Virginia 26506

For

National Aeronautics and Space Administration
Langley Research Center
Hampton, Virginia   23365

November 15, 1974

Acknowledgement

TABLE OF CONTENTS

LIST OF FIGURES

Figure   Page

LIST OF TABLES

I. INTRODUCTION

1.1 Background

Continuous monitoring of ocean surfaces, utilizing the remote
sensing capability of microwave radiometers, may provide important
information applicable in the fields of oceanography, meteorology,
marine transportation, and other related areas. Ocean surface
characteristics such as salinity, molecular temperature, roughness,
and sea ice content can be determined from electromagnetic measure-
ments, as reviewed by Tomiyasu [1]. These properties are parameters
of the function describing the brightness temperature of the water,
which is also dependent on the frequency, polarization, and viewing
angle of the system. The radiometer however, does not measure the
brightness temperature directly. Instead, it measures the antenna
temperature, which is the brightness temperature "smoothed" by the
system weighting function (antenna pattern). The blurring of the
brightness temperature distribution is experienced by all realizable
antennas.

To calculate the water brightness temperature from the measured
antenna temperature, an antenna desmoothing problem is encountered.
This is a classical problem in the field of radio astronomy [2]-[4],
and some of the earlier methods used to solve this problem will be
adapted to the remote sensing radiometer system under investigation.
However, radio astronomers have been able in recent years to reduce

the smoothing effect of the antenna by using highly efficient
narrow beam aerials. This allows the observed antenna temperature
distribution to closely approximate the brightness temperature pro-
file, thus eliminating the desmoothing problem. To achieve this
high resolution in the antenna pattern at microwave frequencies, it
is necessary to construct aerials with relatively large physical
dimensions. However, the radiometer systems used for continuous
ocean monitoring are air-borne, placing considerable size limi-
tations on the antenna. It may not even be desirable to use narrow
beam aerials for fast moving air-borne radiometers, since half of
the main beam must remain in the target area throughout the
measuring period [5]. In any case, desmoothing methods must be
applied to the wide beam antennas used in the remote sensing system.

Desmoothing of the antenna temperature distribution is
dependent on the successful calculation of a unique solution for a
Fredholm integral equation of the first kind. This integral
equation occurs in other indirect measurement problems such as
filter spectrometry, inference of structure from diffraction
patterns, etc. [6]-[8]. In every case the Fredholm equation is
highly unstable and yields unrealistic results when the measurements
are known only with moderate accuracy (ill-posed). Several matrix
techniques have been developed [8]-[11], along with the necessary
smoothing procedures, which will invert the integral. For this
antenna desmoothing problem, a more efficient Fourier transform

inversion method was developed and was then applied to an experimental finite wave tank system, taking into account the temperature contributions from the surrounding sources (earth and sky).

With the advent of the Fast Fourier Transform (FFT) algorithm [12],[13], the discrete frequency spectrums of various functions are computed very efficiently and economically. By placing the antenna temperature equation (Fredholm equation) into a crosscorrelation form, Fourier transform methods utilizing the FFT algorithm, allows the inversion of the integral to proceed efficiently. Also, since the frequency spectrum of the power pattern is made available by the FFT, a better understanding of the smoothing effect of the aerial may be obtained from examination of its spectrum.

1.2 Objective

Microwave radiometer antennas tend to blur and smooth the brightness temperature profile of a target due to the coarse main beam and side-lobe level of the weighting function (power pattern). To recover the true brightness temperature distribution, FFT techniques are used to invert the antenna temperature measurements. It is the purpose of this research to

a. verify the validity of the two-dimensional modeling, reported in reference [14], by comparing it with three-dimensional computations.

b. determine the stability and sensitivity of the Fourier inversion

method to profiles of errors in the antenna temperature.

c. isolate the causes of instability and illustrate them with examples.

d. recommend and implement modifications to smooth (filter) the inherent instabilities in the inversion.

e. investigate the stability and sensitivity of the modified method.

f. apply the modified techniques to actual measurements.

II. THEORY

2.1 Brightness Temperature Modeling

All bodies that maintain a molecular temperature above absolute zero radiate electromagnetic energy that can be measured as a brightness temperature at a specific frequency. If the radiating object is not a black body, then the brightness temperature will be less than that of an ideal radiator. For opaque bodies, the brightness temperature can be expressed from Kirchoff's law [15] as

$$T_b = \epsilon T_m \tag{1}$$

in which T_b is the brightness temperature, ϵ is defined as the ability of a body to radiate energy (emissivity), and T_m is the molecular temperature. Since water is considered to be opaque, its brightness temperature will be given by (1).

When (1) is used to describe the brightness temperature of water, two polarizations of its emissivity must be considered. These polarized emissivities can be described by the Fresnel

equations for smooth flat water surfaces as

$$\varepsilon_{\substack{v \\ h}} = 1 - \mid \Gamma_{\substack{v \\ h}} \mid^2 \qquad (2a)$$

where

$$\Gamma_v = \frac{\dot{\varepsilon} \cos \emptyset - \sqrt{\dot{\varepsilon} - \sin^2 \emptyset}}{\dot{\varepsilon} \cos \emptyset + \sqrt{\dot{\varepsilon} - \sin^2 \emptyset}} \qquad \Gamma_h = \frac{\cos \emptyset - \sqrt{\dot{\varepsilon} - \sin^2 \emptyset}}{\cos \emptyset + \sqrt{\dot{\varepsilon} - \sin^2 \emptyset}} \qquad (2b)$$

and where $\emptyset$ is the incidence angle of the energy, $\dot{\varepsilon}$ is the complex relative dielectric permittivity of the water, and v,h indicate vertical and horizontal polarizations, respectively. Substituting (2b) into (2a) for the vertical (horizontal) polarization, the corresponding emissivities can be written as

$$\varepsilon_v = \frac{4(p\varepsilon' + q\varepsilon'')\cos\emptyset}{(\varepsilon' \cos\emptyset + p)^2 + (\varepsilon'' \cos\emptyset + q)^2} \qquad \varepsilon_h = \frac{4 p \cos\emptyset}{(\cos\emptyset + p)^2 + q^2} \qquad (3a)$$

where

$$
\begin{aligned}
p &= \sqrt{r} \cos\gamma \\
q &= \sqrt{r} \sin\gamma \\
r &= \sqrt{[(\varepsilon' - \sin^2\emptyset)^2 + (\varepsilon'')^2]} \\
\gamma &= \frac{1}{2} \tan^{-1} \left(\frac{\varepsilon''}{\varepsilon' - \sin^2\emptyset}\right)
\end{aligned}
\qquad (3b)
$$

in which ε' and ε'' are the real and imaginary parts of the complex relative permittivity ($\dot{\varepsilon} = \varepsilon' - j\varepsilon''$). These equations are derived in Appendix I assuming that the air-water interface is a smooth flat surface.

To complete the water's emissivity model, the Debye equation, as modified by Stogryn [16], is assumed for the complex permittivities of (3). This equation is

$$\varepsilon' - j\,\varepsilon'' = \varepsilon_\infty + \frac{\varepsilon_0 - \varepsilon_\infty}{1 - j2\pi\tau f} + j\,\frac{\sigma}{2\pi\varepsilon_0^* f} \qquad (4)$$

where

ε_0 = static dielectric constant of the solvent

ε_∞ = high frequency dielectric constant of the solvent (4.9)

ε_0^* = permittivity of free space (farads/m)

σ = ionic conductivity of the dissolved salt (mhos/m)

τ = relaxation time (seconds)

Stogryn has expressed the static dielectric constant ε and the relaxation time τ as semi-empirical equations which, based on a number of measurements, are written as

$$\varepsilon_0 \ (T_m,N) = \varepsilon_0(T_m,0) \ a \ (N) \qquad (5)$$
$$2\pi\tau(T_m,N) = 2\pi\tau(T_m,0) \ b \ (N,T_m) \qquad (6)$$

where

$$\varepsilon_0(T_m,0) = 87.74 - 0.40008 \ T_m + 9.398 \times 10^{-4} T_m^2 + 1.410 \times 10^{-6} T_m^3 \qquad (7)$$

$$a(N) = 1.0 - 0.2551N + 5.151 \times 10^{-2} \ N^2 - 6.889 \times 10^{-3} N^3 \qquad (8)$$

$$2\pi\tau(T_m,0) = 1.1109 \times 10^{-10} - 3.824 \times 10^{-12} \ T_m + 6.938 \times 10^{-14} T_m^2$$
$$- 5.096 \times 10^{-16} T_m^3 \qquad (9)$$

$$b(N,T) = 0.1463 \times 10^{-2} NT_m + 1.0 - 0.04896N - 0.02967N^2 \qquad (10)$$

and

T_m = water molecular temperature ($0 \leq T_m \leq 40^0C$)

N = normality ($0 \leq N \leq 3$)

The normality in (5) and (6) can also be calculated from a semi-empirical equation in terms of the salinity. This equation is

$$N=9[1.707\times10^{-2} + 1.205\times10^{-5} \; S + 4.058\times10^{-9} \; S^2] \qquad (11)$$

where

S = salinity in parts per thousand ($0 \leq S \leq 260$)

The ionic conductivity of sea water found in (4) can be formulated as a function of temperature and salinity. This equation is semi-empirical in nature and has the form of

$$\sigma_{sea \; water} \; (T_m,S) = \sigma_{sea \; water} \; (25,S) \; exp \; (-\Delta\zeta) \qquad (12)$$

where

$$\sigma_{sea \; water} \; (25,S) = S[0.182521-1.46192\times10^{-3}S + 2.69324\times10^{-5}S^2$$
$$-1.28205\times10^{-7}S^3] \qquad (13)$$

$$\zeta = 2.033\times10^{-2} + 1.266\times10^{-4}\Delta + 2.464\times10^{-6}\Delta^2 - S[1.849\times10^{-5}$$
$$-2.551\times10^{-7}\Delta + 2.551\times10^{-8}\Delta^2] \qquad (14)$$

$$\Delta = 25 - T_m \qquad (15)$$

which is valid for $0 \leq S \leq 40$. Equations (3)-(15) require only the salinity, molecular temperature, and frequency to calculate accurate profiles of the vertically and horizontally polarized emissivities of sea water.

To get a more accurate representation of the water brightness temperature, equation (1) is modified to include the reflection of the sky's brightness temperature from the water surface. The

modification of (1) is

$$(T_{bw})_{\substack{v \\ h}} = \epsilon_{\substack{v \\ h}} T_{m} + (1-\epsilon_{\substack{v \\ h}}) T_{\substack{bs \\ h}} \tag{16}$$

in which T_{bw} is the water brightness temperature, and T_{bs} is the sky brightness temperature. This equation was formulated assuming that there were no contributions from any other atmospheric sources.

To complete the modeling of all the brightness temperatures considered in the system, profiles must be selected for the earth and sky. For the lack of more reliable distributions, it will be assumed that the radiation emitted from the earth and sky is unpolarized and for the earth will be fixed at a constant value of $300^{\circ}K$. The brightness temperature of the sky is best described [17] by the equation

$$T_{bs} (\emptyset) = T_{eff} (1 - e^{\tau_0 \sec(\pi-\emptyset)}) \tag{17}$$

where

$$T_{eff} = 1.12 \, T_{air} - 50^{\circ}K \tag{18}$$

$$\tau_0 = - \ln (1 - 3/T_{eff}). \tag{19}$$

in which $T_{air} = 284^{\circ}K$ in all sky profiles modeled throughout the rest of this report. This model takes into account atmospheric absorption by the two main contributions, oxygen and water vapor, and is a reasonable good approximation for horizontally stratisfied atmosphere.

Equations (17)-(19) present sufficient information for (16) to yield a fairly accurate water brightness temperature distribution. In Fig. 1 typical profiles of water brightness temperatures for
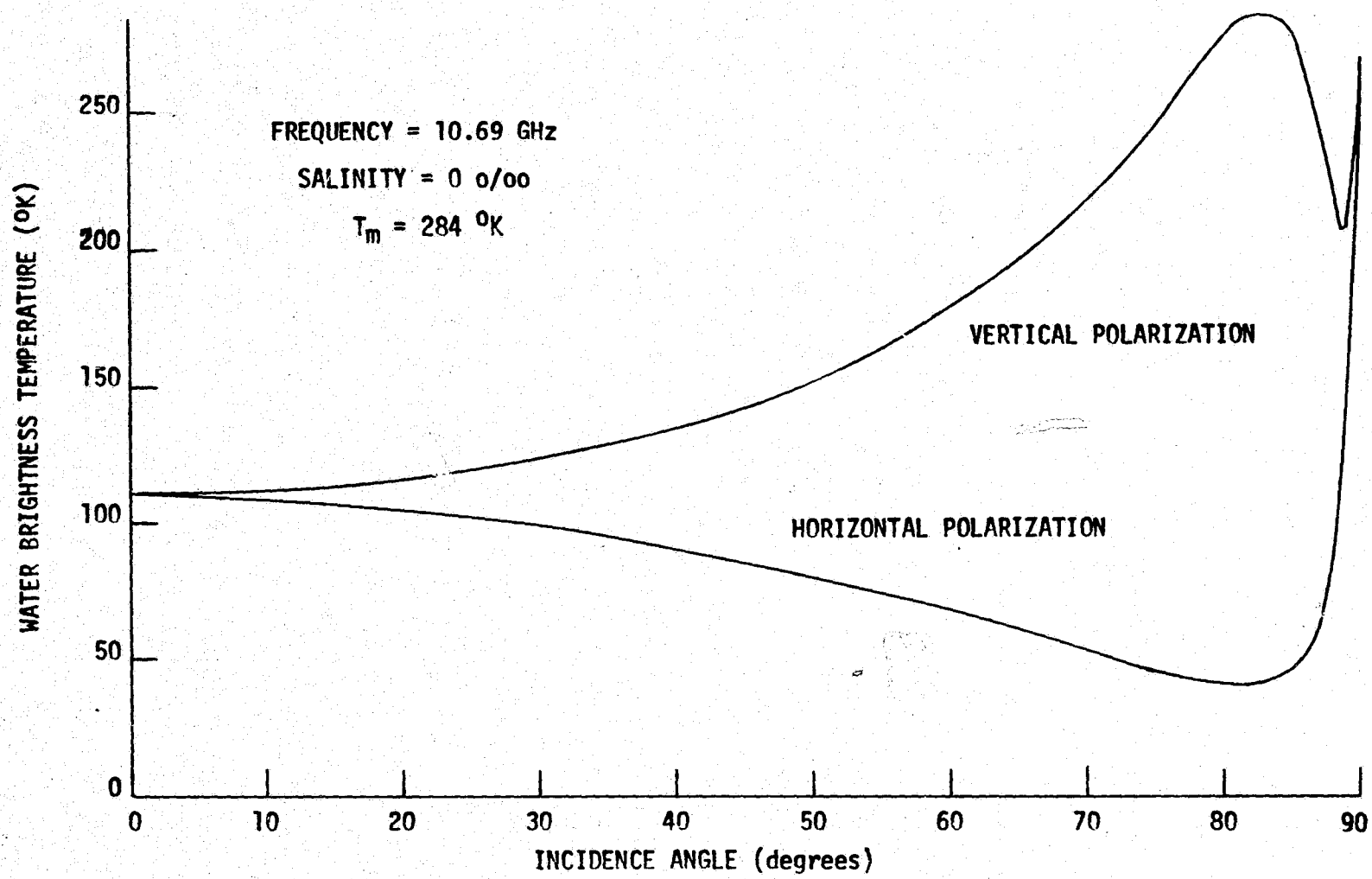
Fig. 1. Brightness temperature profiles for vertical and horizontal polarizations.

vertical and horizontal polarizations are plotted using the emissivity modeling described by (2)-(15). This model was calculated for the parameters indicated in the figure and will be used throughout the investigation.

2.2 Description of Laboratory System

Formulation of the antenna temperature equations describing the performance of the laboratory microwave radiometer system, shown pictorially in Fig. 2 and geometrically in Fig. 3, is simplified by assuming a two-dimensional modeling. The system is now available at the Flight Instrumentation Division of NASA, Langley Research Center, Hampton, Virginia. The square wave tank is 14 feet wide and has the ability of controlling the molecular temperature, salinity, foam, and wave height of the water. The antenna and radiometer, located at x', y', z', of Fig. 3, are positioned above the wave tank of width w, and can travel along an arc of constant radius ρ. The radial distance from the displaced antenna system to the center of the tank forms an incidence angle with a normal to the tank surface, referred to as the system rotation angle α. For each rotation angle α, the system has the mobility to perform a complete $360°$ scan. The antenna's maximum radiation is directed along the observation scan angle β. The θ variations are assumed to be negligible, thus forming a two-dimensional system the validity of which remains to be proven.

For the particular experimental installation under investigation,
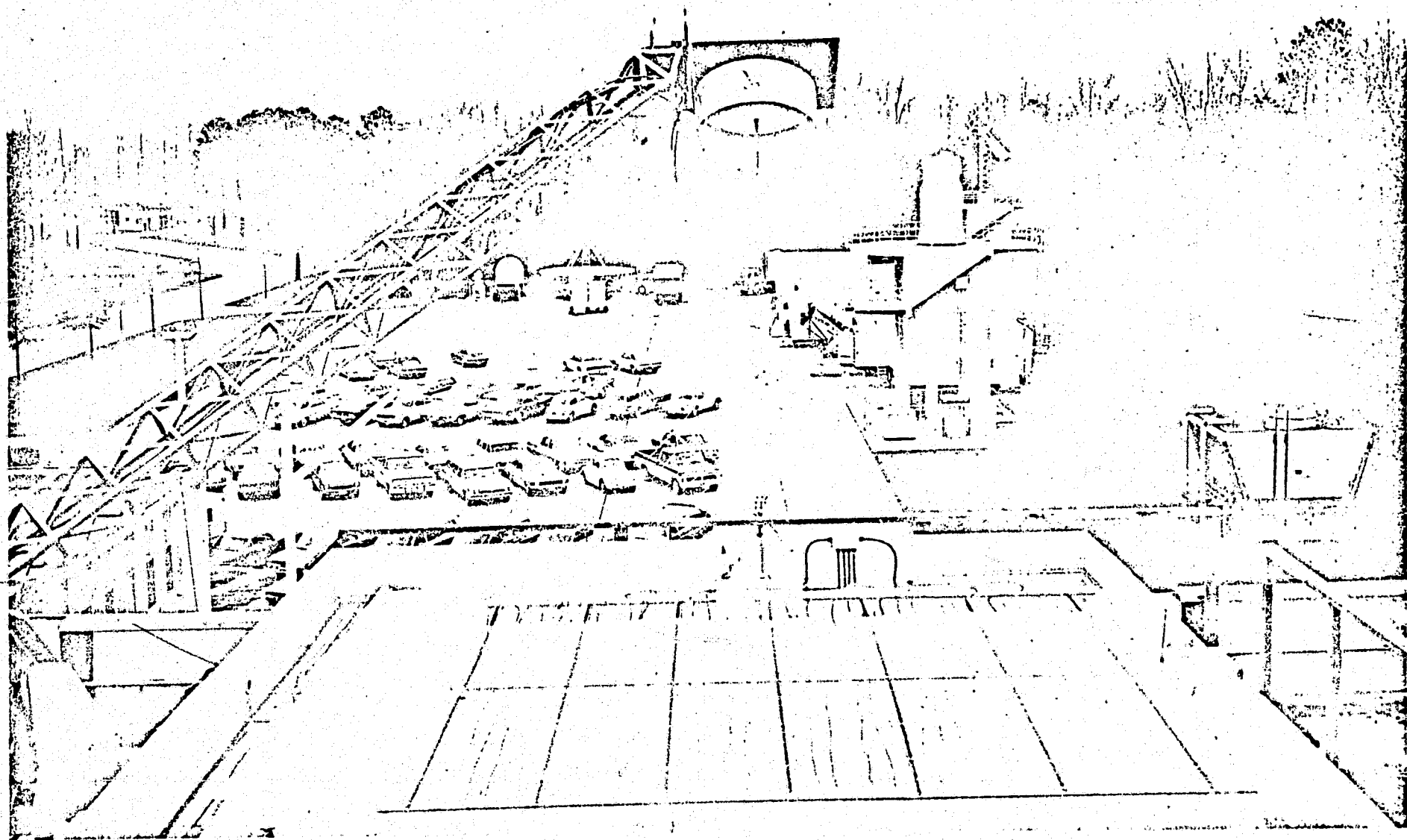
Fig. 2. Pictorial view of wave tank system.
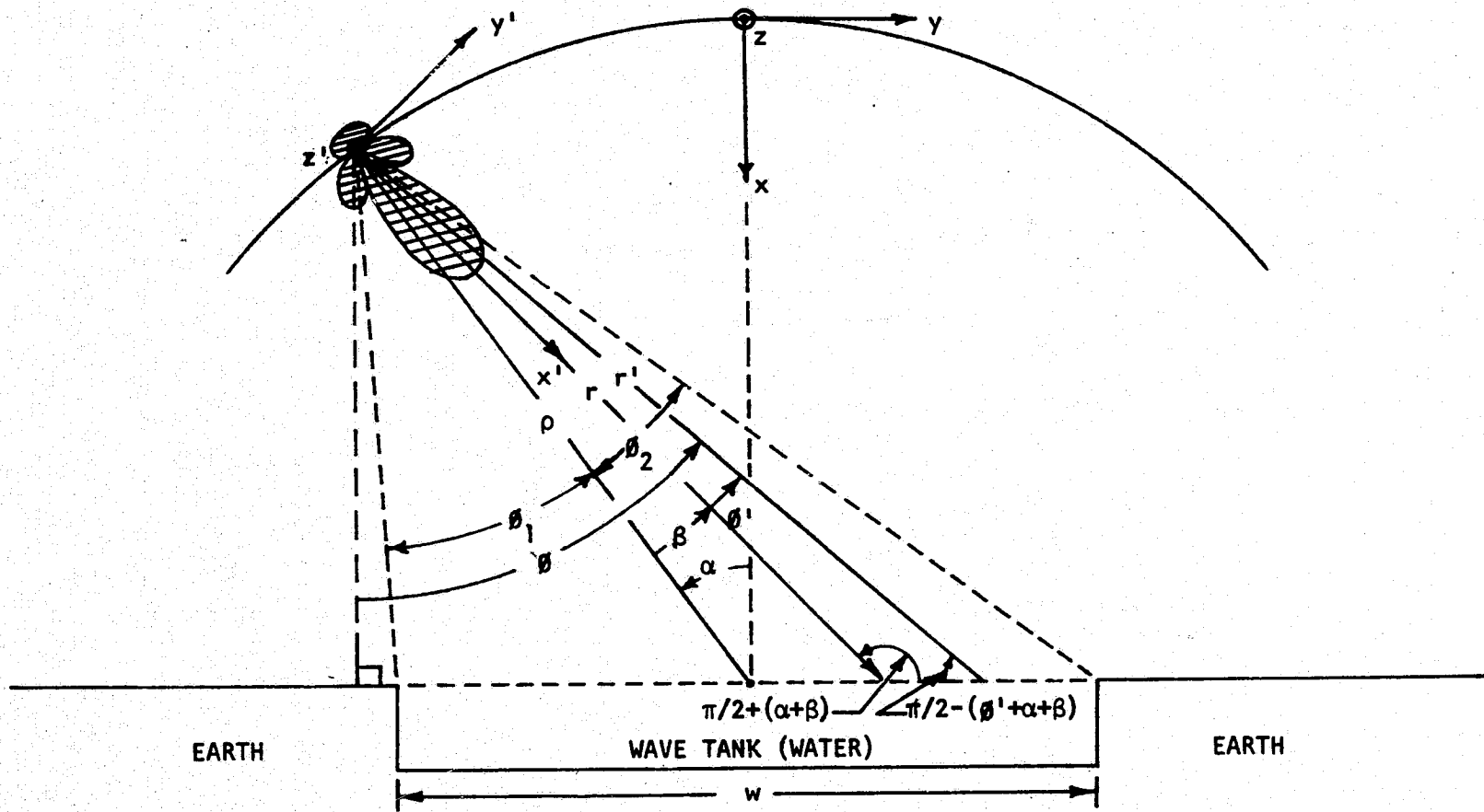
Fig. 3. Geometry of wave tank system.

the total antenna temperature is due to three different sources; namely the water, earth, and sky. Assuming no contributions from any other atmospheric sources, the total antenna temperature is then expressed as

$$T_a (\beta) = T_{aw} (\beta) + T_{ae} (\beta) + T_{as} (\beta) \tag{20}$$

where T_a is the total antenna temperature, T_{aw} is the antenna temperature due to the water, T_{ae} is the antenna temperature due to the earth, and T_{as} is the antenna temperature due to the sky. All of the inversion methods yet to be developed will be applied to T_{aw}, which can be isolated easily from (20).

2.3 Antenna Temperature Equations

For two-dimensional considerations, Fisher [14] has shown that each contribution of (20) can be written as

$$T_{aw} (\beta) = \int_{-\phi_1}^{\phi_2} T_{bw} (\phi' + \beta + \alpha) \, G \, (\phi') \, d \phi' \tag{21}$$

$$T_{ae} (\beta) = \int_{\alpha^+}^{-\phi_1} T_{be} (\phi' + \beta + \alpha) \, G \, (\phi') \, d \phi'$$

$$+ \int_{\phi_2}^{\alpha^-} T_{be} (\phi' + \beta + \alpha) \, G \, (\phi') \, d \phi' \tag{22}$$

$$T_{as}(\beta) = \int_{\pi}^{\alpha^+} T_{bs}(\emptyset' + \beta + \alpha) \, G(\emptyset') \, d\emptyset'$$

$$+ \int_{\alpha^-}^{-\pi} T_{bs}(\emptyset' + \beta + \alpha) \, G(\emptyset') \, d\emptyset' \qquad (23)$$

$$G(\emptyset') = P(\emptyset') \bigg/ \int_{0}^{2\pi} P(\emptyset') \, d\emptyset' \qquad (24)$$

and the limits of integration are found from the geometry of Fig. 3 as

$$\emptyset_{1,2} = \tan^{-1} \left[\frac{w/2 + \rho \sin\alpha}{\rho \cos \alpha} \right] \pm \alpha \qquad (25)$$

$$\alpha^+ = \frac{\pi}{2} + \alpha \qquad\qquad \alpha^- = \frac{\pi}{2} - \alpha \qquad (26)$$

where $P(\emptyset')$ is the power pattern of the aerial, $G(\emptyset')$ is the normalized gain function of the antenna, T_{bw}, T_{be}, and T_{bs} are the brightness temperatures of the water, earth, and sky, respectively. The brightness temperatures in (21)-(23) were described in section 2.1. Each term in (21)-(23) was intentionally placed in the form of a crosscorrelation and can be evaluated, in the Fourier transform domain, by a multiplication. From the crosscorrelation theorem, the antenna temperature equations (21)-(23) can be written in general as

$$T_a(\omega) = T_b(\omega) \, G^*(\omega) \qquad\qquad (27)$$

where $T_a(\omega)$ is the Fourier transform of $T_a(\beta)$ defined by

$$T_a(\omega) = \int_{-\infty}^{\infty} T_a(\beta) \, e^{-j\omega\beta} d\beta \qquad\qquad (28)$$

$T_b(\omega)$ and $G^*(\omega)$ are similarly the transform of $T_b(\beta)$ and the conjugate of the transform of $G(\beta)$, respectively. The computational advantages of (27) are realized from the use of the FFT algorithm to calculate the direct and inverse transforms of the functions involved.

A better understanding of the smoothing effect of the gain function is obtained by examining its spectrum's influence on (27). This equation emphasizes the importance of zeros in $G^*(\omega)$. It is apparent from (27) that for those frequencies ω_k for which

$$G^*(\omega_k) = 0 \qquad\qquad (29)$$

the information contained in $T_b(\omega_k)$ is lost in the smoothing process. This means that $T_a(\omega)$ has no knowledge of $T_b(\omega)$ at $\omega = \omega_k$ no matter what the magnitude of $T_b(\omega_k)$. Even if $G^*(\omega)$ only approaches zero, spectral information is severely attenuated. It is reasonable to expect $G^*(\omega)$ to be small in magnitude at some large ω since continous functions, such as antenna patterns, have high frequency components that approach zero.

Fig. 4 demonstrates the aerial smoothing effect in the transform domain for arbitrary functions. The point labeled ω_c may be described as being a cutoff frequency beyond which $G(\omega)$ is at or near zero. Starting with $T_b(\omega)$ (Fig. 4a) and multiplying by $G(\omega)$
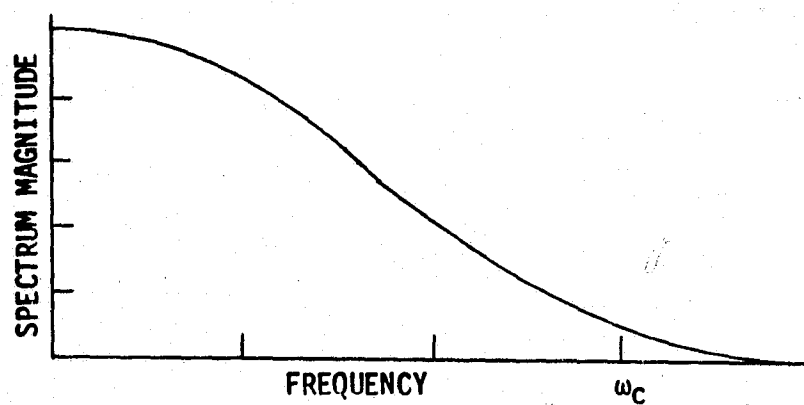
(a) BRIGHTNESS TEMPERATURE SPECTRUM $[T_b(\omega)]$
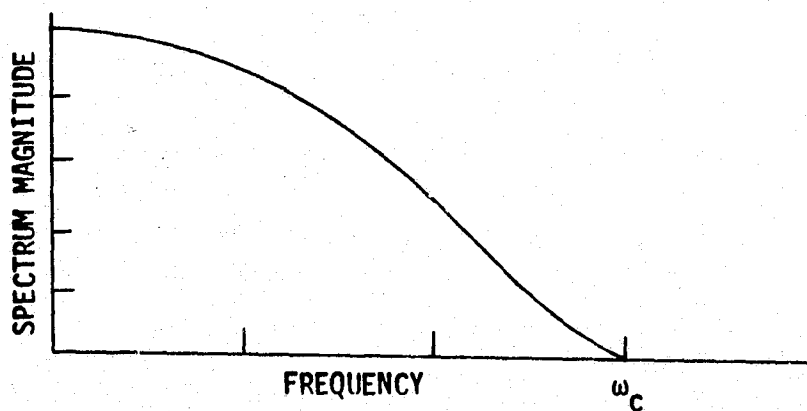
(b) GAIN PATTERN SPECTRUM $[G(\omega)]$
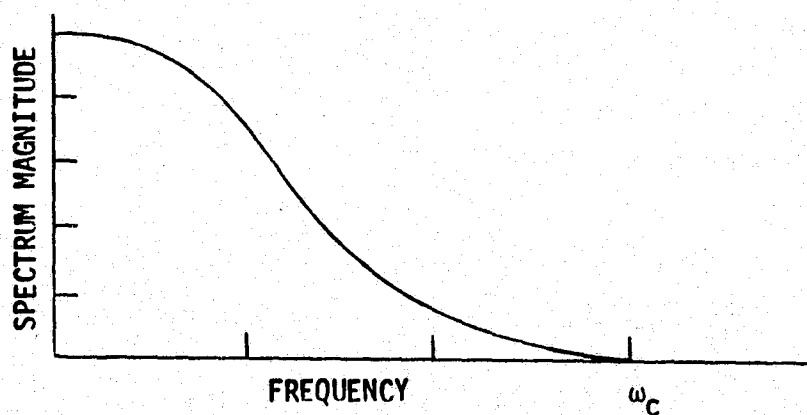
(c) ANTENNA TEMPERATURE SPECTRUM $[T_a(\omega)]$

Fig. 4. The smoothing effect in the transform domain.

(Fig. 4b) results in the spectrum of $T_a(\omega)$ (Fig. 4c). This procedure may be explained as being a filtering process in which the input signal $T_b(\omega)$ is filtered by the system's transfer function $G(\omega)$, resulting in the ouput signal $T_a(\omega)$. The figure shows that the frequencies above ω_c are completely lost and below ω_c reduced in magnitude according to the gain function spectrum variation. The end result of the two areas of spectral attenuation is the smoothing of the brightness temperature distribution in the spatial domain.

As was stated in the introduction, radio astronomers have been able to by-pass the antenna smoothing problem. They accomplish this by using highly efficient narrow beam aerials which allow the antenna temperature to approximate the brightness temperature. This approximation is accurate because the gain function of the high efficiency antenna approaches the Dirac delta function. If $G(\emptyset)$ is a delta function, $T_a(\omega)$ equals $T_b(\omega)$ in (27). In this case, there is no loss of spectral information which results in the measurement of a highly resolved profile. However, the antennas used for remote sensing must meet rigid constraints that force the use of aerials with pattern frequency spectrums that decrease and approach zero at high frequencies.

The existence of ω_c, that was discussed previously, places $G(\omega)$ in the role of a low-pass filter that rejects the high frequency signals subjected to it. This implies the possible existence of brightness temperature profiles that may be virtually

undetectable, such as

$$T_b(\emptyset) = \sum_m A_m \exp(j\omega_m\emptyset) \qquad (30)$$

where the A_m are arbitrary and ω_m are larger than ω_c of Fig. 4.
These temperature distributions may be called invisible distri-
butions, since they are not accepted and not recorded by the system.
Although the presence of what (30) represents in nature is
impossible, since it would require the measurement of negative
absolute temperatures, it may however occur on top of a realizable
detectable distribution such as T ($\emptyset$) forming

$$T_b(\emptyset) = T(\emptyset) + \sum_m A_m \exp(j\omega_m\emptyset) \qquad (31)$$

The plausibility of (31) in water brightness temperature investi-
gations is questionable, although its usage in the study of the
stability of inversion methods is advantageous.

2.4 Inversion of the Integral Equation

Experiments have been devised to investigate the state of water
by remote sensing techniques. For this investigation, the actual
measurements would represent the antenna temperature, as given by
(20), where the parameter of importance is the brightness
temperature of the water (T_{bw}) which is part of the integrand of
(21). It would then be important to be able to determine the
functional variation within the integral from a knowledge of the
integral itself (measurements). This process is known as inversion.

Since (21) can be cast into a multiplication form in the

transform domain, as shown by (27), $T_{bw}(\beta)$ can then be determined by

$$T_{bw}(\beta) = F^{-1}[\frac{T_{aw}(\omega)}{G^{*}(\omega)}] \qquad (32)$$

where F^{-1} is the inverse Fourier transform and $T_{aw}(\omega)$ is the antenna temperature due to the water in the frequency domain. It should be pointed out that T_{aw} is obtained from (20) after the contributions from the earth (T_{ae}) and sky (T_{as}), calculated using (22) and (23) and a knowledge of T_{be} and T_{bs}, have been subtracted from the total measured antenna temperature. The advantage of using (32) for inverting (21) is that the T_{bw} for all observation angles (β's) and one system position (α) are processed in one efficient calculation with the aid of the FFT algorithm. This makes the method very attractive in the evaluation of large quantities of data.

2.5 Stability Investigation of the Inversion

Calculating a T_{aw} from a known T_{bw} by (27) and then inverting this T_{aw} using (32) gives a T_{bw} different from the original by only $\pm 0.02^{\circ}K$, as was demonstrated in [14]. This would indicate that (32) is an accurate inversion method. However, this method was examined only with exact T_{aw}. Therefore, it is important to investigate the sensitivity and stability of (32) when $T_{aw}(\beta)$ is known with only moderate accuracy, that is to say when (21) is ill-posed.

The integral equation of (21) is in a crosscorrelation form and is a special case of the Fredholm integral equation of the first kind. However, the stability of the more stringent general form of the Fredholm equation will be inspected, and the conclusions drawn from this investigation will apply to the special case of (21). In the course of the stability investigation, the following relationship is required.

$$\lim_{R \to \infty} \int_a^b K(x,y) \sin(Rx)dx = 0 \quad ; a \leq x \leq b \qquad (33)$$

The proof of (33) is given in [18] and is repeated in Appendix II.

The general form of the Fredholm integral equation of the first kind is

$$g(y) = \int_a^b K(x,y) f(x) dx \quad ; a \leq x \leq b \qquad (34)$$

where $g(y)$ is a known (measured) function, $K(x,y)$ is the kernel of the integral equation, $f(x)$ is the unknown function, and a,b are constant limits of integration. If for any A, $A\sin(Rx)$ is added on to $f(x)$ and $R \to \infty$, then from (33), $g(y)$ remains unchanged and (34) may be written as

$$g(y) = \int_a^b K(x,y) [f(x) + A\sin(Rx)] dx \quad ; a \leq x \leq b \qquad (35)$$

However, if R is given some finite large value rather than infinity, then an arbitrary small variable $\delta(y)$ is added to $g(y)$ forming

$$g(y) + \delta(y) = \int_a^b K(x,y) \, [A\sin Rx + f(x)] \, dx \quad ; \quad a \leq x \leq b \qquad (36)$$

If the left side of (36) represents measured data, that differs from the correct measurements $g(y)$ by some small experimental error $\delta(y)$, the inversion would then yield large amplitude, high frequency oscillations attached to the correct solution of $f(x)$. This indicates that the solutions to the Fredholm integral equation of the first kind are not unique when experimental errors are considered.

The solutions of the ill-posed integral equation of the first kind will result in sporadic oscillations, regardless of the inversion method used. This also applies to the Fourier inversion technique of (32). The source of the instability in the Fourier inversion becomes apparent if the spectrum of the gain function $G(\omega)$ is examined, as was done in section 3.2.

To explain the instability in the Fourier inversion, (32) is rewritten as

$$T_{bw}(\beta) = F^{-1} \left[\frac{T'_{aw}(\omega)}{G^*(\omega)} + \frac{T_e(\omega)}{G^*(\omega)} \right] \qquad (37)$$

where $T_e(\omega)$ is the additive experimental error in the transform domain, and $T'_{aw}(\omega)$ is the spectrum of the error-free antenna temperature. For some ω near or above ω_c of Fig. 4b, the second

term on the right side of (37) may be large because $T_e(\omega)$ is amplified considerably from its division by the small $G(\omega)$ components. In the extreme case where $G(\omega_k)$ is exactly zero, the inversion of the ill-posed (21) will blow up since $T_{bw}(\beta)$ will have components of infinite magnitude for any trace of $T_e(\omega_k)$. This means that the inversion inadvertently exaggerates the A_m terms of the invisible portion of (31). This inversion method can not be used in practical applications and a modification to the technique must be developed.

2.6 Restoration Method

The discussion on equation (37) showed that it is impossible to obtain an exact solution using (32) when T_{aw} contains experimental errors. To reduce the oscillations of the solution, a smoothing procedure must be included, as was done for the matrix inversion techniques [8]-[11]. This will require the filtering of the large high frequency error terms of (37).

Writing $1/G^*(\omega)$ of (32) as $1/1-[1-G^*(\omega)]$, and then performing a series expansion [2] results in

$$T_{bw}(\beta) = F^{-1} \{T_{aw}(\omega) [1+(1-G^*(\omega)) + (1-G^*(\omega))^2 + (1-G^*(\omega))^3$$

$$+....+ (1-G^*(\omega))^n +....]\} \tag{38}$$

The infinite series expansion of $1/G^*(\omega)$ converges provided that $|1-G^*(\omega)| < 1$. For most antenna systems used in radiometry, their gain patterns are symmetrical, smooth varying functions which

insure that $G^*(\omega)$ is always real and in most cases positive. For some cases where $G^*(\omega)$ is negative, the amplitudes are very small compared to the positive values. Since $G(\omega)$ has been normalized so that its maximum value is unity, convergence of $1/G^*(\omega)$ insures the recovery of a unique T_{bw} only if T_{aw} does not contain any error. The inclusion of error in T_{aw} leads to nonunique and oscillating solutions for T_{bw} since the convergence of $1/G^*(\omega)$ equates (38) to (37). The oscillating forms of T_{bw} are mainly attributed to the inclusion of higher order terms in the series expansion of $1/G^*(\omega)$. Thus, $T_{bw}(\beta)$ can be restored to the extent depending on the error present in $T_{aw}(\omega)$. The oscillations can be minimized by properly truncating the series expansion, which in effect filters the high frequency error terms. In practice, only the first few terms of (38) are necessary, as will be shown later.

The rewriting of (32) in a series form as in (38), places the equation in a convenient form to develop a smoothing procedure in the recovery of $T_{bw}(\beta)$. The technique involves a truncation of the infinite series and then a multiplication of the $T_{aw}(\omega)$ by the truncated series. The inclusion of one, two, three, or more terms of the series can be interpreted as letting the values of T_{bw} be equal, respectively, to

$$T_{bwo} = T_{aw} \tag{39a}$$

$$T_{bw1} = T_{bwo} + (T_{aw} - G*T_{bwo}) \tag{39b}$$

$$T_{bw_2} = T_{bw_1} + (T_{aw} - G*T_{bw_1}) \qquad (39c)$$

$$\vdots$$

$$T_{bwn} = T_{bw\,(n-1)} + (T_{aw} - G*T_{bw(n-1)}) \qquad (39d)$$

where * implies crosscorrelation. The altered inversion procedure reduces to an iterative method, as indicated by (39a)-(39d),and will be referred to as restoration [2]. The second term in (39b)-(39d) is a correction factor which is added to the values of the previous restored brightness temperature to obtain the newly created function. It should be emphasized that this iterative method allows restoration of the brightness temperature of the water for all viewing angles within the limits of the wave tank.

The restoration method approximates well the correct T_{bw} solution from the truncation of (38). This filtering process not only reduces the oscillatory part of the solution, but it also smooths the true T_{bw} where high frequency terms are required to describe the rapidly varying parts of the curve. However, the T_{bw} curve is a fairly smooth function in itself. The restoration method will smooth only the discontinuous edges of the wave tank profile or those temperatures near the horizon, depending on the size of the wave tank. This property of the restoration process will be demonstrated later.

III. COMPUTATIONS

3.1 Calculation of the Antenna Temperature

Computations for the investigation of the Fourier inversion technique will be conducted using the 5° Half Power Beam Width (HPBW) antenna of Fig. 5, whose beam efficiency to the first null, assuming rotational symmetry, is 99.97%. This beam efficiency is typical of antenna patterns used in state-of-the-art radiometers nowadays [19]. To use the FFT algorithm developed by Cooley and Tukey [12] to perform a discrete Fourier transform, requires that 2^N sampling points be known (N is an integer). All functions used throughout this investigation are sampled 256 times in one reveloution (360°) of its observation angle. Two hundred fifty six points allow 128 harmonics of the fundamental frequency ($f_0 = \frac{1}{2\pi}$) of the function to be calculated. Ninety (90) harmonics of the normalized spectrum of the 5° HPBW antenna are shown in Fig. 6. Although an exact ω_c can not be located in this figure, the spectral characteristics of Fig. 6 and Fig. 4b are equivalent.

To prove the validity of the two-dimensional modeling of the wave tank system, T_{aw} of (21) was calculated from T_{bw} of Fig. 1 using different methods. A three-dimensional model [20], using numerical integration for computations, is compared to the two-dimensional Fourier transform technique in Table I. These results were obtained for various system rotation angles (α's) while the radiometer was looking toward the center of the wave tank ($\beta=0$).
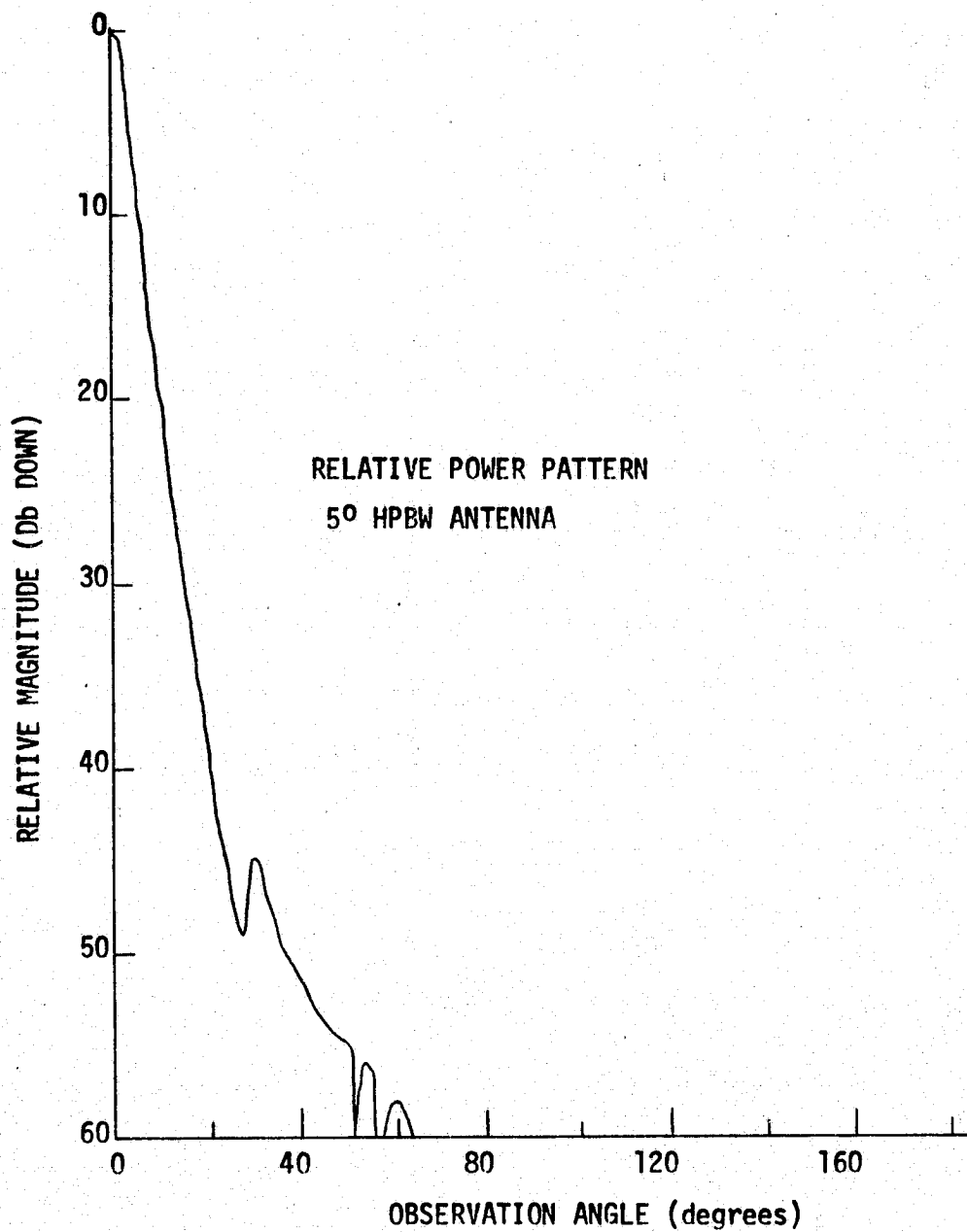
Fig. 5. Predicted pattern of 5° half power beam width (HPBW) corrugated horn antenna.
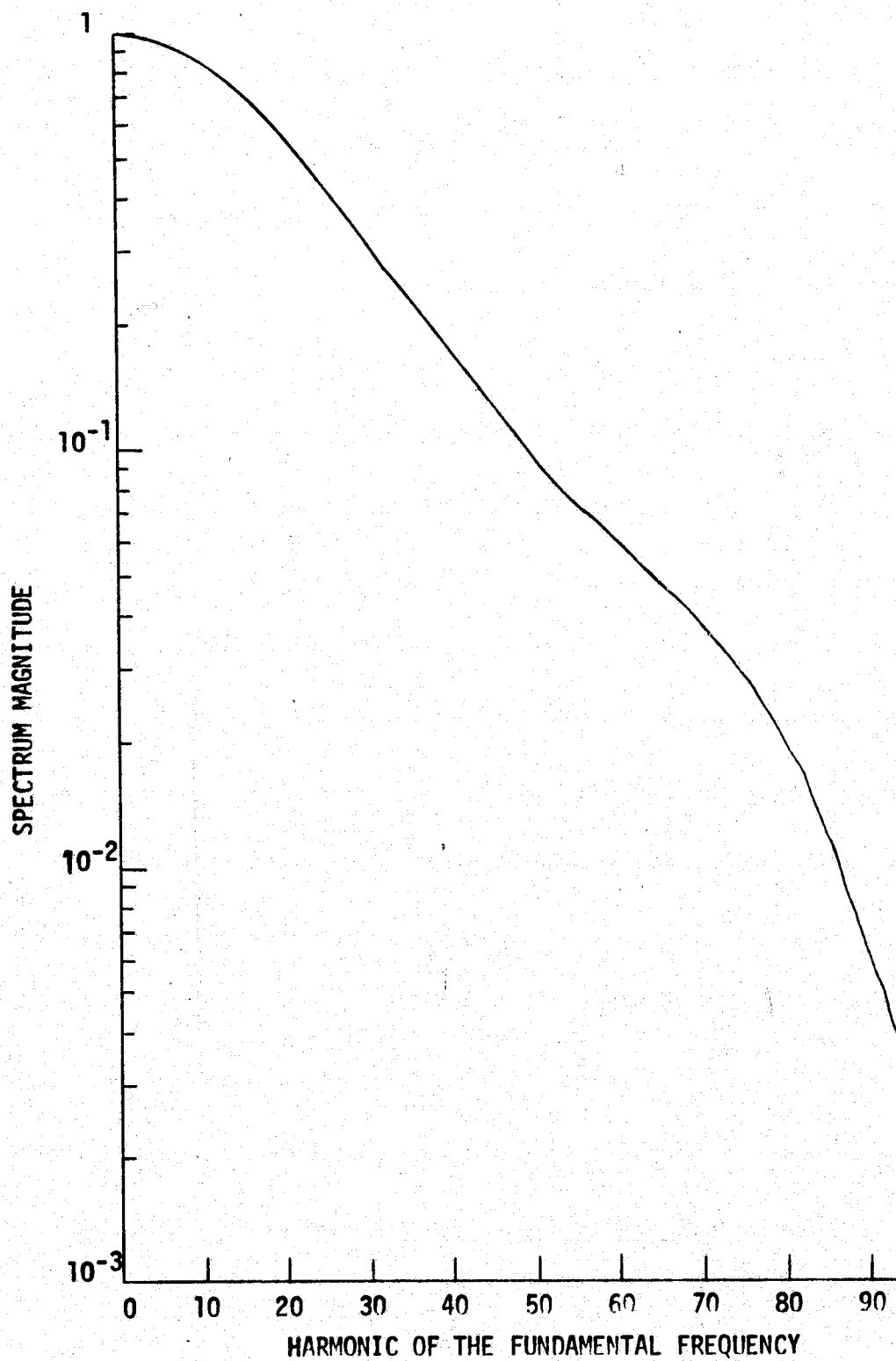
Fig. 6. Frequency spectrum of 5° HPBW antenna.

TABLE 1

ANTENNA TEMPERATURES OF WATER (T_{aw})
FOR VERTICAL AND HORIZONTAL POLARIZATIONS

	WATER ANTENNA TEMPERATURE (T_{aw}, °K)			$w = 14$ feet $\rho = 13$ feet	WATER ANTENNA TEMPERATURE (T_{aw}, °K)		
	VERTICAL POLARIZATION				HORIZONTAL POLARIZATION		
SYSTEM ROTATION ANGLE	WATER BRIGHTNESS TEMPERATURE (T_{bw}, °K)	3-D NUMERICAL INTEGRATION	2-D FAST FOURIER TRANSFORMS		WATER BRIGHTNESS TEMPERATURE (T_{bw}, °K)	3-D NUMERICAL INTEGRATION	2-D FAST FOURIER TRANSFORMS
$\alpha = 0°$	109.10	109.09	109.23		109.10	109.09	108.96
$\alpha = 20°$	114.44	114.48	114.59		104.16	104.14	104.01
$\alpha = 40°$	133.19	133.40	133.42		89.26	89.19	89.07
$\alpha = 60°$	176.88	176.86	176.93		64.71	64.52	64.51
$\alpha = 80°$	269.70	231.32	232.84		37.97	34.24	34.17

As Table I indicates, the two methods agree favorably and the T_{aw}'s are nearly the same as the corresponding T_{bw}'s for incidence angles up to about 60°. For radiometer systems with less efficient radiation characteristics and dominant crosspolarization components, larger differences between brightness and antenna temperatures will be found for all incidence angles and the two-dimensional modeling will not then be as valid.

3.2 Sensitivity Investigation of the Fourier Inversion and Restoration Methods

As was explained previously using (37), the instability in the Fourier inversion is dependent on the spectrums of the error $(T_e(\omega))$ and gain function $(G(\omega))$. To demonstrate this, three sinusodial errors of different frequencies (10th, 30th, and 50th harmonics) and of constant magnitude (1°K) were individually examined. Each of the sine errors were added on to the error-free vertically and horizontally polarized water antenna temperature (T_{aw}) calculated using the water brightness temperature of Fig. 1. The spectrums of the errors $T_e(\beta)$ are spikes placed at their corresponding frequencies, as shown in Fig. 7. Even though the magnitude of $T_e(\beta)$ is the same in each case, the error in the inverted T_{bw} increases as the frequency of the error term increases (Figs. 8 and 9). This is expected from examination of Fig. 6 which shows $G(\omega)$ decreasing as ω increases, causing the higher frequency error to be amplified in
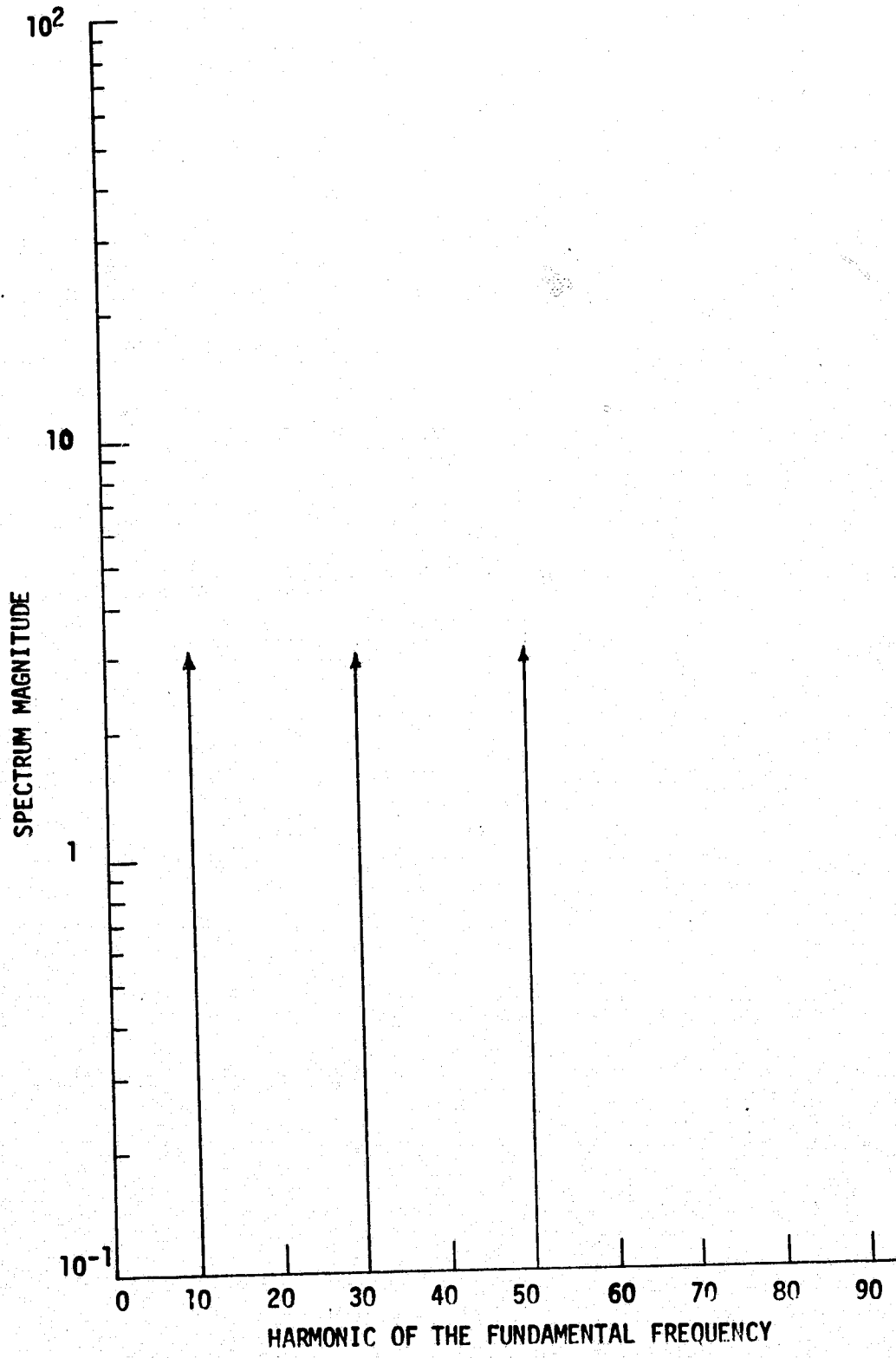
Fig. 7.   Spectrums of the sinusodial errors.
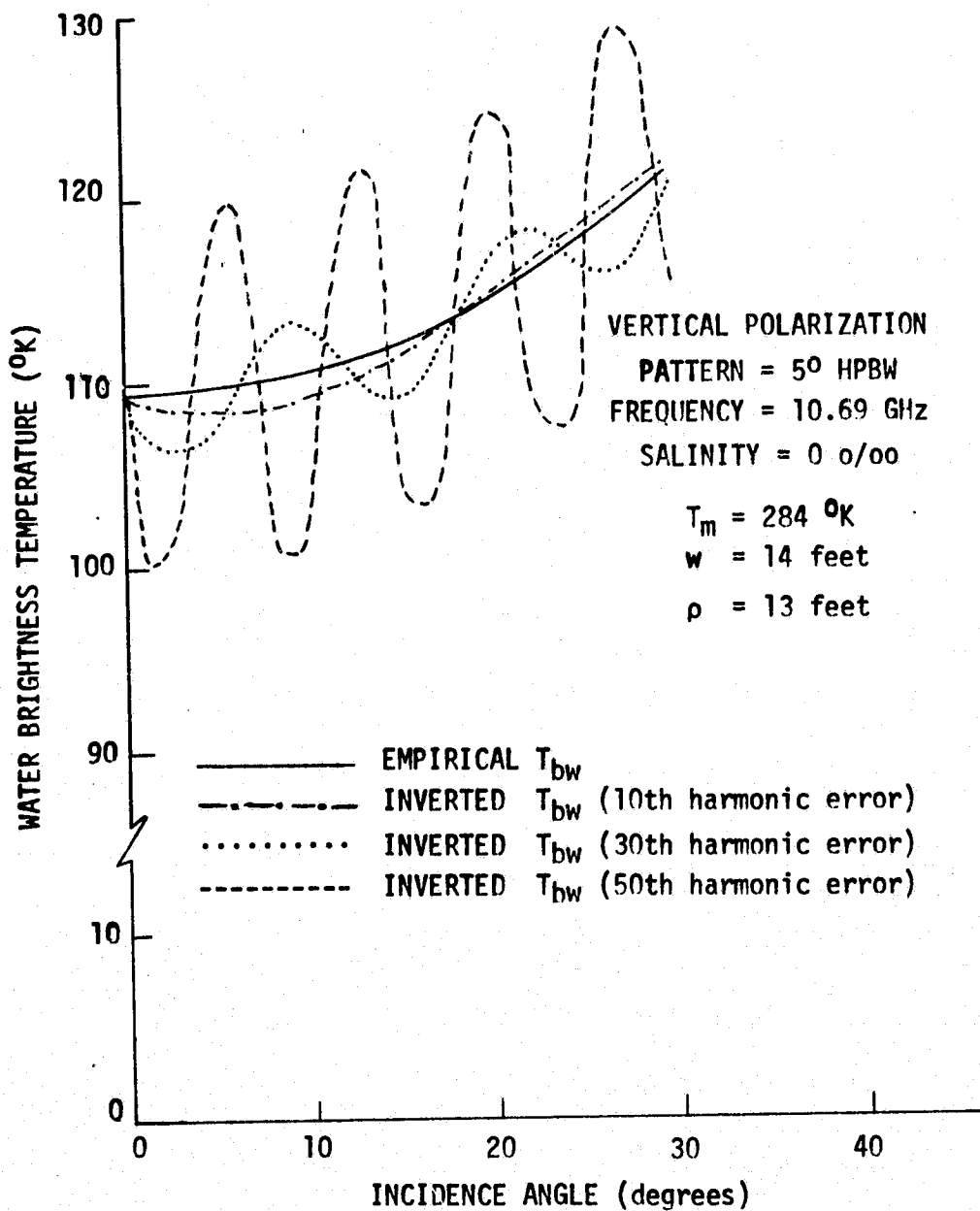
Fig. 8. Empirical and inverted (with sinusoidal errors) vertically polarized brightness temperature profiles.
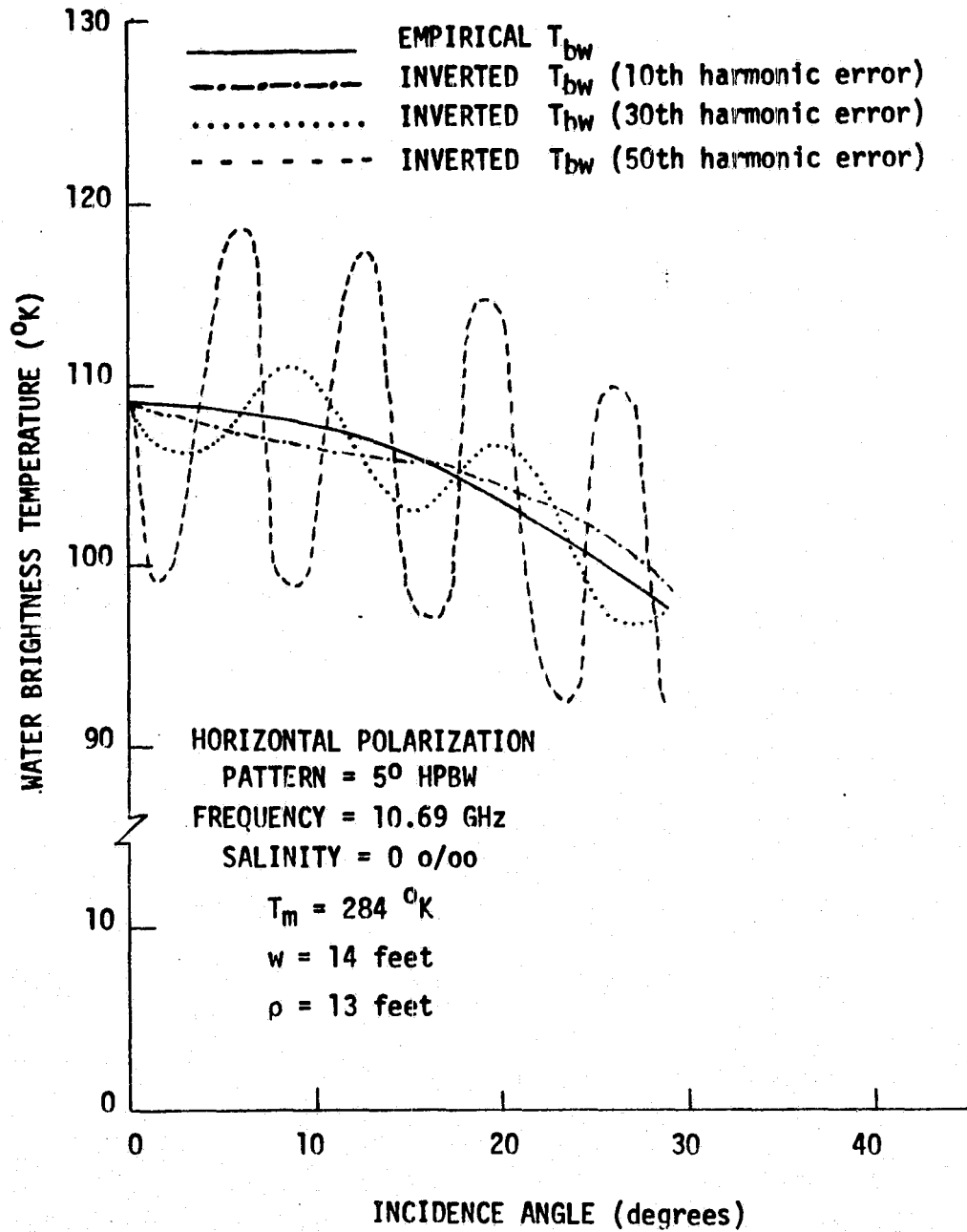
Fig. 9. Empirical and inverted (with sinusoidal
errors) horizontally polarized brightness
temperature profiles.

the inversion process, since it is divided by smaller numbers. The amplification of high frequency error terms is true for all wide beam antennas (narrow frequency spectrum), as was explained in section 4.2.

Another type of error that can be examined is that which occurs when only one out of the two hundred fifty six T_{aw} measurements is incorrect. This is impulse error and has spectral characteristics similar to white noise (Fig. 10). The spectrum of the impulse error is constant and extends to all frequencies. Therefore, the oscillations that result from the division of this $T_e(\omega)$ by $G^*(\omega)$ are sporadic in nature and are large in magnitude. This is demonstrated in Figs. 11 and 12 whose curves were calculated from a T_{aw} that contained a 10° impulse error at the edge of the wave tank. Since these inversions are completely unacceptable, the restoration technique was then applied to the T_{aw} containing the impulse error (Fig. 13). This method yields an accurate T_{bw} curve out to an incidence angle of approximately 17° using only three restorations (four terms of (38)). The discrepancies, that occur at incidence angles greater than 17°, are due mostly to the distortion of the true T_{bw} by the filtering effect of the restoration process.

The sine and impulse errors were introduced to show the sensitivity of the inversion method to the spectrum of the error, and are not representative of errors in actual measurements. An example of a more realistic error is demonstrated by considering
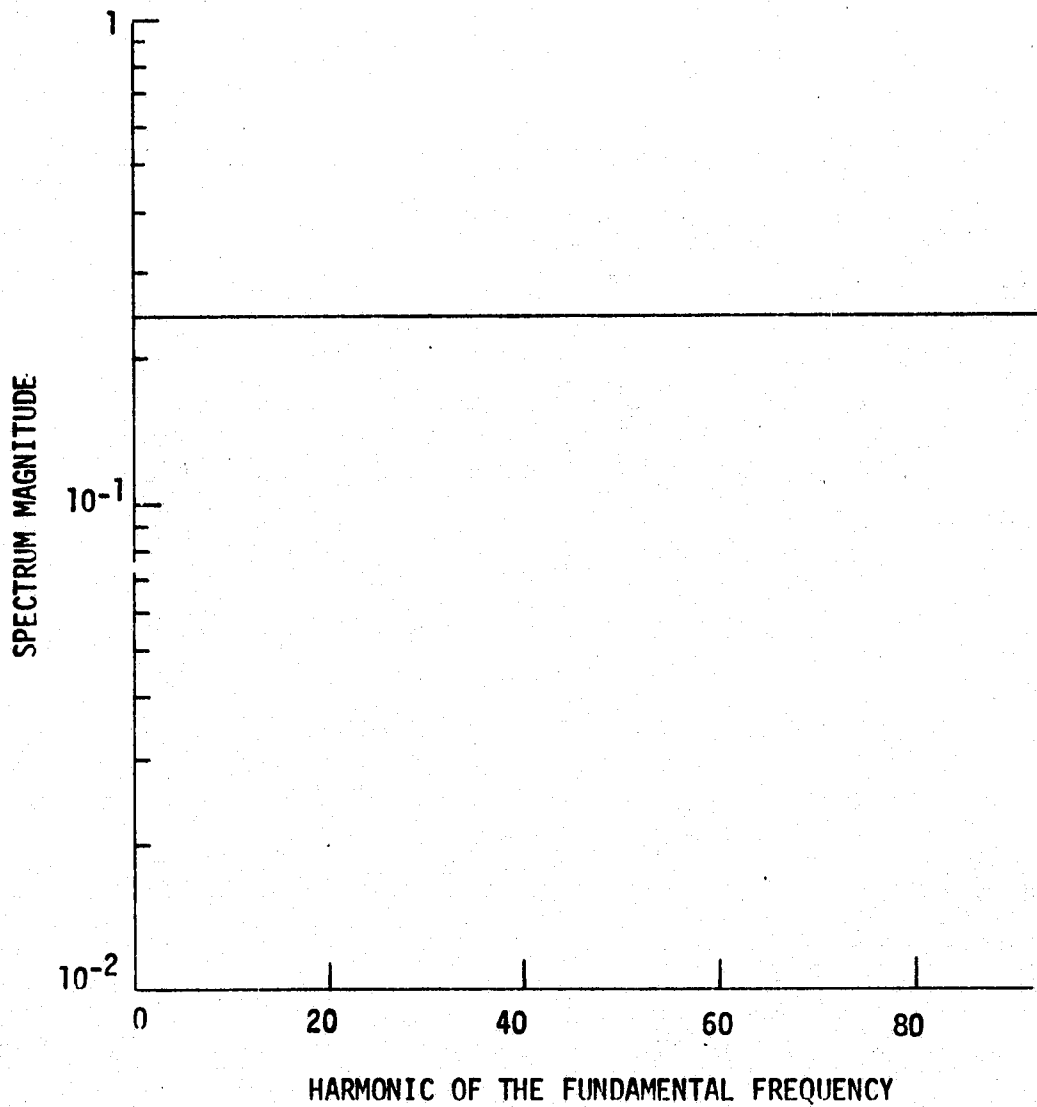
Fig. 10. Spectrum of 10^0 impulse error.
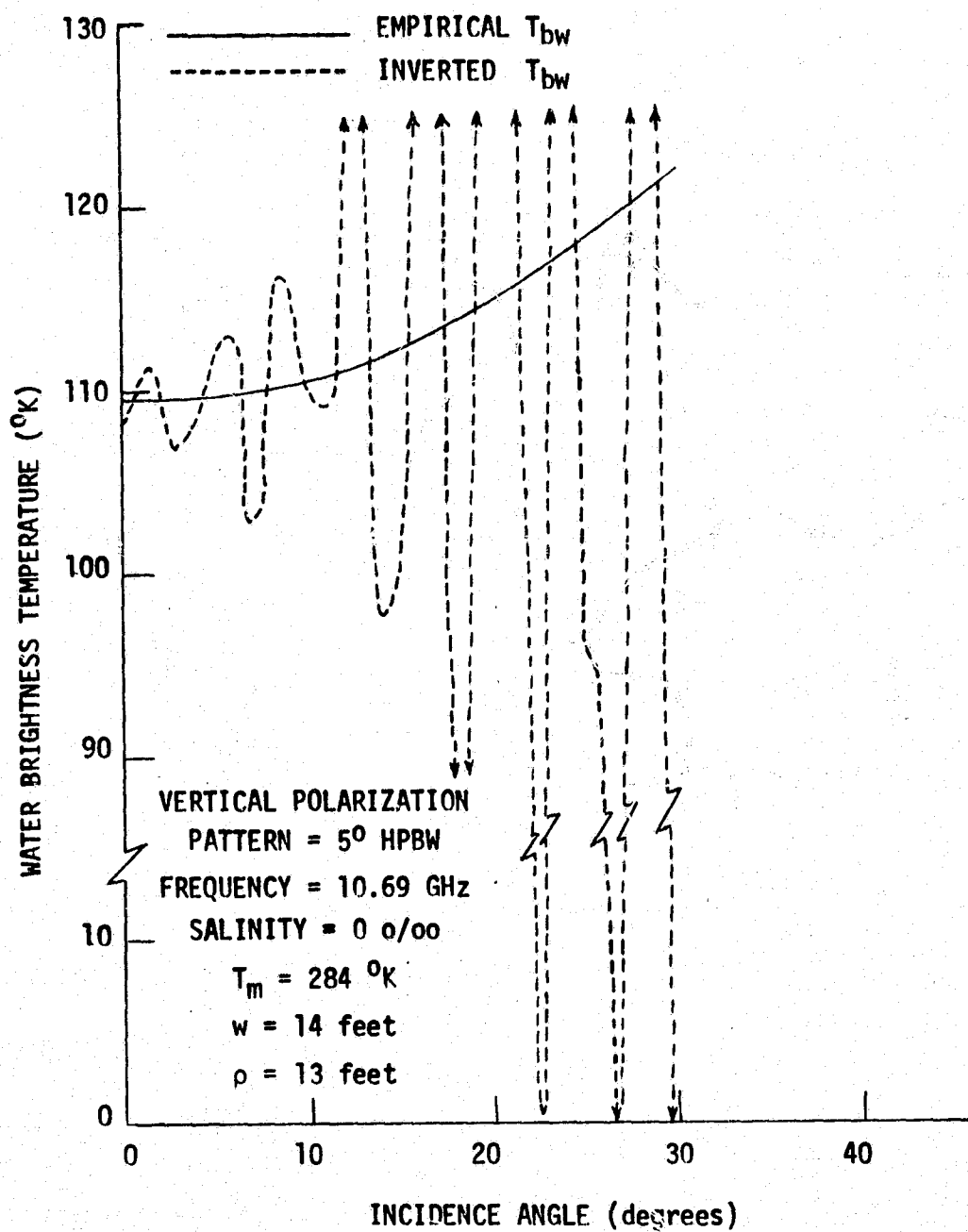
Fig. 11. Empirical and inverted (with 10° impulse
error) vertically polarized brightness
temperature profiles.
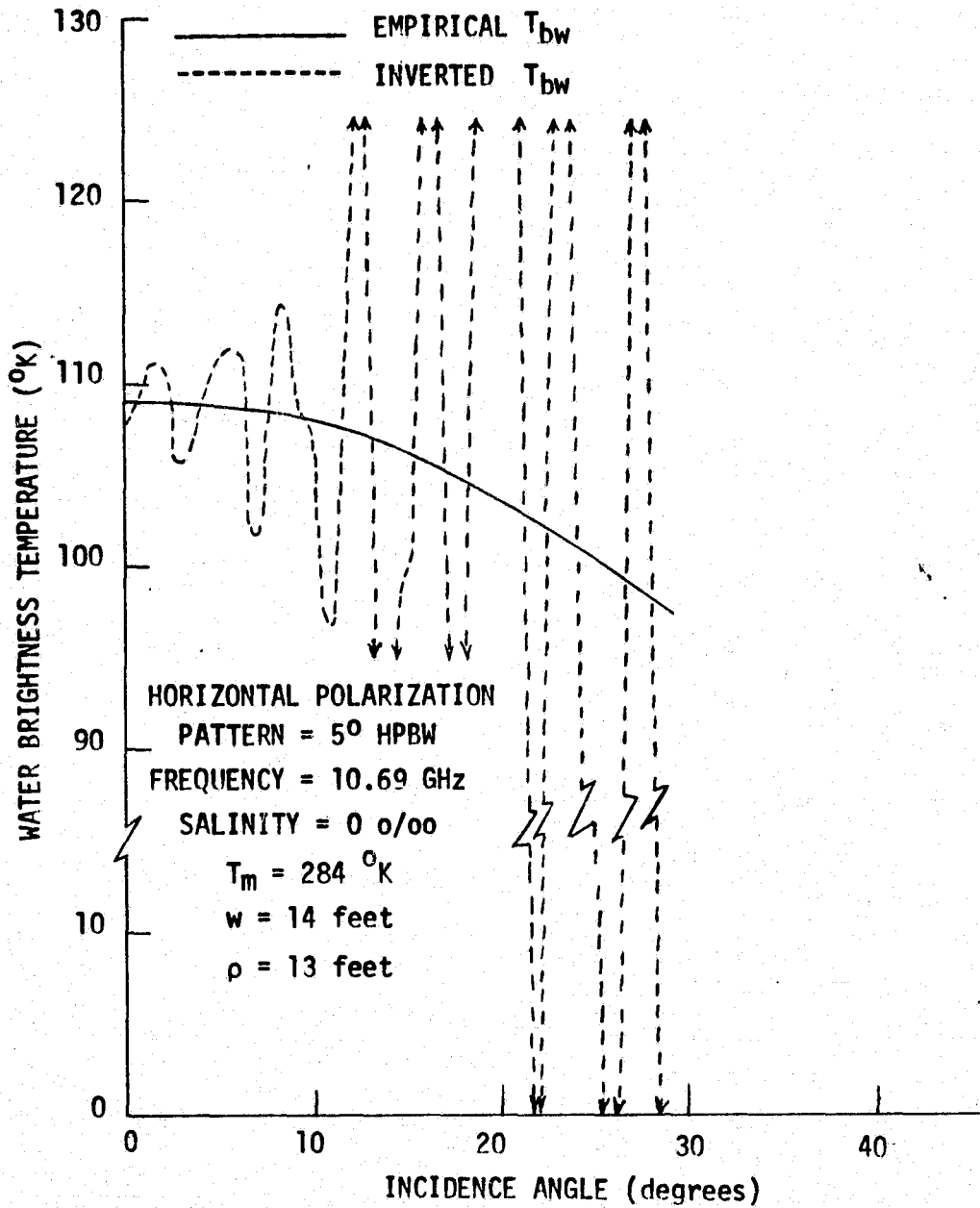
Fig. 12. Empirical and inverted (with 10° impulse error) horizontally polarized brightness temperature profiles.
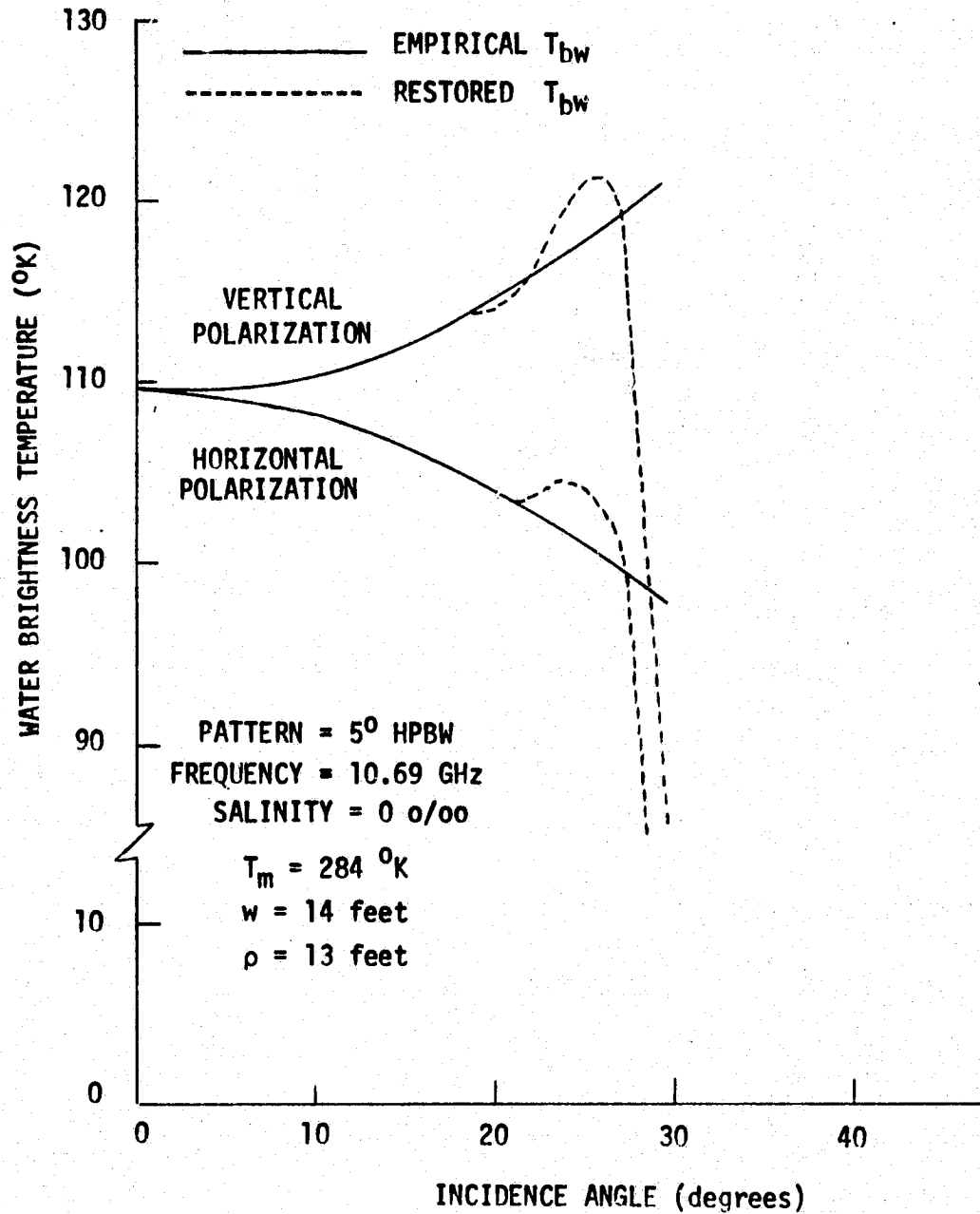
Fig. 13. Empirical and restored (with assumed
injected impulse error) brightness
temperature for vertical and horizontal
polarization.

the operating procedures for the measurements and the manner in which they will be utilized to perform the inversion. To complete the inversion, it is necessary to have measured data for a complete revolution (360^0). Since it was decided that a sampling of about every 1.4^0 was sufficient, two hundred fifty six (256) points will be required for each inversion. Making 256 measurements necessitates long periods of time, and it is not a very practical pro - cedure. Measurements are usually made every 5^0 or 10^0 and the others, necessary for the inversion, can be inferred by interpolating between measured points.

To see what errors are introduced from the procedure described, in Fig. 14 the error-free T_a for vertical polarization was plotted every 5^0 (denoted by stars) for the first 40^0 and every 10^0 thereafter. A curve was then drawn through the points (*--*--*) to represent a profile of T_a for all observation angles. The same procedure was followed for the horizontal polarization with the results shown in Fig. 15. The true T_a is also shown with these curves (——) and seems to indicate very little difference between the two. However, closer observation shows large vertical differences around the rapidly varying parts of the curves. These errors have considerable high frequency content in their spectrums, resulting in the unrealistic inversions of Fig. 16 and 17. If part of the data (0^0-40^0) is from the solid (——) curve of Fig. 14 and the remaining (40^0-180^0) from the dashed (--*--*--) curve of the
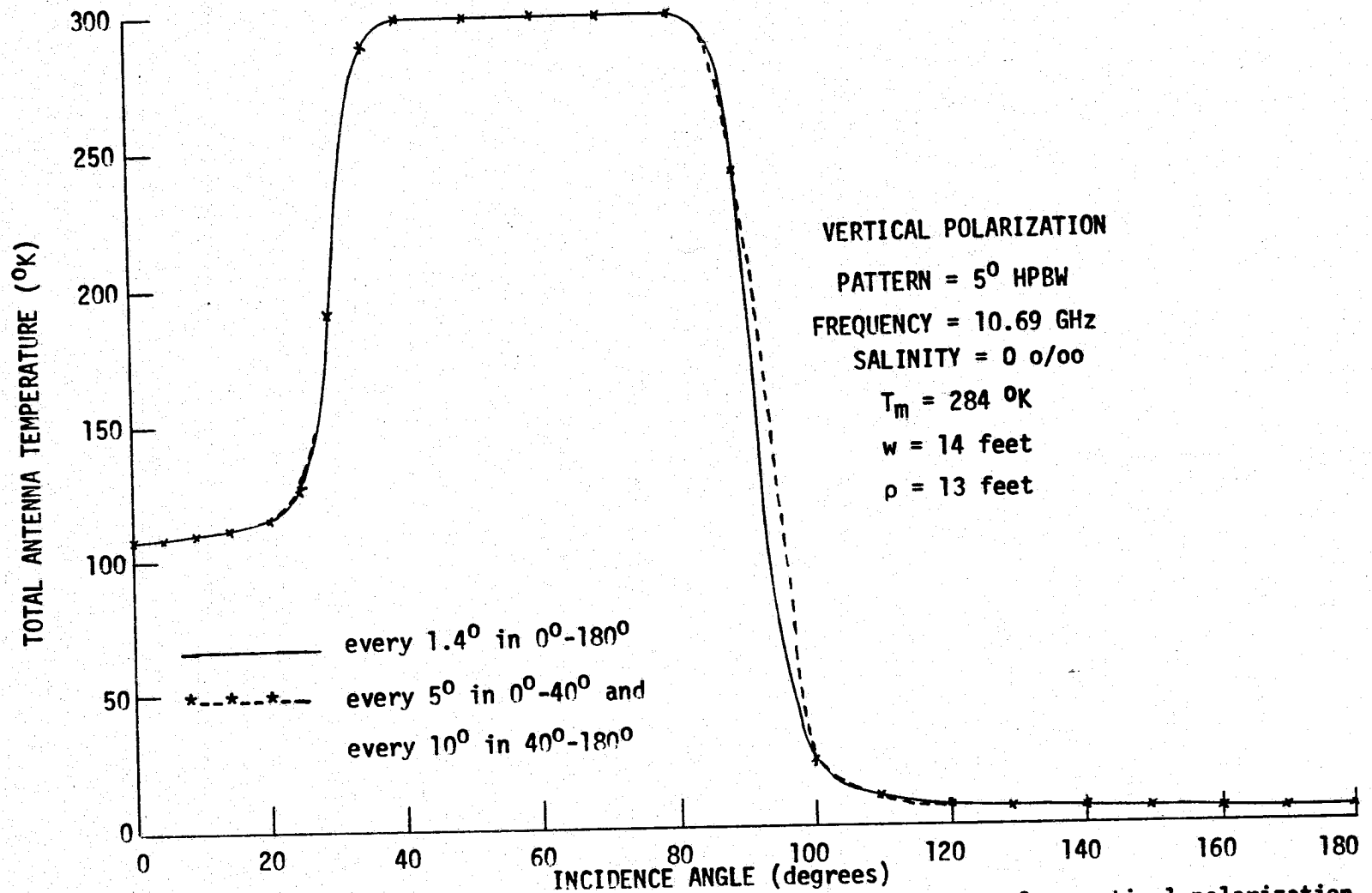
Fig. 14. Exact (———) and approximate (--*--*--) total antenna temperature for vertical polarization.
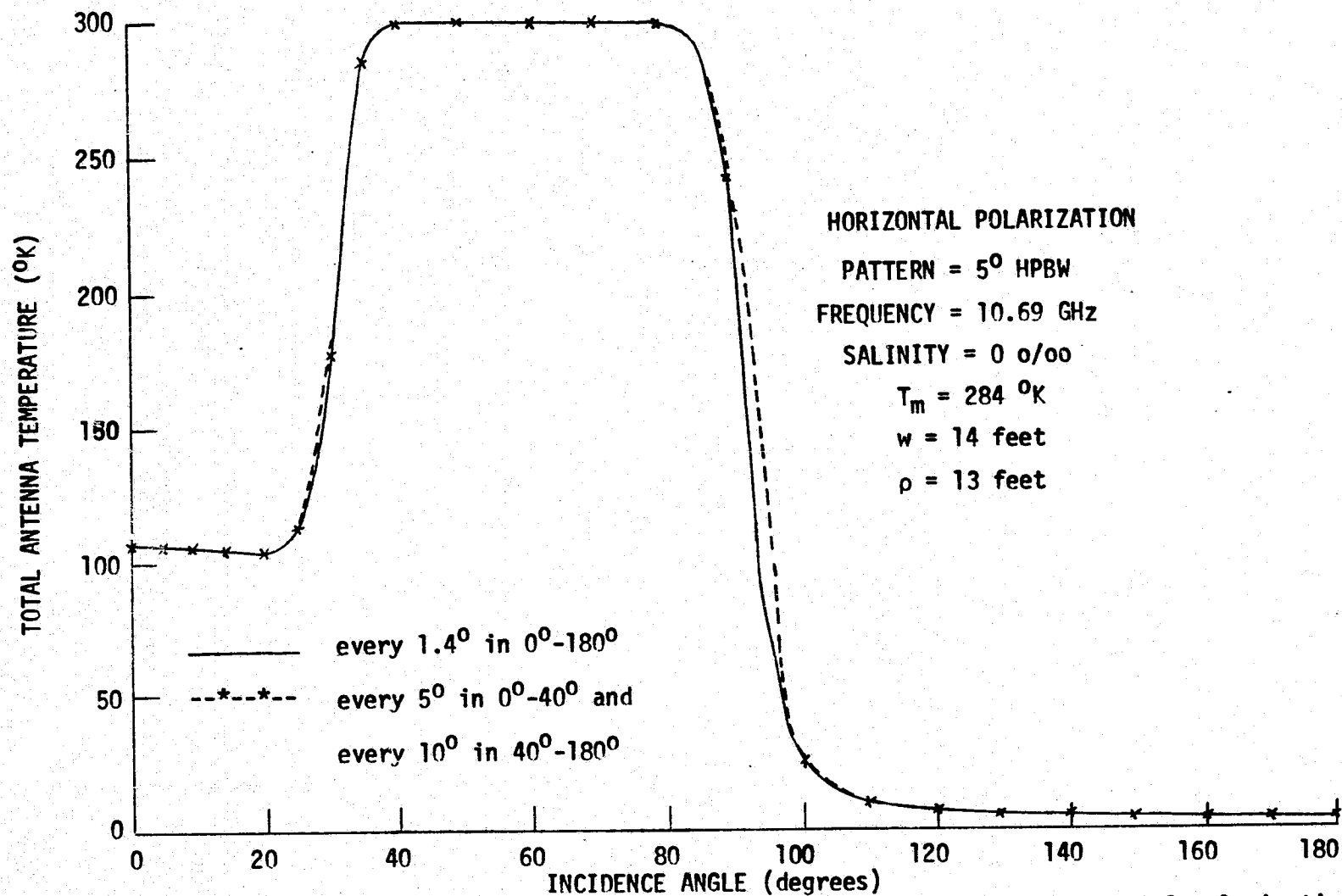
Fig. 15. Exact (——) and approximate (--*--*--) total antenna temperature for horizontal polarization.
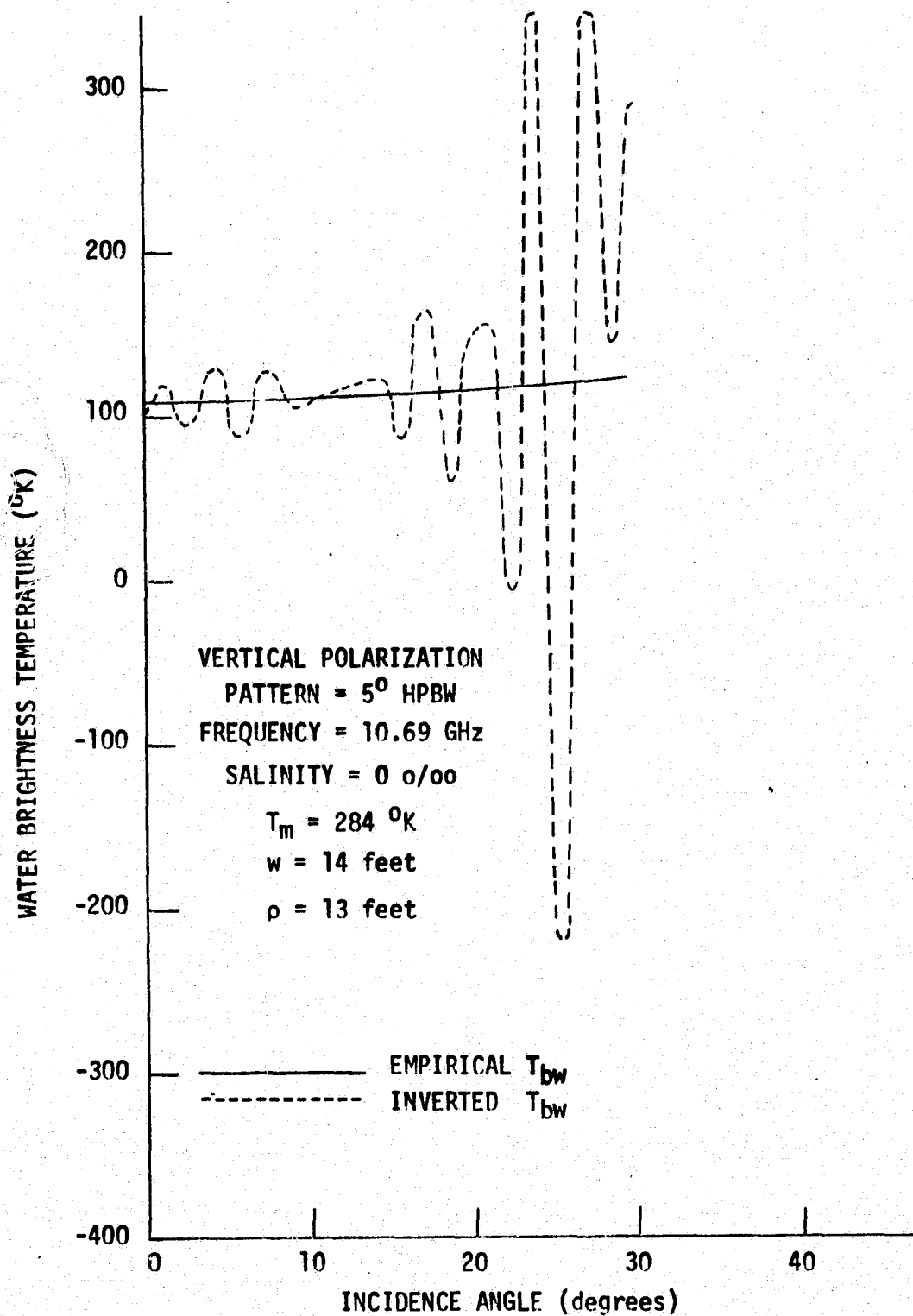
Fig. 16. Empirical and inverted (based on data from —*—*— curve of Fig. 14) water brightness temperatures for vertical polarization.
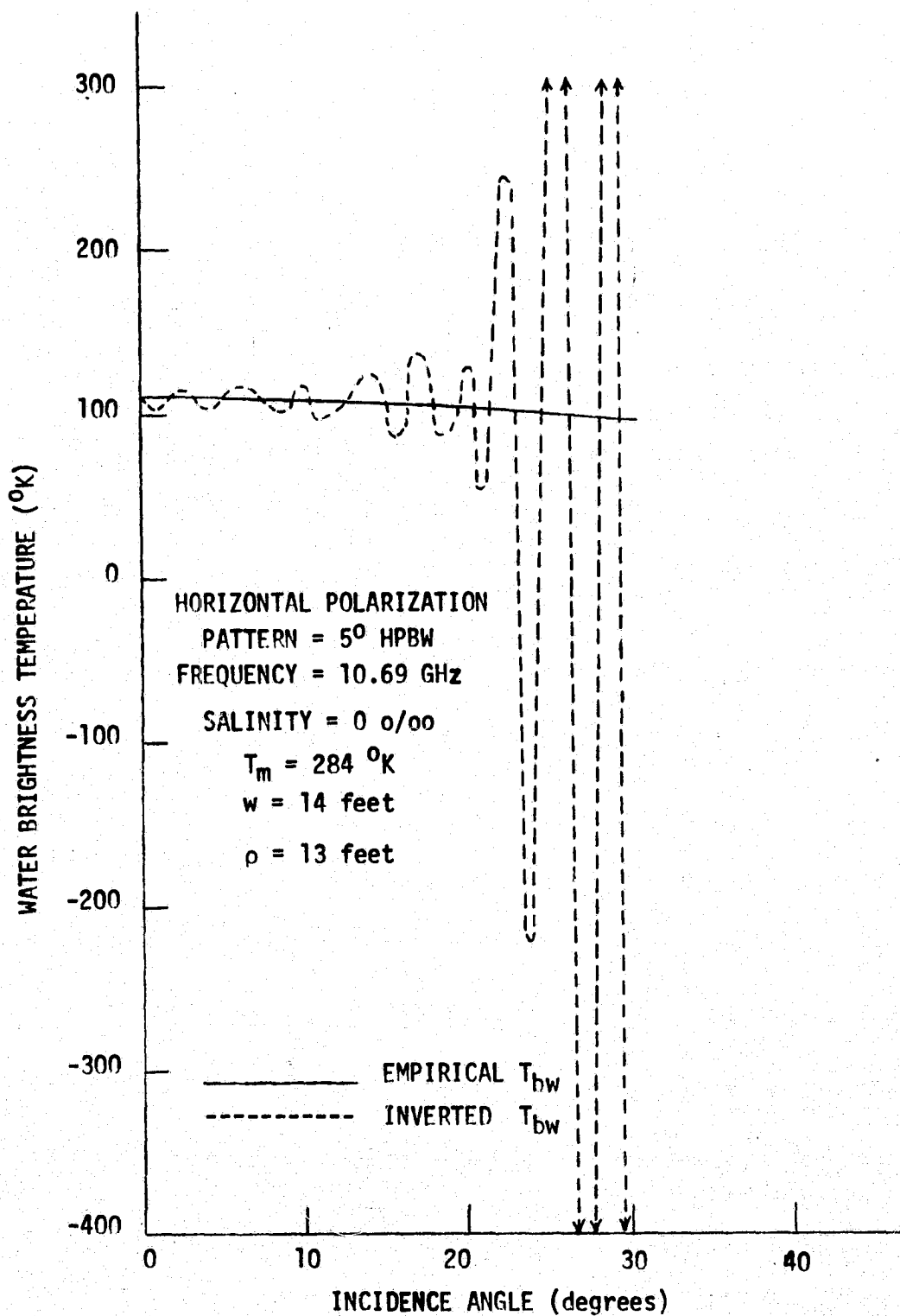
Fig. 17. Empirical and inverted (based on data from —*—*— curve of Fig. 15) water brightness temperatures for horizontal polarization.

same figure, the inversions are still undesirable as shown in Fig. 18. The same is true for the horizontal polarization as shown in Fig. 19 as obtained from the data of Fig. 15.

Since complete inversion, using (31), of the data shown in Figs. 14-19 resulted in quite unrealistic solutions, the restoration procedure of (38) was used to smooth the instabilities. Performing only three restorations on the data used to calculate Figs. 16-19, the restored vertical and horizontal polarizations of T_{bw} are compared to the true T_{bw} in Figs. 20 and 21. When T_a is measured every 5° over the first 40°, discrepancies in the restored T_{bw} occur at angles near the edge of the wave tank because of the diffi- culty in measuring the T_a around this rapidly varying part of the profile. If the correct T_a is used over the wave tank (every 1.4^o over the 0°-40° range), then less disagreement is observed between the true and restored T_{bw}. The difference between the curves in the second case is not due to the error in T_a completely. Instead, as was discussed previously, this discrepancy results from the filtering process of the restoration which attenuates the high frequency terms in the solution.

All of the high frequency components, made available by the FFT algorithm, are required to describe the discontinuous edge of the wave tank's brightness temperature profile. By eliminating some of these terms in the restoration process, a smoothed edge is formed. The discontinuous edge can be restored if more terms in (38) are
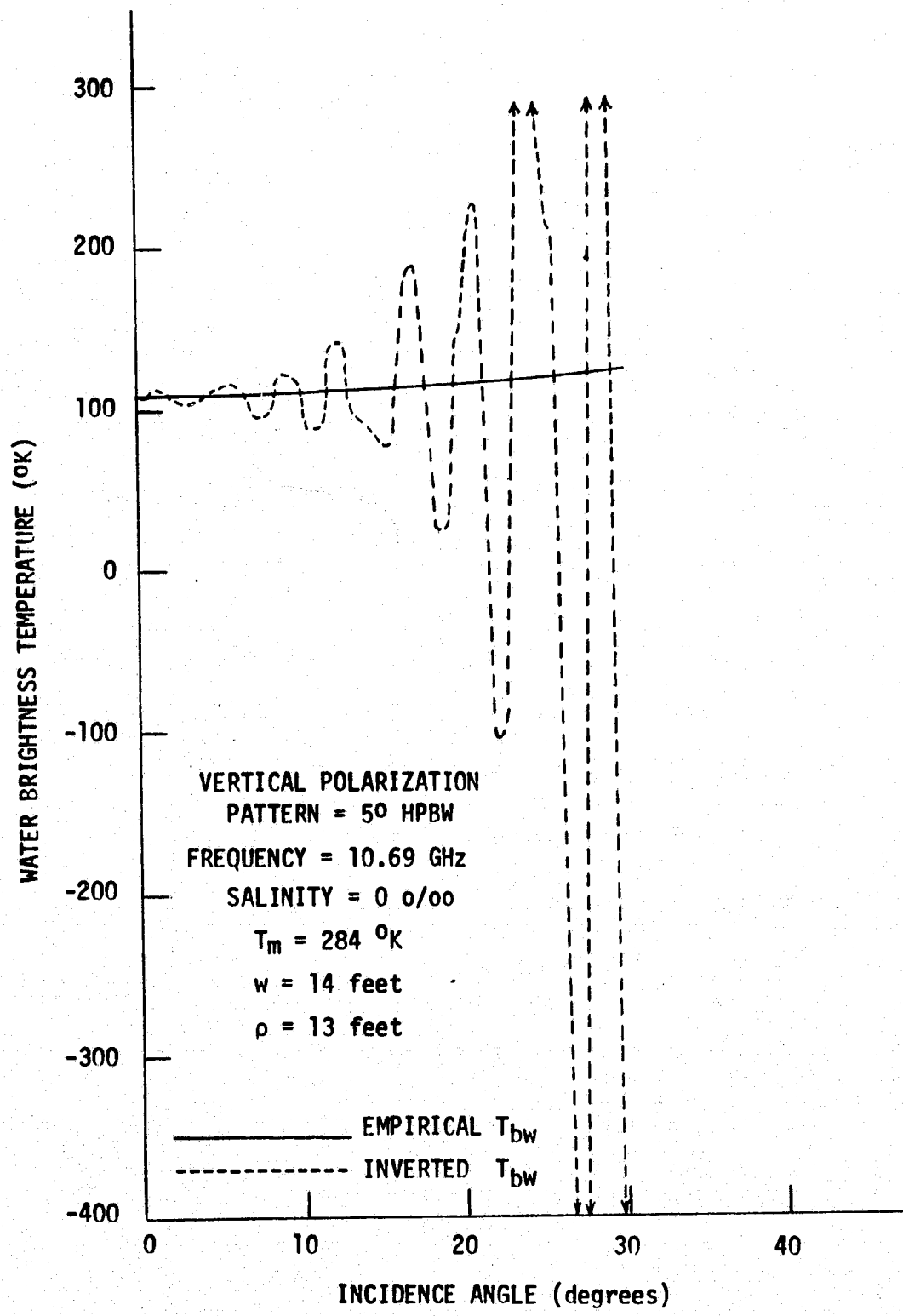
Fig. 18. Empirical and inverted (using data from Fig. 14) water brightness temperatures for vertical polarization.
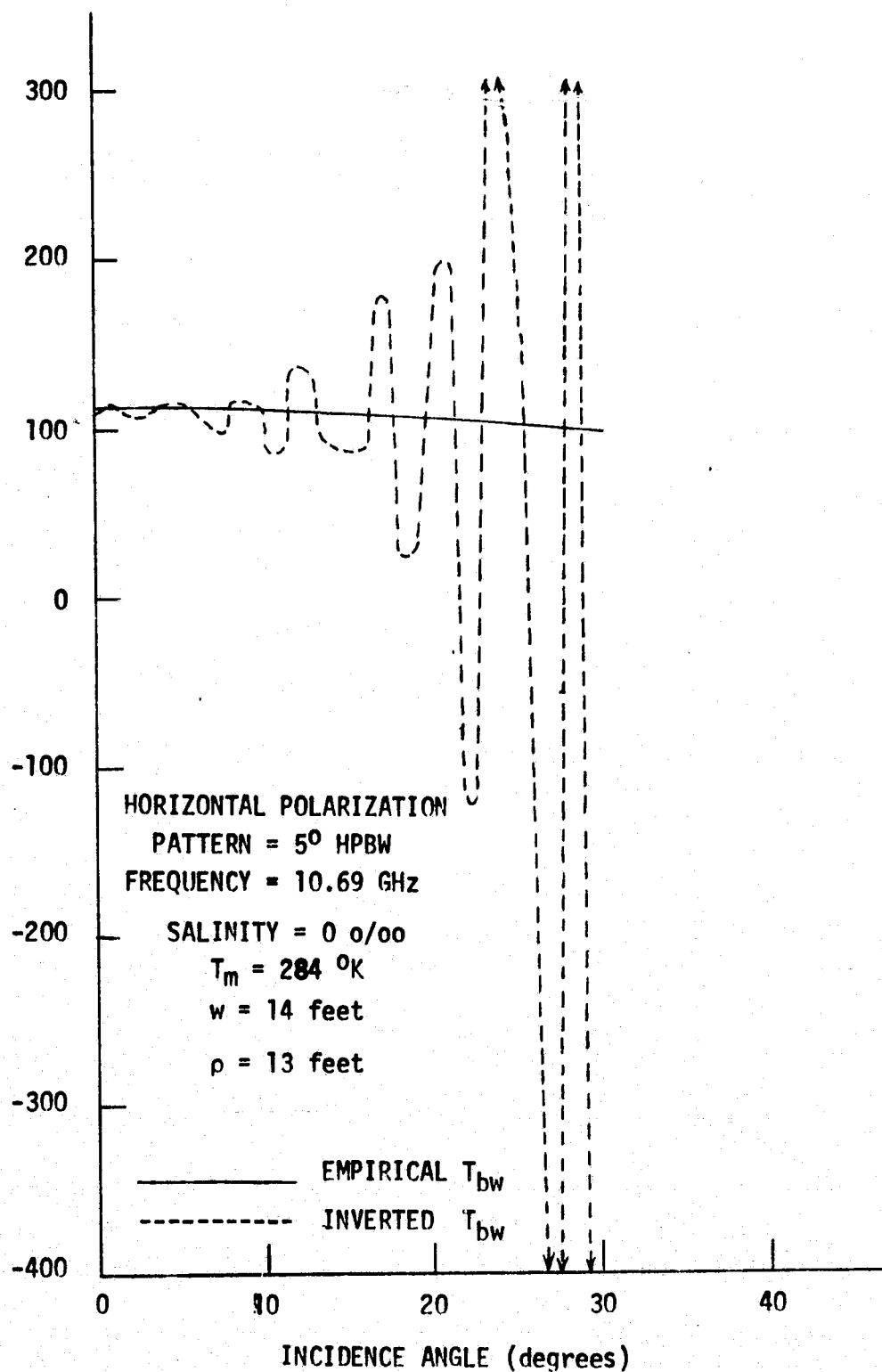
Fig. 19. Empirical and inverted (using data from Fig. 15) water
brightness temperatures for horizontal polarization.
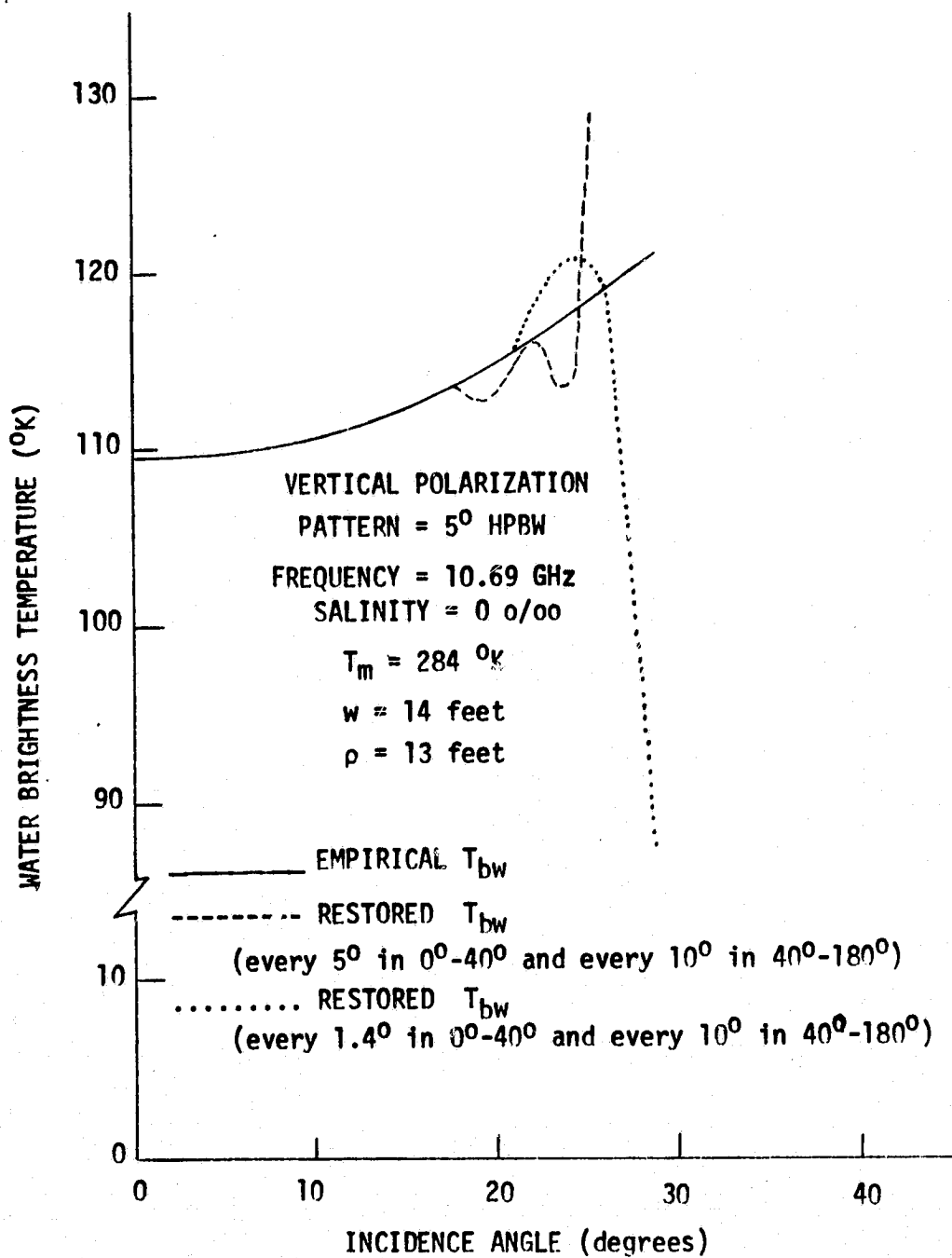
Fig. 20. Computed and restored brightness temperature profiles of water for vertical polarization.
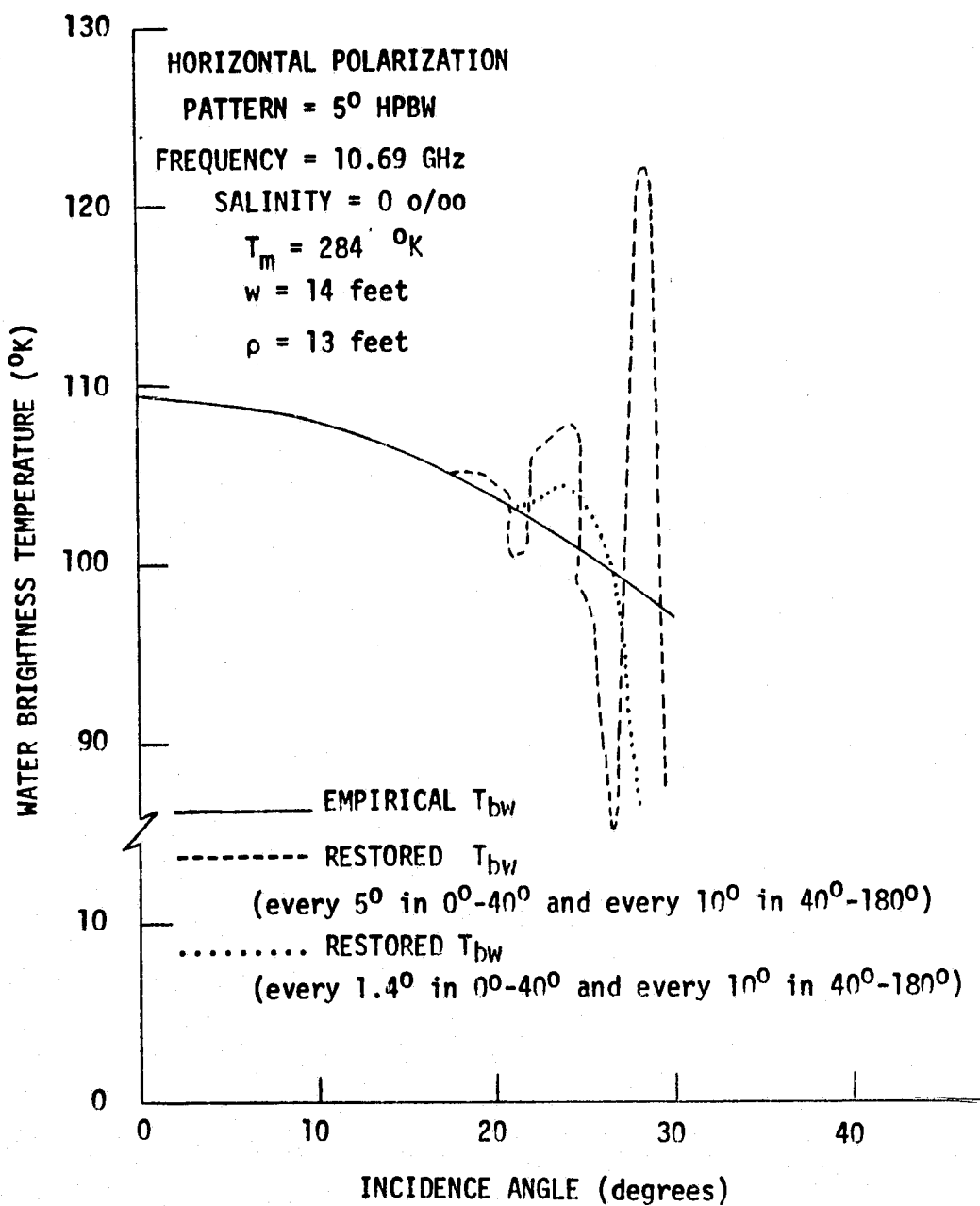
Fig. 21. Computed and restored brightness temperature
profiles of water for horizontal polarization.

considered, but this would enhance the errors in T_a and would approach the unstable inversions of Figs. 16-19. It was observed that three restorations is usually the limit for most measured data, which was also concluded in [3] and [21].

3.3 Refined Measuring Procedure

To calculate the water's brightness temperature profile for large incidence angles using a finite size wave tank, the system's rotation angle (α) must be varied. Since only a small number of restorations will normally be performed on measurements, the usable portion of each restored profile, for a given antenna position along the arc, will be limited. Therefore, to maximize the benefits of the restoration process, the selection of the best first estimate for T_{bw} of (39a) must be examined.

Performing three restorations on measurements permits only three corrections to the first estimate of T_{bw} in (39). This raises the question of whether T_a might be a better estimate of T_{bw} rather than T_{aw}, in which case its use would result in improved solutions from the limited number of restorations performed. To aid in the selection of the term to be placed in (39a), the curves in Figs. 22, 23 (ρ = 13 feet) and Figs. 24,25 (ρ = 26 feet), were calculated by restoring the error-free T_{aw}. These plots can be compared to the curves of Figs. 26-29 which were calculated by restoring the error-free T_a. These figures indicate that for small α the accuracy and range of the restored profiles are approximately the same whether
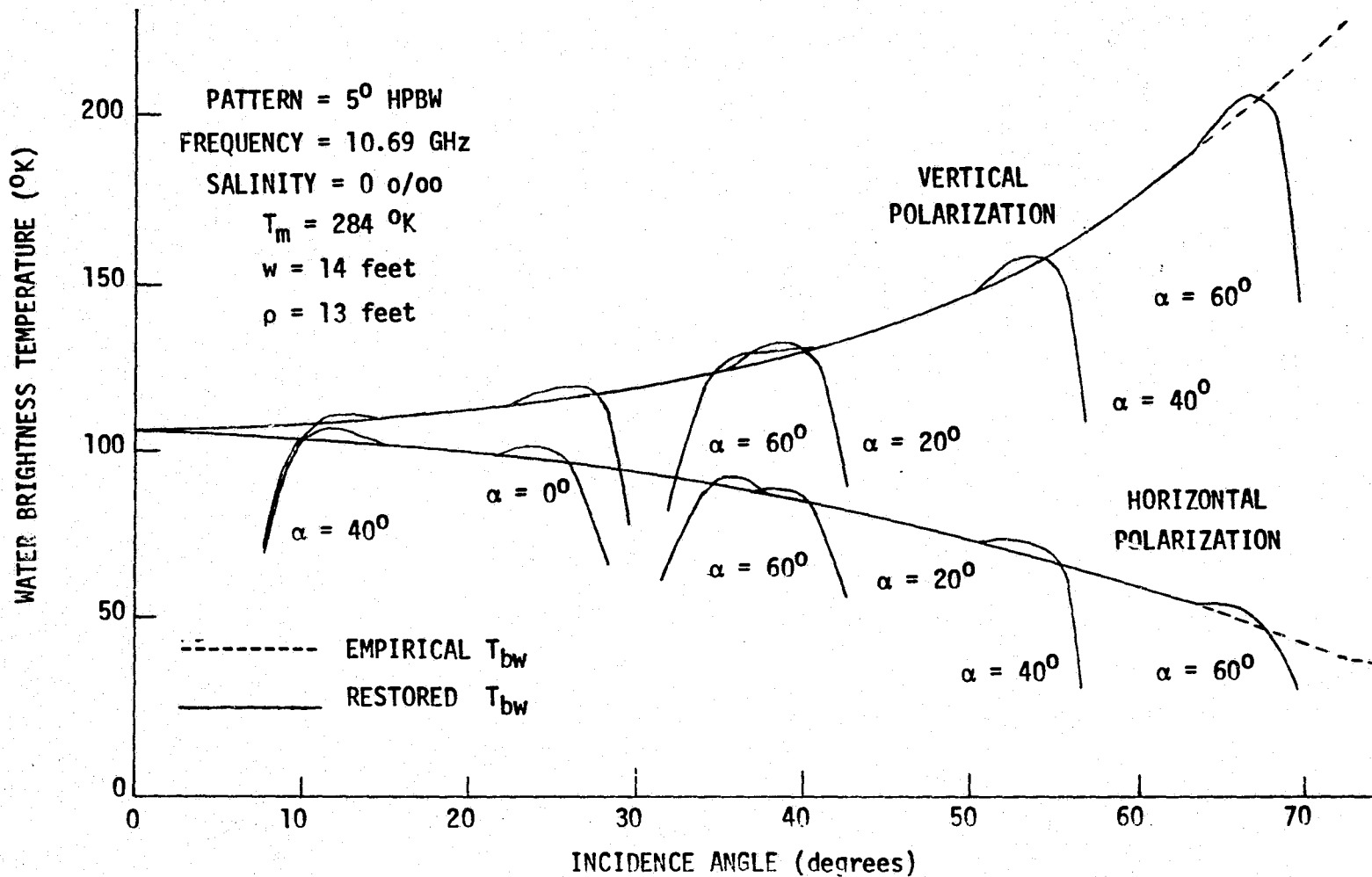
Fig. 22.   Restored brightness temperature profiles of T_{aw} for even α and ρ = 13 feet.

PATTERN = 5° HPBW
FREQUENCY = 10.69 GHz
SALINITY = 0 o/oo
T_m = 284 ^{O}K
w = 14 feet
ρ = 13 feet

VERTICAL POLARIZATION

HORIZONTAL POLARIZATION

$\alpha = 60^O$
$\alpha = 40^O$
$\alpha = 60^O$
$\alpha = 20^O$
$\alpha = 0^O$
$\alpha = 40^O$
$\alpha = 60^O$
$\alpha = 20^O$
$\alpha = 40^O$
$\alpha = 60^O$

- - - - - - - - EMPIRICAL T_{bw}
——————— RESTORED T_{bw}

WATER BRIGHTNESS TEMPERATURE (^{O}K)

INCIDENCE ANGLE (degrees)
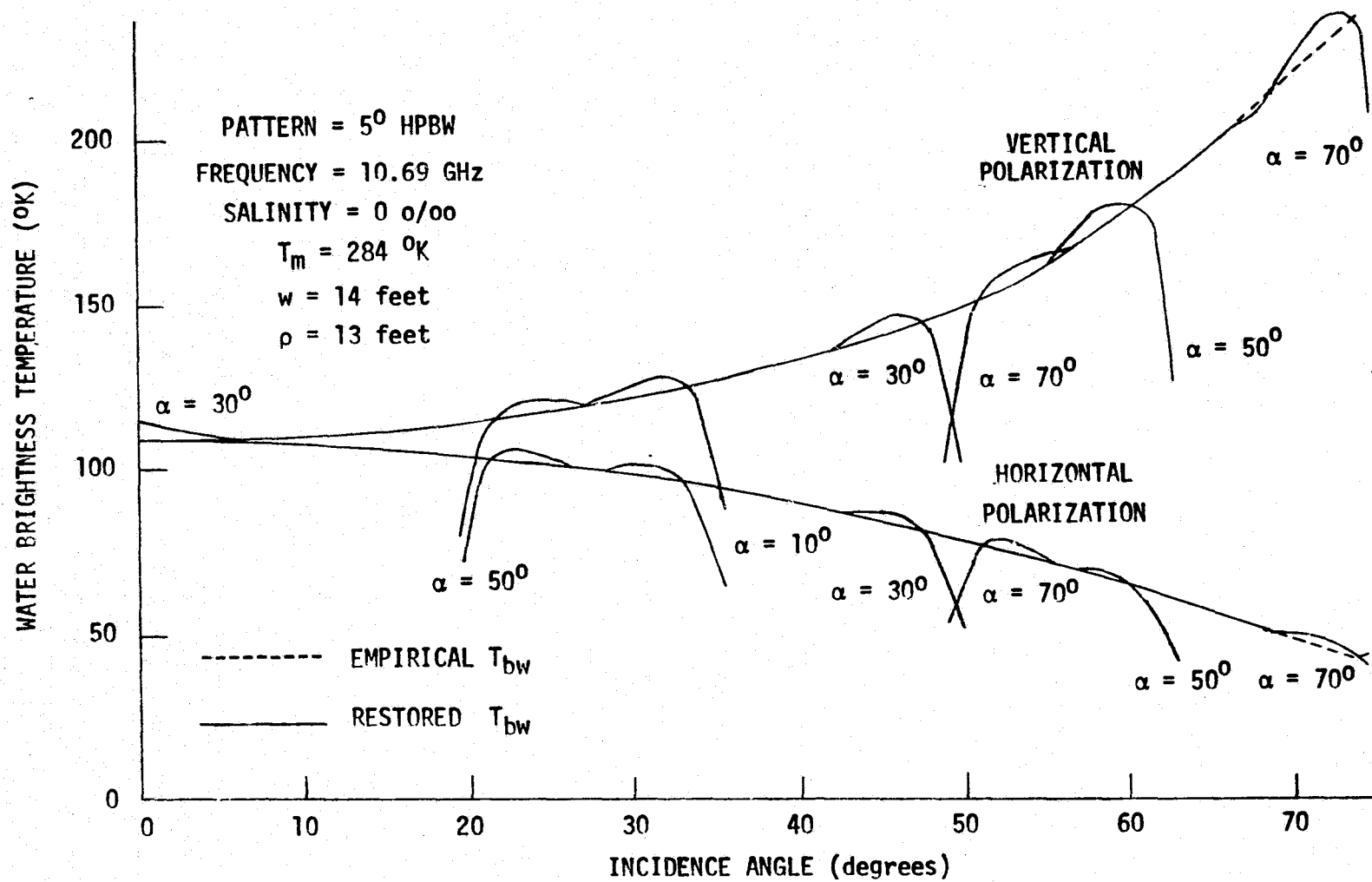
Fig. 23. Restored brightness temperature profiles of T_{aw} for odd α and ρ = 13 feet.
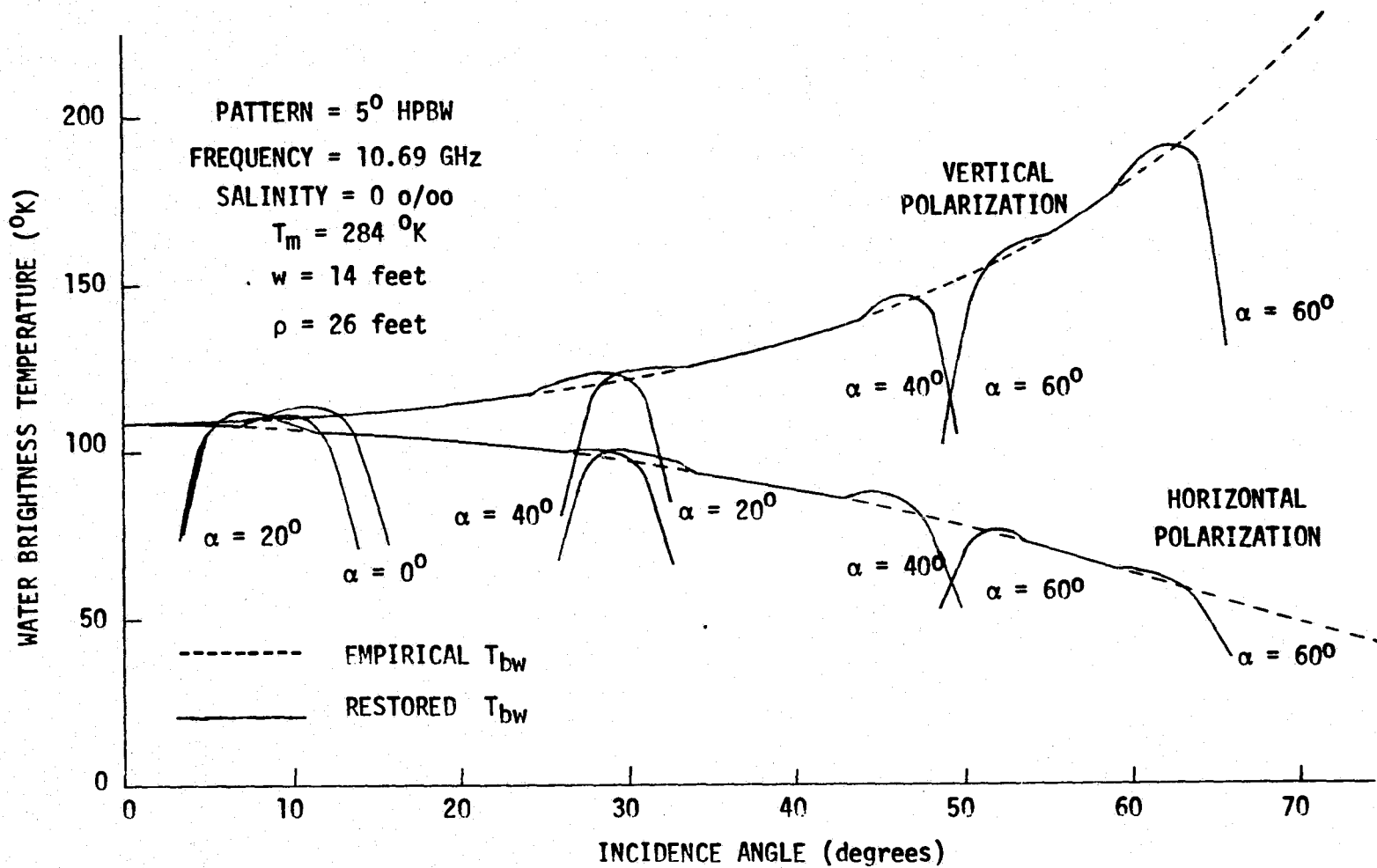
Fig. 24.   Restored brightness temperature profiles of T_{aw} for even α and $\rho = 26$ feet.
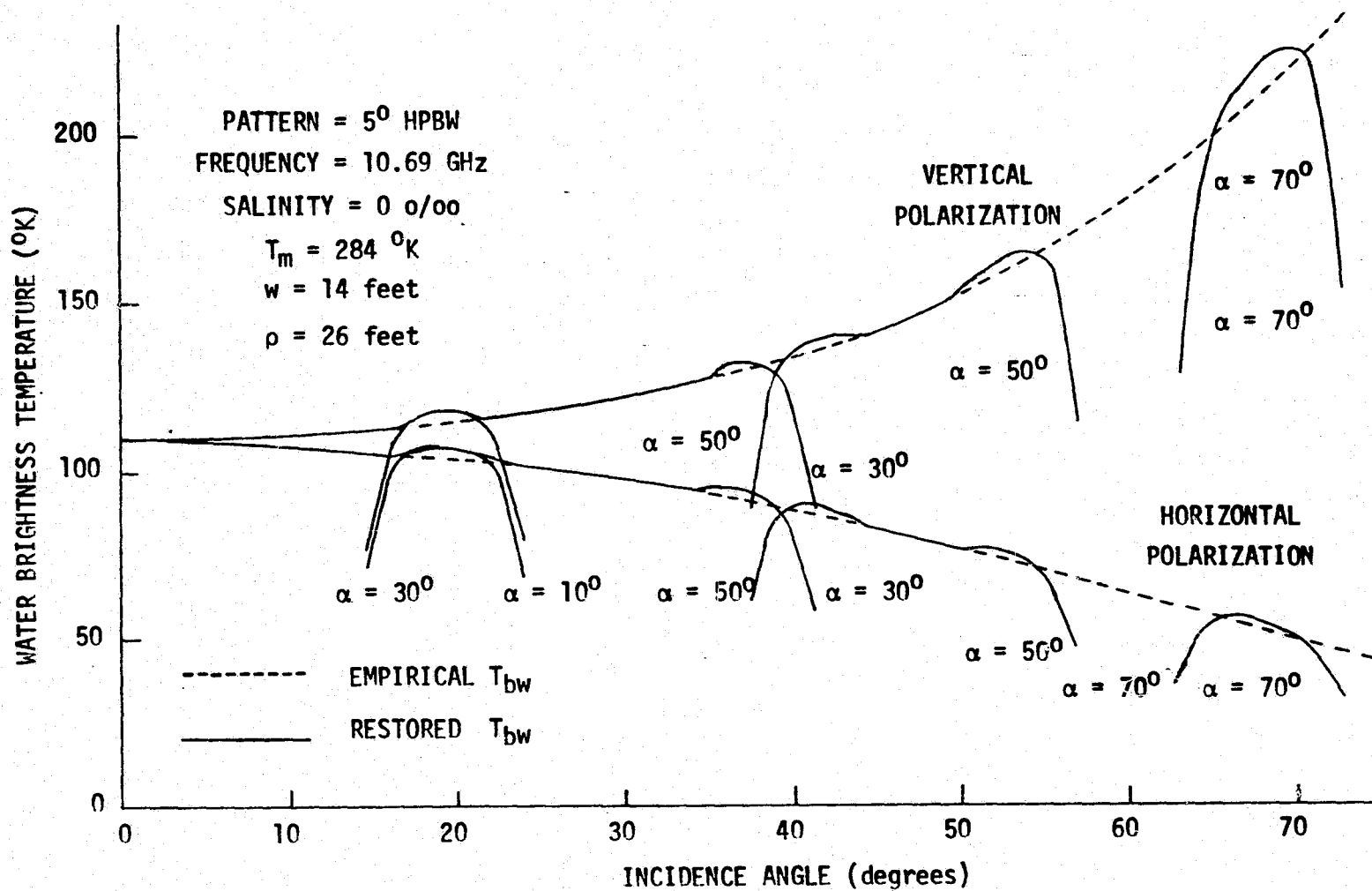
Fig. 25.   Restored brightness temperature profiles of T_{aw} for odd α and ρ = 26 feet.
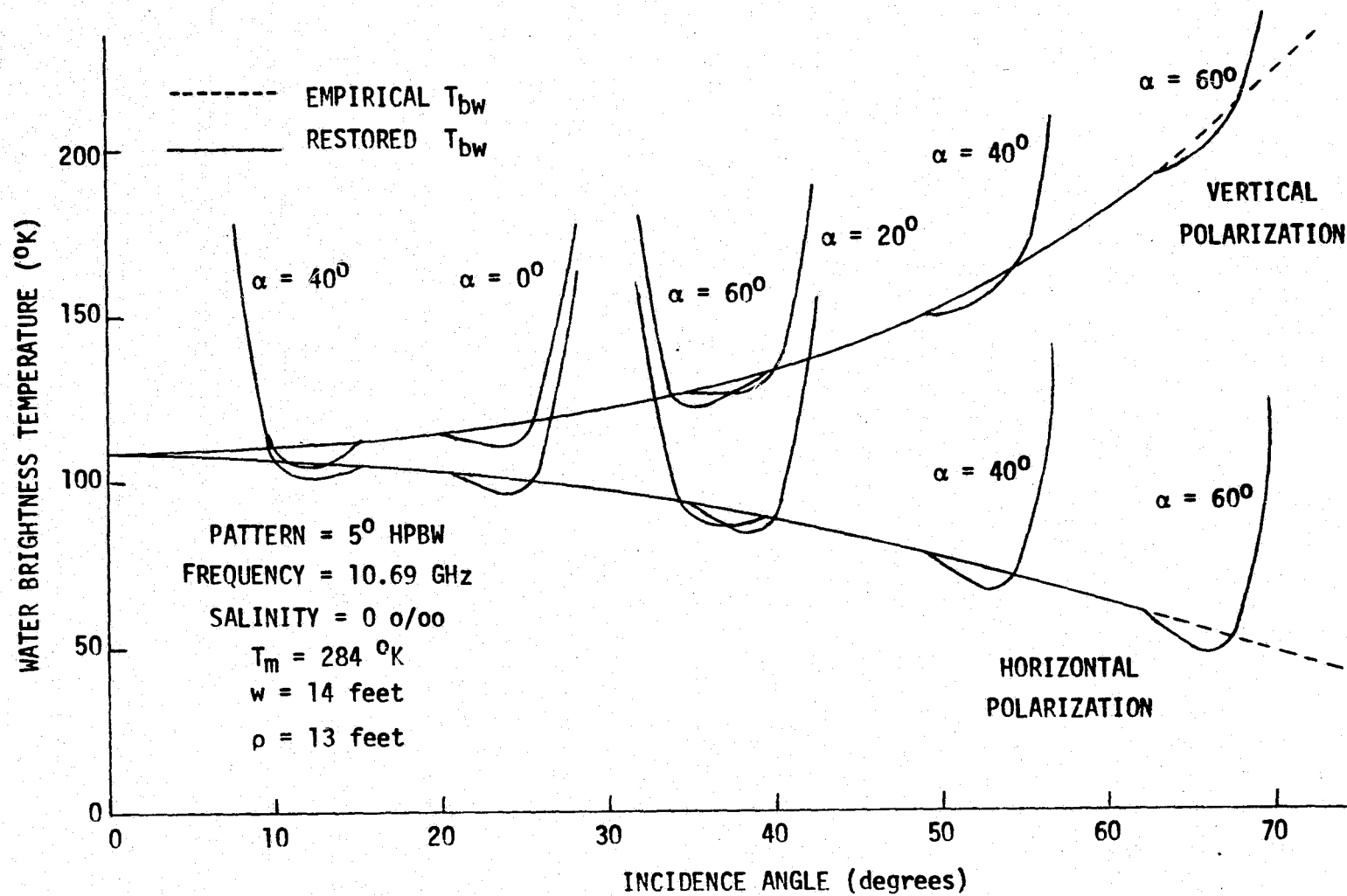
Fig. 26. Restored brightness temperature profiles of T_a for even α and ρ = 13 feet.

53
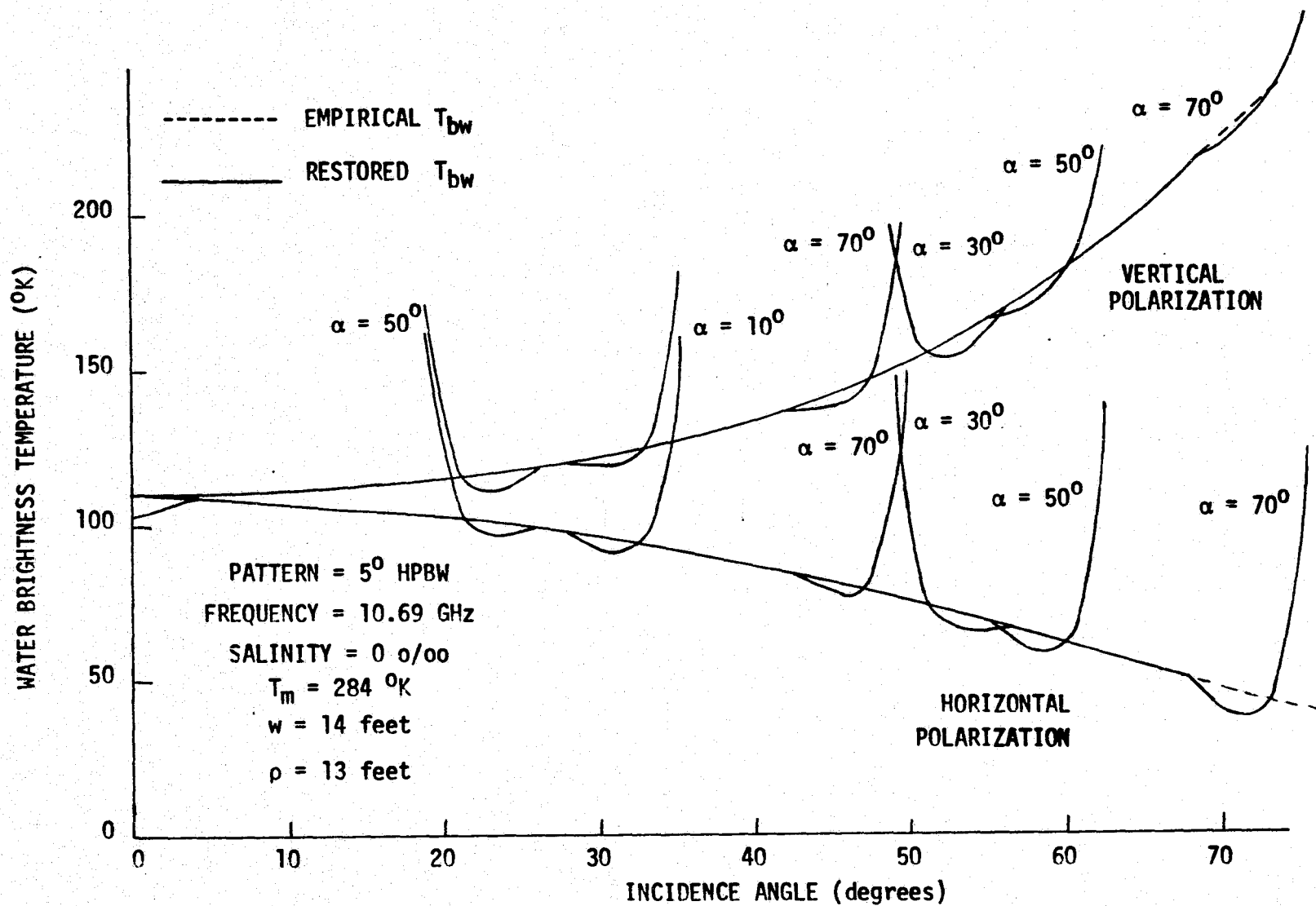
Fig. 27. Restored brightness temperature profiles of T_a for odd α and ρ = 13 feet.
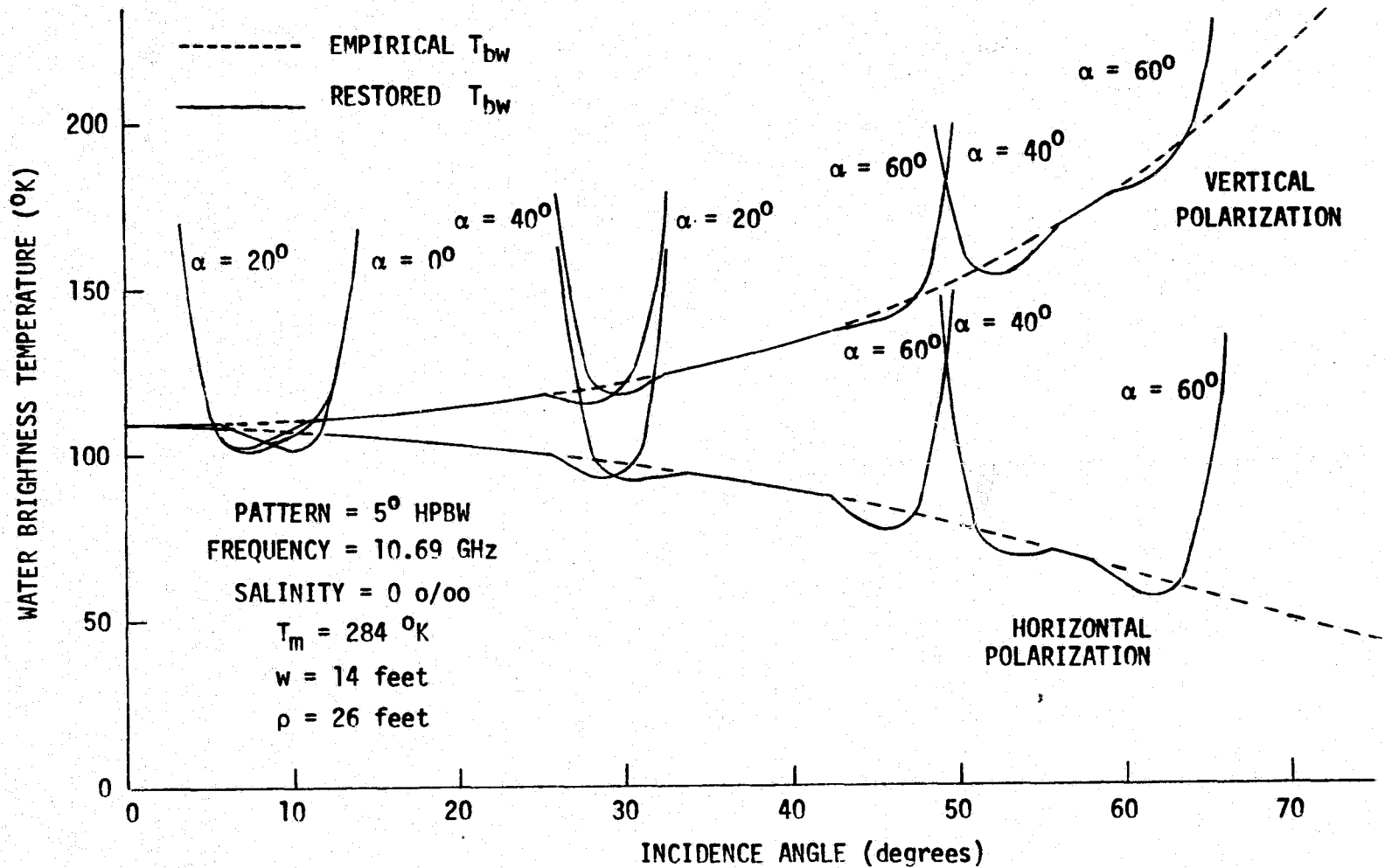
Fig. 28. Restored brightness temperature profiles of T_a for even α and ρ = 26 feet.
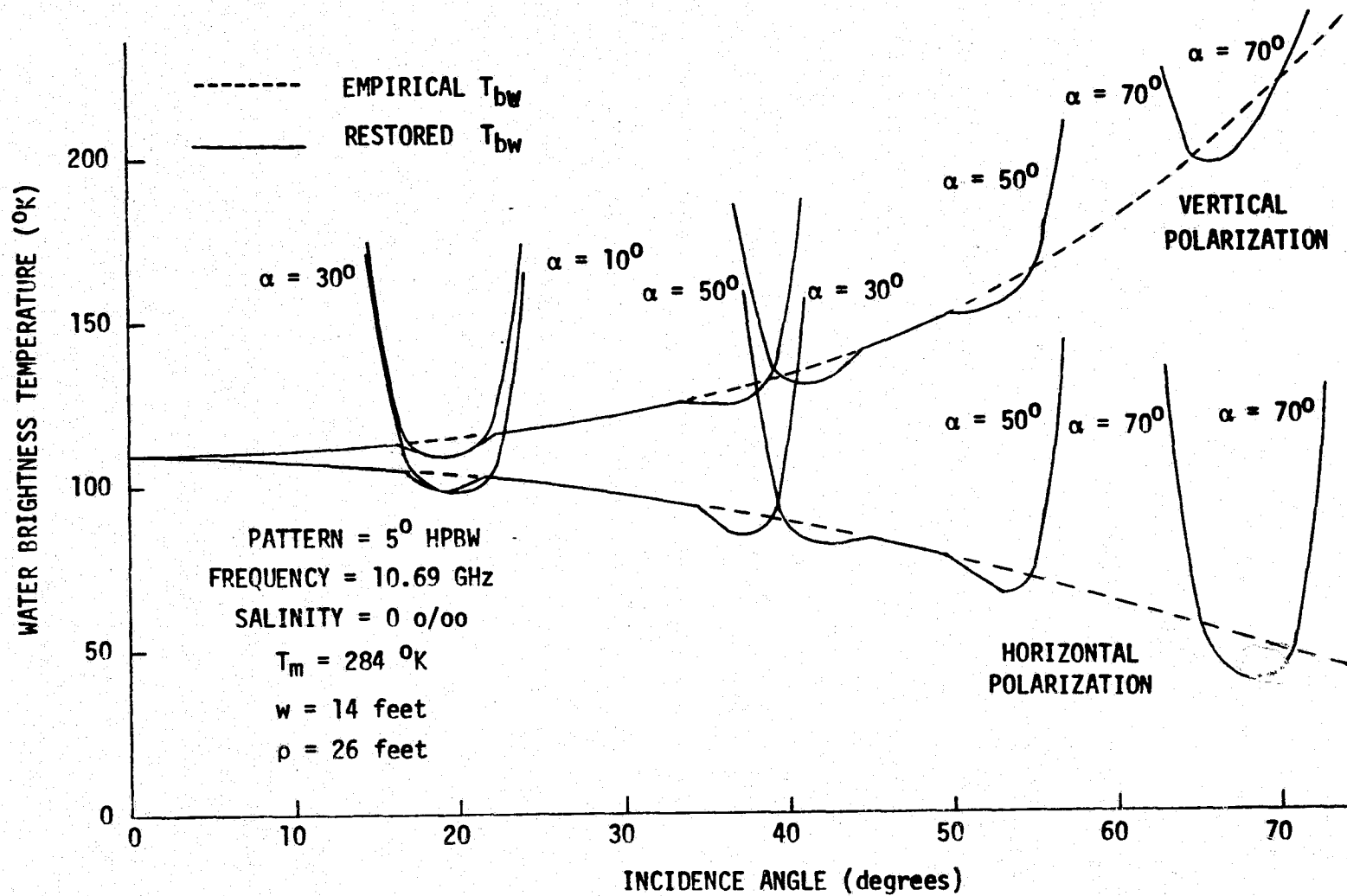
Fig. 29. Restored brightness temperature profiles of T_a for odd α and ρ = 26 feet.

- Y-axis: WATER BRIGHTNESS TEMPERATURE ($^\circ$K)
- X-axis: INCIDENCE ANGLE (degrees)

Legend:
- - - - - - - EMPIRICAL T_{bw}
———— RESTORED T_{bw}

PATTERN = 5° HPBW
FREQUENCY = 10.69 GHz
SALINITY = 0 o/oo
T_m = 284 $^\circ$K
w = 14 feet
ρ = 26 feet

VERTICAL POLARIZATION
HORIZONTAL POLARIZATION

$\alpha = 30^\circ$ $\alpha = 10^\circ$ $\alpha = 50^\circ$ $\alpha = 30^\circ$ $\alpha = 50^\circ$ $\alpha = 70^\circ$ $\alpha = 70^\circ$ $\alpha = 50^\circ$ $\alpha = 70^\circ$ $\alpha = 70^\circ$

the restoration is being performed on the T_a's or T_{aw}'s. However, when large α are considered, it can be concluded that the restoration should be performed on the T_a's for vertical polarizations and T_{aw}'s for horizontal polarizations. This occurs because both T_{bw_v} and T_a curve up for large incidence angles, as T_{bw_h} and T_{aw} both curve down for the same angles which results in a better first estimate for T_{bw} of (39a).

The profiles of Figs. 22-29 show the overlapping of each α curve, and the limits of the usable data may be set in each case. These profiles however were calculated from data taken at 1.4^0 intervals. Since it is not practical to make measurements at this interval, a compromised measuring scheme was developed. It is indicated from [22] that measurements can be made every 2.8^0 over the wave tank and every 5.6^0 over the rest of the observation angles. This routine would be repeated for all α from 0^0 to 80^0 in 10^0 steps.

The measuring scheme described requires interpolation to produce the 256 temperatures necessary for the restoration technique. Straight line interpolation will be used for all measurements. This type of interpolation will introduce more error into the earth and sky measurements than it will for the wave tank measurements, since earth and sky data are taken at larger intervals. However, Figs. 20 and 21 show that the restoration technique is not sensitive to errors over the earth and sky when only three restorations are performed.

A second source of error must be considered when T_{aw} is isolated in (20) for the restoration of horizontally polarized data. In actual measurements T_{be} and T_{bs} are not known. To obtain a good approximation to these profiles, the portion of T_a over the earth and sky is assumed for T_{be} and T_{bs}, respectively. This allows the evaluation of T_{ae} and T_{as} used in (20). To improve the approximate T_{be} profile, it will be assumed that

$$T_{be}(\emptyset) = T_a(-\emptyset_1 - 12^0) \qquad (40)$$

for $-\emptyset_1 - 12^0 \leq \emptyset \leq \bar{\emptyset}_1$ and $\emptyset_2 \leq \emptyset \leq \emptyset_2 + 12^0$. It is more reasonable to assume that T_{be} remains at this constant value in this range rather than decreasing as T_a does, since the earth is homogenous in the area near the wave tank's edge.

The final two-dimensional restoration program, utilizing the measuring scheme discussed, is shown as a subroutine in Appendix III. If the appropriate T_a measurements are made using the T_{bw}'s of Fig. 1 and placed in the computer program, the T_{bw} profiles of Figs. 30 and 31 can then be calculated. These curves show that for the system parameters considered, the restored T_{bw} profile is accurate to within 1^0K out to an incidence angle of 67^0 for $\rho = 26$ feet. Although the calculated T_{bw} beyond these limits have less accuracy than 1^0K, they are closer to the true T_{bw} than any other data available.

The large incorrect T_{bw} that occur in the calculations of Figs. 30 and 31 are rejected by the computer program, which accounts
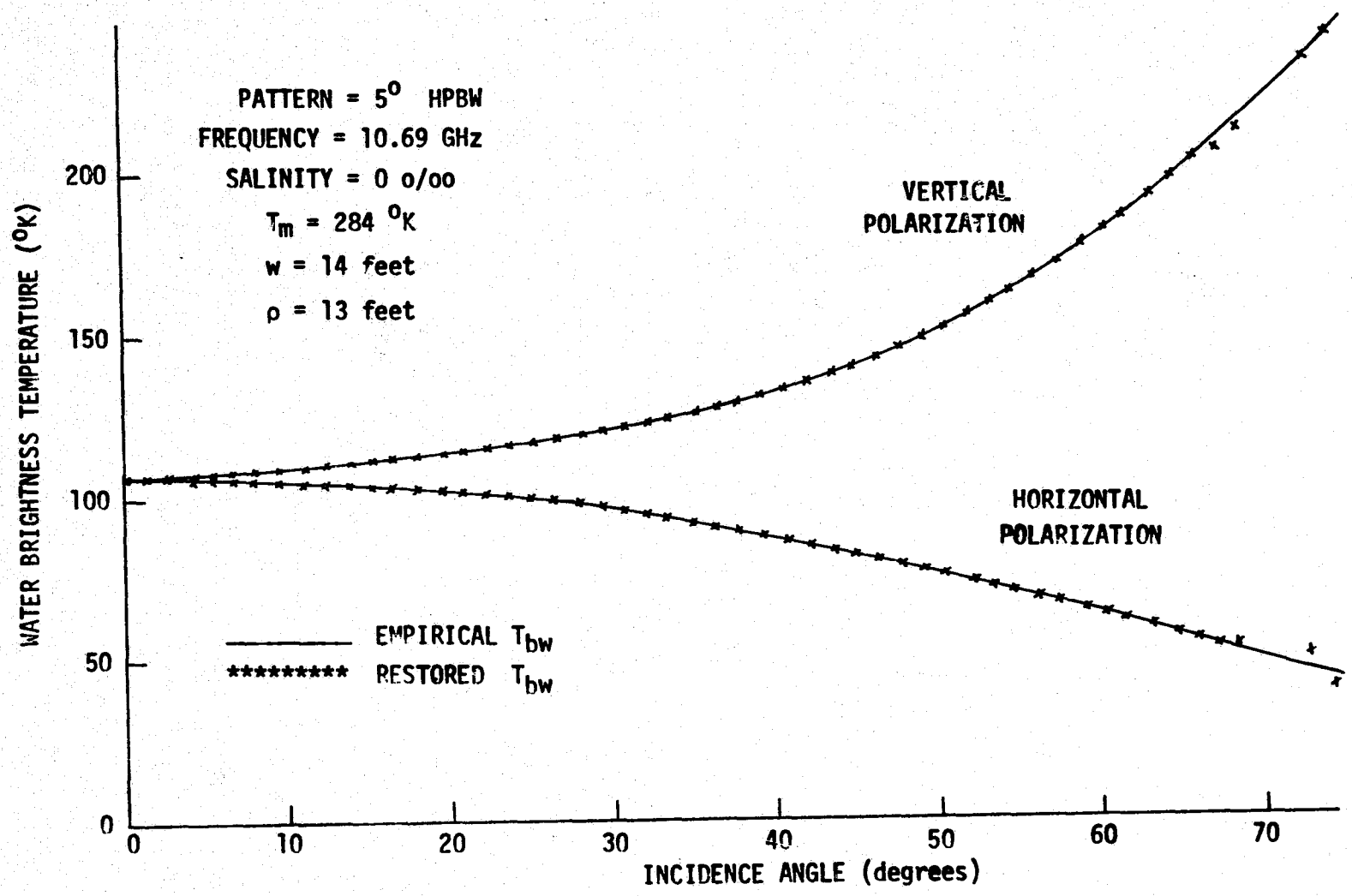
Fig. 30. Water brightness temperatures for ρ = 13 feet computed from empirical (———) and edited restored α profiles (****).
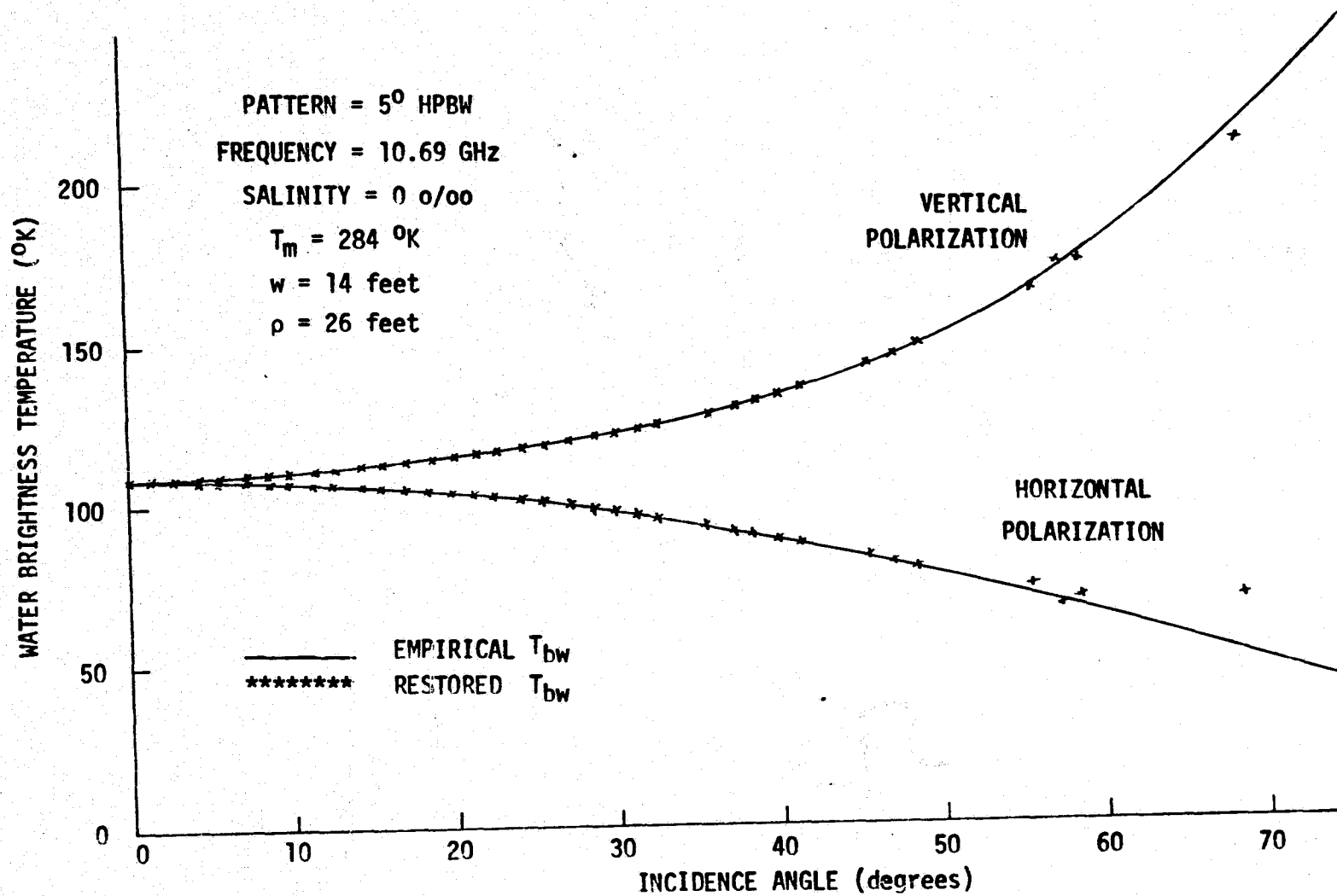
Fig. 31. Water brightness temperature for ρ = 26 feet computed from empirical (———) and edited restored α profiles (****).

for the breaks in the restored profile. These discrepancies are
due mainly to the interpolation of the measured data, and are more
prominent when a 26 foot antenna boom is considered. This occurs
because the range of β within the limits of the wave tank for the
26 foot boom is small, causing the rapidly varying antenna
temperatures to be interpolated with considerable error. The result
is a reduction in the usable portion of each α profile, producing
the breaks in the edited T_{bw} curves shown. However, it is possible
to fit a curve through the points made available by the computer
program, yielding a fairly accurate and continuous T_{bw} profile.

The discrepancy in the restored T_{bw} for each α curve near the
edge of the wave tank in Figs. 22-29 is explained as being caused
by the attenuation of the high frequency terms of the solution.
When an infinite wave tank is considered, the high frequency terms
are needed to describe the rapid changes in the T_{bw} at the horizon.
This is shown in Fig. 32 where the restored T_{bw} is calculated from
an error-free T_{aw}. Since both vertical and horizontal polarizations
of T_{bw} vary rapidly at the horizon, nothing is gained by restoring
T_a instead of T_{aw}. Therefore, an accurate restored T_{bw} can be
expected out to an incidence angle of about 80° for infinite wave
tank considerations, which is representative of open sea
measurements.

The restoration method, demonstrated in this section, restores
the water brightness temperature with good computational efficiency.
The computer time required to perform each additional restoration,
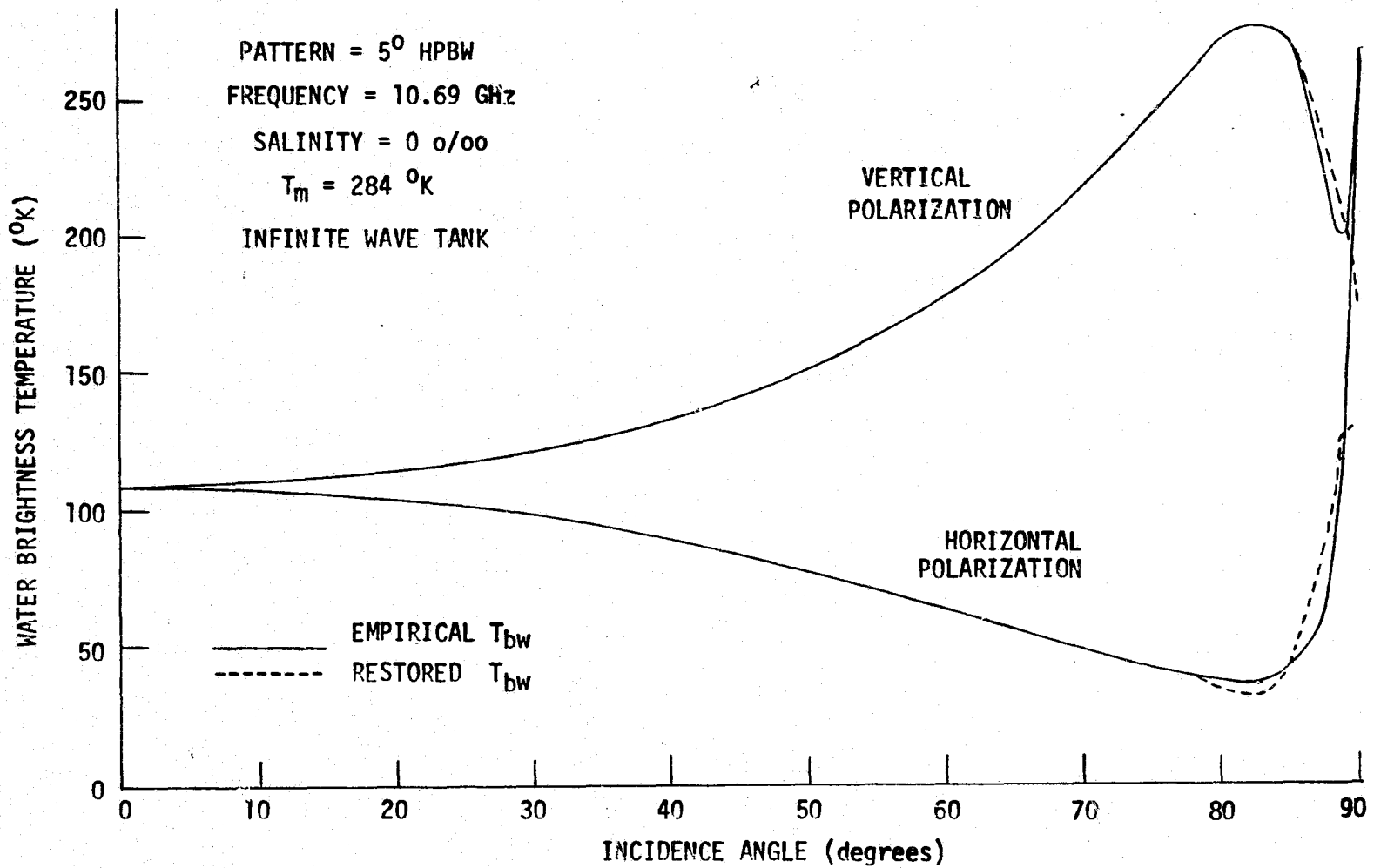
Fig. 32. Computed and restored brightness temperature profiles for an infinite wave tank geometry.

once the Fourier transforms of all pertinent functions have been found, is on the order of 0.05 seconds. A total time of about 1-2 seconds is required to perform a complete restoration for one α and for one polarization. The computational advantages of this method are beneficial in the evaluation of large quantities of data.

3.4 Restoration of Sea Water Measurements

Radiometric measurements of sea water at 7.55 GHz were made at Cape Cod canal, as reported by Swift [23]. The E- and H-plane patterns of the antenna used for the measurements are given in Fig. 33 with beam efficiencies of 80.34/69.34, 88.98/76.76, 95.68/88.94, 97.06/92.66, 98.06/95.55, 99.81/99.83% for the E-/H- planes within the observation angles of 10°, 20°, 32°, 40°, 58°, and 108°, respectively [20]. The spectrum of the E- and H-plane patterns are given in Figs. 34 and 35, and show some negative terms. These negative components are small in magnitude and will have little effect on the solution for the small number of restorations performed.

Using infinite wave tank geometry approximations, a T_{bw} was calculated by performing three restorations on the measurements reported by Swift. The restored T_{bw} and the measured T_a are shown in Fig. 36. A very close agreement between the two is indicated for incidence angles up to about 75°, as would be expected for efficient antennas with negligible crosspolarization components.
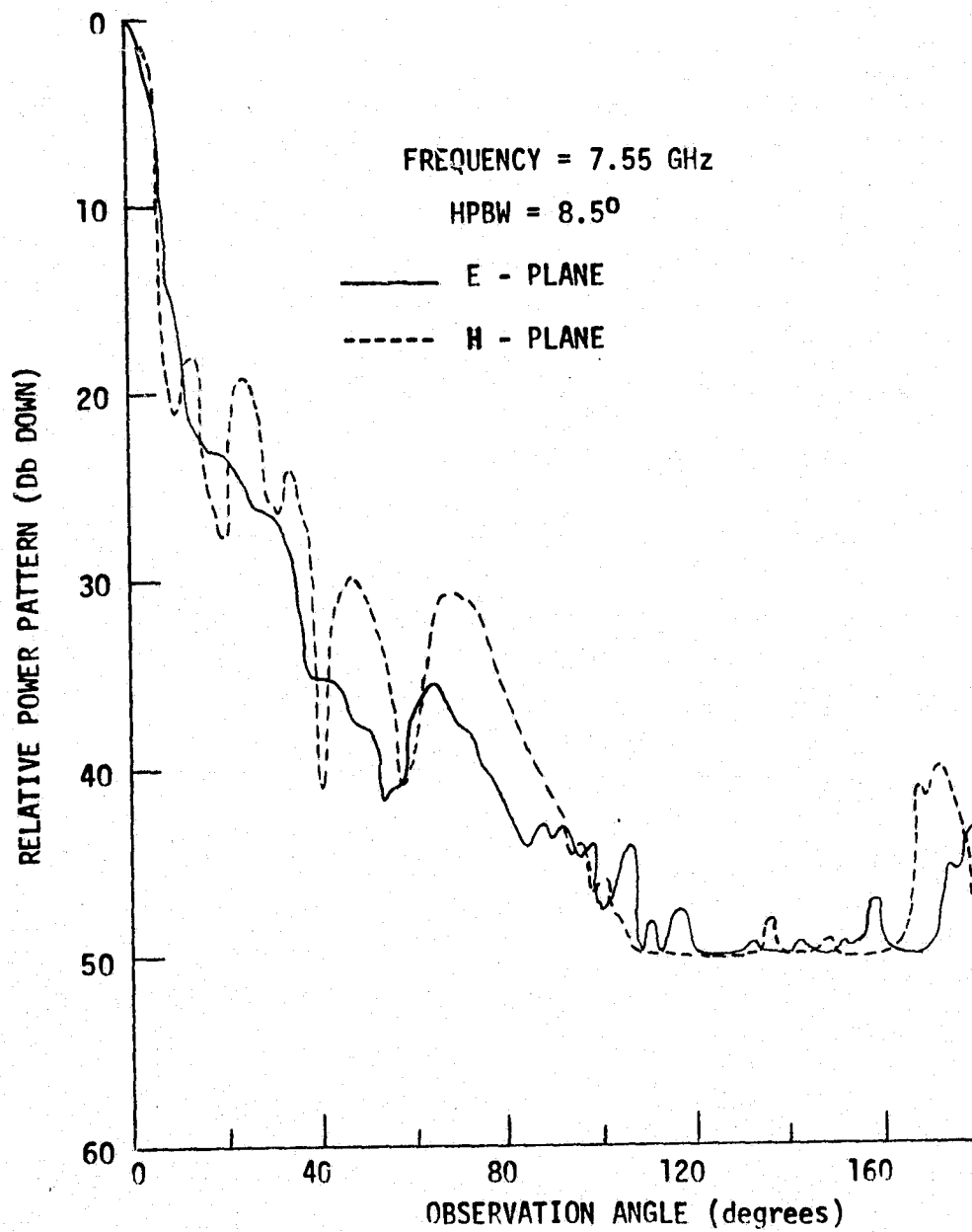
Fig. 33. Measured E- and H plane patterns for antenna
system used for Cape Cod canal experiment.
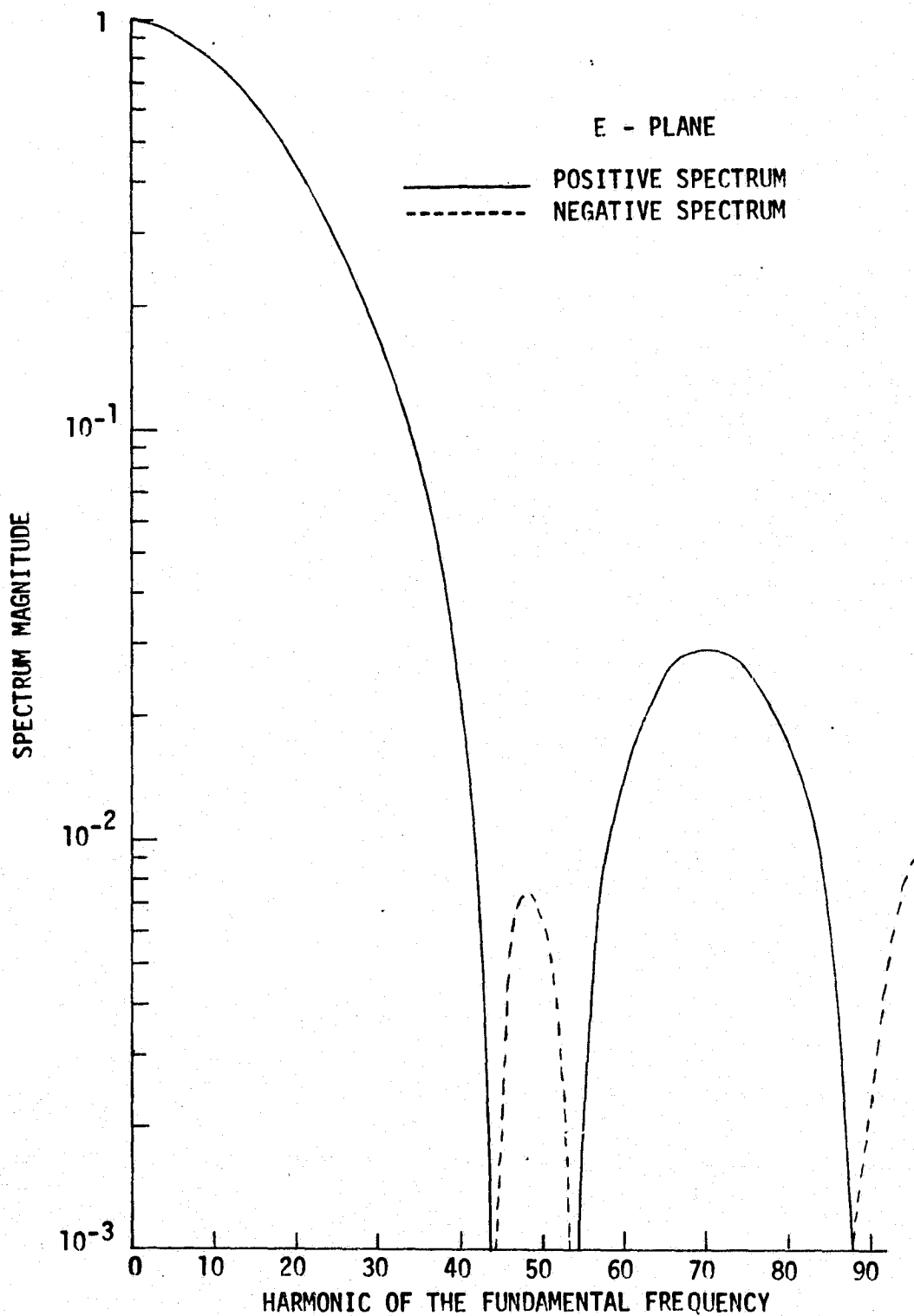
Fig. 34.   Frequency spectrum of 8.5° HPBW E-plane pattern.
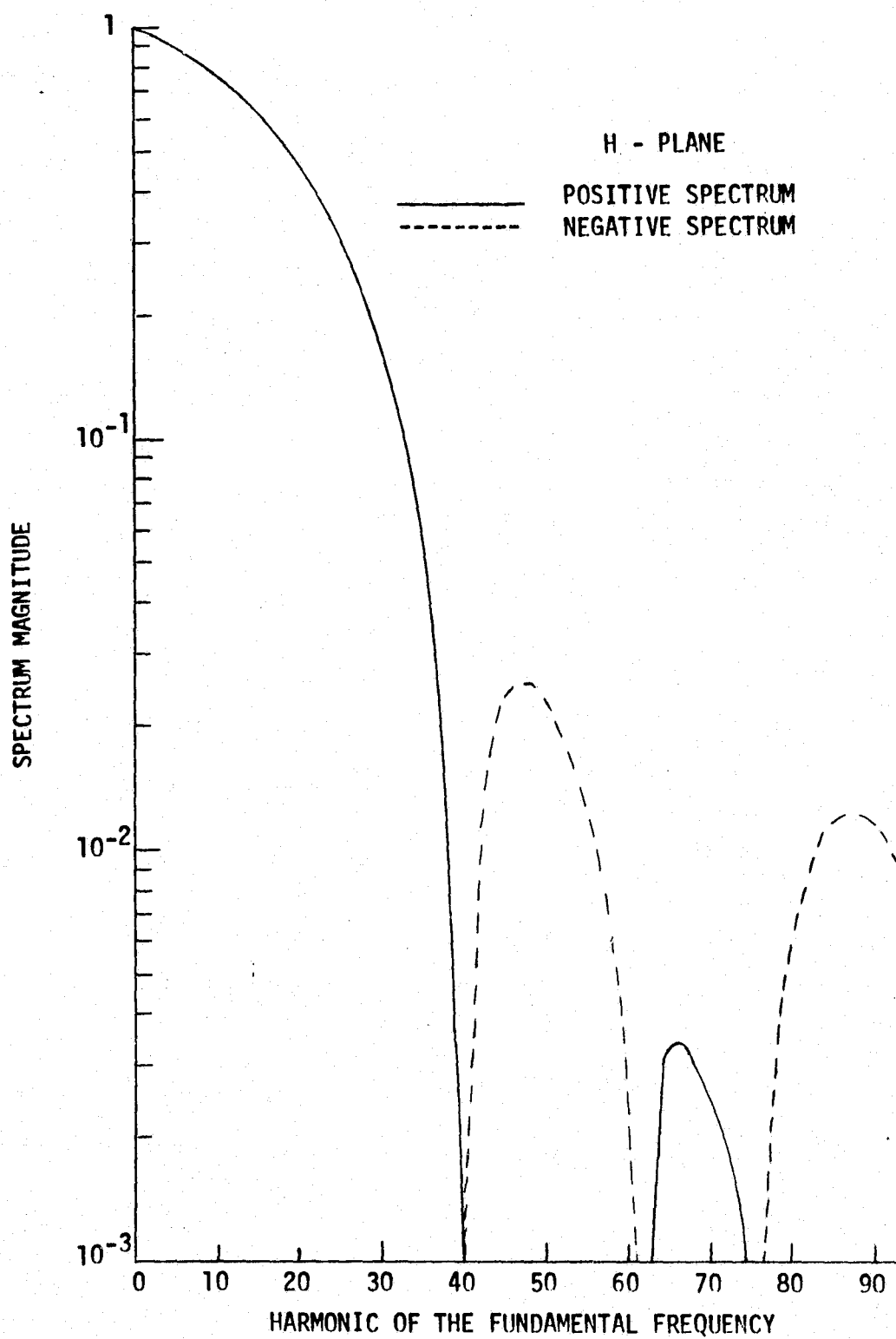
Fig. 35. Frequency spectrum of 8.5^o HPBW H-plane pattern.
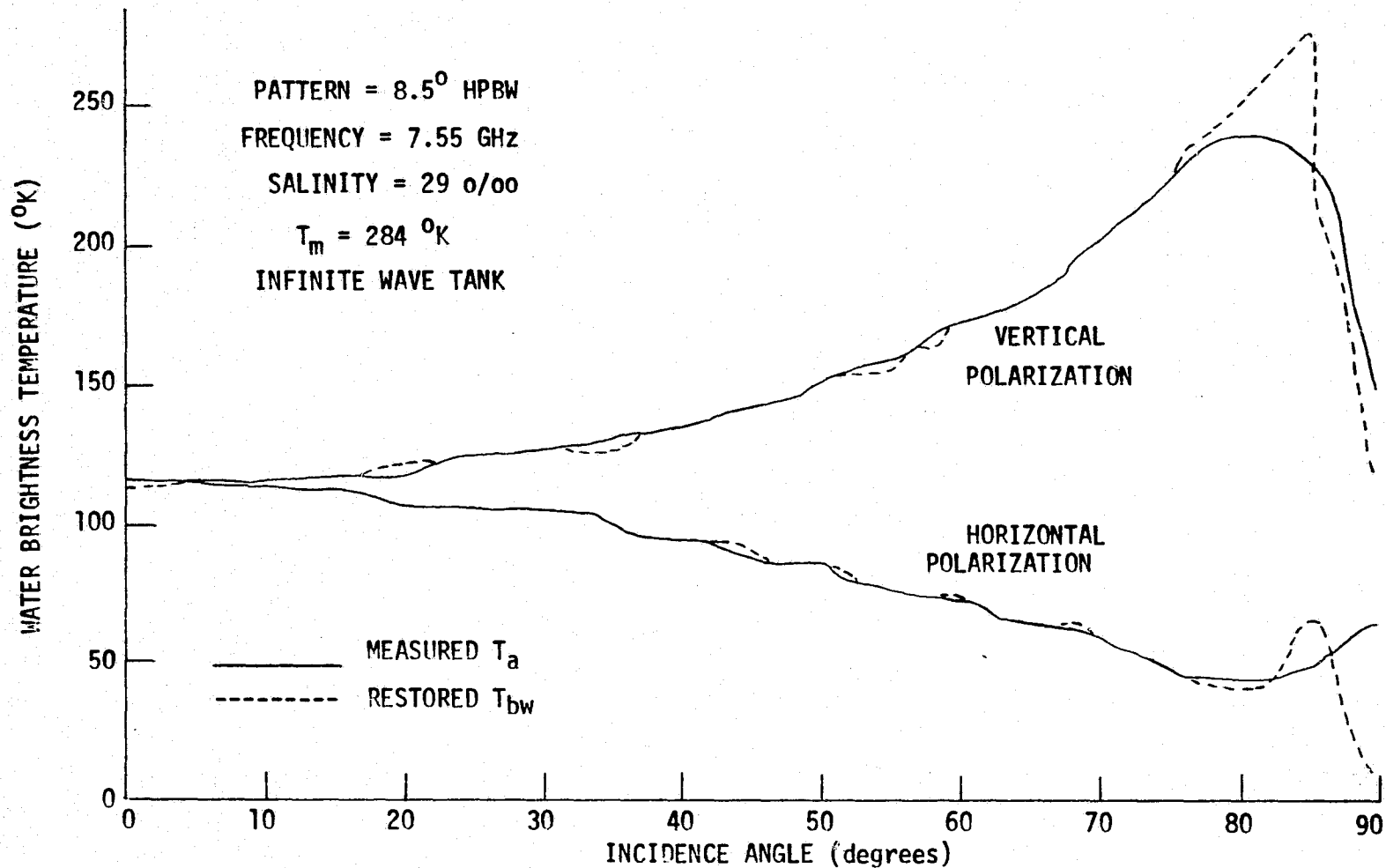
Fig. 36. Measured total antenna temperatures at Cape Cod canal and restored water brightness temperature.

Near the edges of the tank there are large disagreements between the two because the sky contributions are beginning to become significant and the crosspolarization contributions become more evident. The measured T_a profile is not smooth, and exhibits flat spots due to uncontrollable parameters such as periodic surface roughness, sunlight reflections, and the close proximity of the irregular shoreline.

To interpret the measurements and to shed some insight in the validity of Stogryn's mathematical model [16], in Fig. 37 the restored T_{bw} was plotted and compared to that obtained using equations (2)-(16) for the parameters indicated, which were measured independently at the site. It is clear that the restored values have the same profile characteristics as the ones computed from the mathematical model. There are some distinct disagreements at large incidence angles, but it should be emphasized that the restoration method is not valid in the region near the edges of the wave tank as was shown in Fig. 32. The computed values were based on a smooth surface mathematical model where the restored temperatures were based on measurements of sea water which may have had some surface irregularities during the course of the experiment.

IV. CONCLUSION

The validity of the two-dimensional modeling used in this investigation was verified for efficient radiometric antennas that
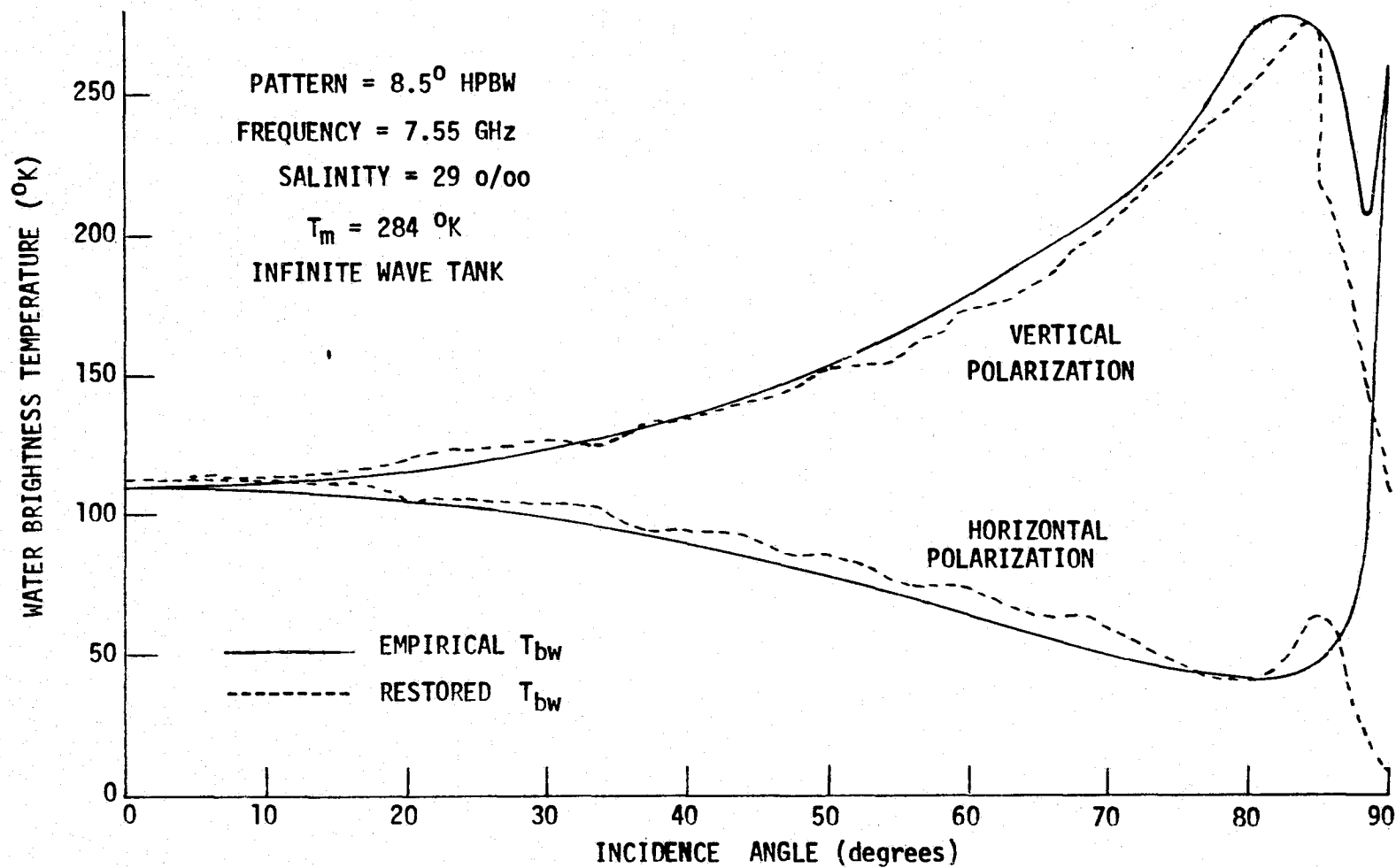
Fig. 37. Computed water brightness temperature from empirical equations and restored
profile from measurements at Cape Cod canal.

contain negligible crosspolarization components. This type of antenna is used in systems employing state-of-the-art radiometers. The validity of the modeling was demonstrated by comparing the calculated antenna temperature of a three-dimensional numerical integration method with that of the two-dimensional Fourier transform method. The results of the two methods agreed favorably for efficient antennas and any differences may be attributed to the neglected θ variations and crosspolarization contributions in the two-dimensional system.

It was shown that the complete inversion of the two-dimensional antenna temperature equation is unstable and yields unrealistic solutions when experimental errors are considered. This is true regardless of the inversion method used, as was proven using the general form of the Fredholm integral equation of the first kind. The instabilities appear in the Fourier inversion because of the division of error terms by small gain pattern components in the transform domain. This was demonstrated by inverting antenna temperatures that contained sine and impulse errors. These examples showed considerable amplification of the high frequency error terms caused by the spectrum of the antenna pattern.

By performing a series expansion of the inversion equation, the inherent instabilities may be filtered by properly truncating the series. This ability of the restoration technique was demonstrated using sampled data of typical measurements which contained error, and indicated an insensitivity to errors in the earth and sky data.

Although the restoration technique filters the true brightness
temperature as well as the instabilities, a large portion of the
water brightness temperature profile is obtainable by editing the
restorations of measurements made at different system positions in
a finite wave tank geometry. For open sea measurements 88% of the
entire profile can be accurately calculated using the restoration
technique.

The solution of the integral equation along with the appro-
priate smoothing technique can be applied to large amounts of data
with ease. The two-dimensional restoration was used to restore sea
water measurements made in an infinite wave tank geometry. These
restorations compared favorably with values obtained from a semi-
empirical mathematical modeling of a smooth surface.

The Fast Fourier Transform algorithm has enabled the solution
of the two-dimensional antenna temperature integral, formulated as
a crosscorrelation, to proceed with the utmost efficiency and speed.
To obtain an accuracy in the restoration method comparable with the
measuring accuracy of the state-of-the-art radiometers (less than
$0.1^\circ K$), the θ variations and crosspolarization contributions must
be considered. This will require a three-dimensional inversion
which is now under consideration. The advantages of the Fourier
restoration method will be felt greatly in this circumstance.

BIBLIOGRAPHY

[1] Tamiyasu, K., "Remote Sensing of the Earth by Microwaves", Proceedings IEEE, vol. 62, pp. 86-92, Jan. 1974.

[2] Bracewell, R.N. and Roberts, J.A., "Aerial Smoothing in Radio Astronomy", Aust. J. Phys., vol. 7, pp. 615-640, Dec. 1954.

[3] Bracewell, R.N., "Restoration in the Presence of Errors", Proceedings IRE, pp. 106-111, Jan. 1958.

[4] Bracewell, R.N., "Two-Dimensional Aerial Smoothing in Radio Astronomy", Aust. J. Phys., vol. 9, pp. 297-314, Sept. 1956.

[5] Hidy, G.M., et al., "Development of a Satellite Microwave Radiometer to Sense the Surface Temperature of the World Oceans", NASA CR-1960, Feb., 1972.

[6] Heneghan, J.M. and Ishimaru, A., "Remote Determination of the Profiles of the Atmospheric Structure Constant and Wind Velocity Along a Line-of Sight Path by a Statistical Inversion Procedure", IEEE Trans. Antennas Propagat., vol. AP-22, pp. 456-464, May 1974.

[7] Waser, J. and Schomaker, V., "The Fourier Inversion of Diffraction Data," Rev. Mod. Phys., vol. 25, pp. 671-690, July, 1953.

[8] Twomey, S., "The Application of Numerical Filtering to the Solution of Integral Equations Encountered in Indirect Sensing Measurements", J. Franklin Inst., vol. 279, Feb.,1965.

[9] Phillips, D.L., "A Technique for the Numerical Solution of Certain Integral Equations of the First Kind", J. Ass. Comput. Mach., pp. 84-97, 1962.

[10] Squire, W., "The Solution of Ill-Conditional Linear Systems Arising from Fredholm Equations of the First Kind", Internal Paper, West Virginia University, 1974.

[11] Claassen, J.P. and Fung, A.F., "The Recovery of Polarized Apparent Temperature Distribution of Flat Scenes from Antenna Temperature Measurements", IEEE Trans. Antennas Propagat., vol. AP-22, pp. 433-442, May, 1974.

[12] Cooley, J.W. and Tukey, J.W., "An Algorithm for the Machine Calculation of Complex Fourier Series", Math. of Comput., vol. 19, pp. 297-301, April 1965.

[13] Fisher, J.R., "Fortran Program for Fast Fourier Transform", NRL Report 7041, April, 1970.

[14] Fisher, V.L., "Fourier Transform Techniques for the Inversion of Radiometric Measurements", MSEE Thesis, West Virginia Univ., Morgantown, May, 1973.

[15] Hyatt, H.A., "Emission, Reflection, and Absorption of Micro-waves at a Smooth Air-Water Interface", J. Quant. Spectrosc. Radiat. Transfer. vol. 10, pp. 217-247, 1970.

[16] Stogryn, A., "Equations for Calculating the Dielectric Constant of Saline Water", IEEE Trans. Microwave Theory and Techniques, pp. 733-736, 1971.

[17] Peake, W.H., "The Microwave Radiometer as a Remote Sensing Instrument", Technical Report 1903-8, Jan., 1969, Electro-Sciences Laboratory, the Ohio State University, Columbus, Ohio.

[18] Dettman, J.W., Mathematical Methods in Physics and Engineering, McGraw-Hill Book Co., pp. 369-370, 1962.

[19] Caldecott, R., Mentzer, C.A., Peters, L., and Toth, J., "High Performance S-Band Horn Antennas for Radiometer Use", NASA CR-2133, prepared by Ohio State University, ElectroScience Laboratory, Columbus, Ohio, Jan., 1973.

[20] Truman, W.M., Private communication, Department of Electrical Engineering, West Virginia University, Morgantown, West Virginia.

[21] Rollett, J.S. and Higgs, L.A., "Correction of Spectroscopic Line Profiles for Instrumental Broadening by a Fourier Analysis Method", Proc. Phys. Soc., vol. 79, 1962.

[22] Jones, W.L., Private communication, NASA Langley Research Center, Hampton, Virginia.

[23] Swift, C.T., "Microwave Radiometer Measurements of the Cape Cod Canal", Radio Science, July, 1974.

Appendix I. Vertically and Horizontally Polarized Water
             Emissivities for Smooth Flat Air-Water
             Interfaces

The emissivity of water that has a smooth flat surface is expressed as

$$\epsilon = 1 - |\Gamma|^2 \qquad \text{(A-1)}$$

where ϵ is the emissivity and Γ is the electromagnetic reflection coefficient. The air-water interface is assumed to be abrupt (Fig. 38), which allows the reflection coefficient to be described by the Fresnel equations as

$$\Gamma_v = \frac{n_0\cos\emptyset - n_1\cos\emptyset'}{n_0\cos\emptyset + n_1\cos\emptyset'} \qquad \text{(A-2a)}$$

$$\Gamma_h = \frac{n_1\cos\emptyset - n_0\cos\emptyset'}{n_1\cos\emptyset + n_1\cos\emptyset'} \qquad \text{(A-2b)}$$

where

$n_0 =$ impedance of the air (free space)

$n_1 =$ impedance of the water

$\emptyset =$ incidence angle of the energy

$\emptyset' =$ refracted angle of the energy

and v,h indicate the vertical and horizontal polarizations, respectively.

Examining the vertically polarized reflection coefficient first, (A-2a) can be written in the form of

$$\Gamma_v = \frac{\sqrt{\dfrac{\mu_0}{\epsilon_0}}\cos\emptyset - \sqrt{\dfrac{\mu_1}{\epsilon_1}}\cos\emptyset'}{\sqrt{\dfrac{\mu_0}{\epsilon_0}}\cos\emptyset + \sqrt{\dfrac{\mu_1}{\epsilon_1}}\cos\emptyset'} \qquad \text{(A-3)}$$

$\mu_0, \varepsilon_0, \eta_0$

Air

$\mu_1, \varepsilon_1, \eta_1$
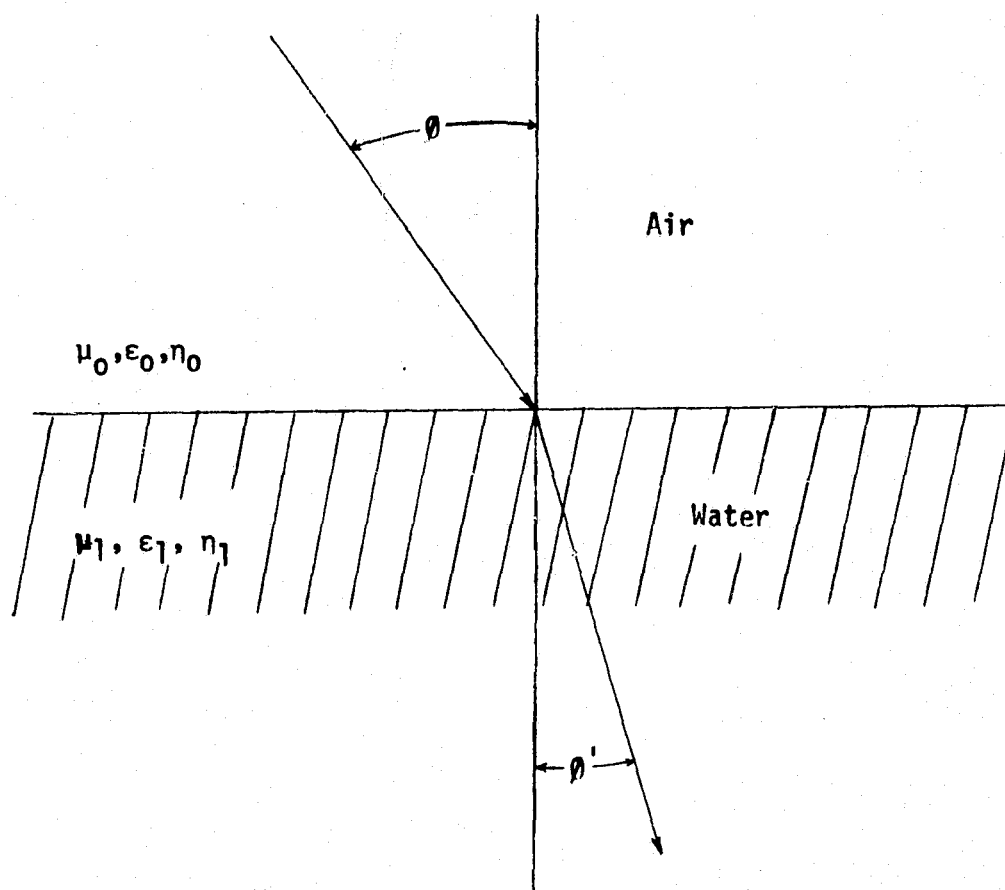
Water

Fig. 38. Geometry of smooth flat air-water interface.

where

$\mu_0 =$ permeability of the air (free space)

$\epsilon_0 =$ permittivity of the air (free space)

$\mu_1 =$ permeability of the water

$\epsilon_1 =$ permittivity of the water

Since the permeability of the water (μ_i) is equal to that of free space (μ_0), Snell's Law of refraction, which expresses the refracted angle in terms of the incidence angle, is given by

$$\sin^2\phi' = \frac{\epsilon_0}{\epsilon_1} \sin^2\phi \qquad (A-4)$$

This allows (A-3) to be written as

$$\Gamma_v = \frac{\sqrt{\frac{1}{\epsilon_0}} \cos\phi - \sqrt{\frac{1}{\epsilon_1}} \sqrt{1 - \frac{\epsilon_0}{\epsilon_1} \sin^2\phi}}{\sqrt{\frac{1}{\epsilon_0}} \cos\phi + \sqrt{\frac{1}{\epsilon_1}} \sqrt{1 - \frac{\epsilon_0}{\epsilon_1} \sin^2\phi}} \qquad (A-5)$$

The permittivity of the water is described by the complex relative permittivity, $\dot{\epsilon} = \frac{\epsilon_1}{\epsilon_0}$, placing (A-5) in the form of

$$\Gamma_v = \frac{\dot{\epsilon} \cos\phi - \sqrt{\dot{\epsilon} - \sin^2\phi}}{\dot{\epsilon} \cos\phi + \sqrt{\dot{\epsilon} - \sin^2\phi}} \qquad (A-6)$$

$\dot{\epsilon}$ is a complex quantity given by

$$\dot{\epsilon} = \epsilon' - j\epsilon'' \qquad (A-7)$$

where ϵ', ϵ'' are the real and imaginary parts of the complex relative permittivity. Therefore,

$$\sqrt{\dot{\epsilon} - \sin^2\phi} = \sqrt{r}\ e^{-j\gamma} \qquad (A-8)$$

in which

$$r = \sqrt{(\varepsilon' - \sin^2\phi)^2 + (\varepsilon'')^2}$$

$$\gamma = \frac{1}{2}\tan^{-1}\left(\frac{\varepsilon''}{\varepsilon' - \sin^2\phi}\right)$$

Placing (A-8) and (A-7) into (A-6) results in

$$\Gamma_v = \frac{\varepsilon'\cos\phi - p + j(q - \varepsilon''\cos\phi)}{\varepsilon'\cos\phi + p - j(q + \varepsilon''\cos\phi)} \tag{A-9}$$

where

$$p = \sqrt{r}\,\cos\gamma$$

$$q = \sqrt{r}\,\sin\gamma$$

Making the denominator of (A-9) real gives

$$\Gamma_v = \frac{(\varepsilon')^2\cos^2\phi - r + (\varepsilon'')^2\cos^2\phi + j(2\varepsilon' q\cos\phi - 2p\varepsilon''\cos\phi)}{(\varepsilon'\cos\phi + p)^2 + (q + \varepsilon''\cos\phi)^2} \tag{A-10}$$

Taking the square of the magnitude of (A-10) results in

$$|\Gamma_v|^2 = \frac{(\varepsilon')^4\cos^4\phi - 2r(\varepsilon')^2\cos^2\phi + 2(\varepsilon')^2(\varepsilon'')^2\cos^4\phi + r^2}{[(\varepsilon'\cos\phi + p)^2 + (q + \varepsilon''\cos\phi)^2]^2}$$

$$+ \frac{-2r(\varepsilon'')^2\cos^2\phi + (\varepsilon'')^4\cos^4\phi + 4(\varepsilon')^2 q^2\cos^2\phi}{[(\varepsilon'\cos\phi + p)^2 + (q + \varepsilon''\cos\phi)^2]^2}$$

$$+ \frac{4p^2(\varepsilon'')^2\cos^2\phi - 8\varepsilon'\varepsilon'' qp\cos^2\phi}{[(\varepsilon'\cos\phi + p)^2 + (q + \varepsilon''\cos\phi)^2]^2} \tag{A-11}$$

The vertically polarized emissivity can be written from (A-1) and (A-11) as

$$\varepsilon_v = \frac{4(p\varepsilon' + q\varepsilon'')\cos\phi[(\varepsilon')^2\cos^2\phi + p^2 + 2\varepsilon' p\cos\phi}{[(\varepsilon'\cos\phi + p)^2 + (q + \varepsilon''\cos\phi)^2]^2}$$

$$+ \frac{(\epsilon'')^2 \cos^2\emptyset + 2\epsilon'' q \cos\emptyset + q^2]^2}{[(\epsilon'\cos\emptyset + p)^2 + (q + \epsilon''\cos\emptyset)^2]^2} \qquad (A-12)$$

which reduces to the final form

$$\epsilon_v = \frac{4(p\epsilon' + q\epsilon'')\cos\emptyset}{(\epsilon'\cos\emptyset + p)^2 + (q+\epsilon''\cos\emptyset)^2} \qquad (A-13)$$

Next, the horizontally polarized reflection coefficient is examined, and (A-2b) can be written as

$$\Gamma_h = \frac{\sqrt{\dfrac{\mu_1}{\epsilon_1}} \cos\emptyset - \sqrt{\dfrac{\mu_0}{\epsilon_0}} \cos\emptyset'}{\sqrt{\dfrac{\mu_1}{\epsilon_1}} \cos\emptyset + \sqrt{\dfrac{\mu_0}{\epsilon_0}} \cos\emptyset'} \qquad (A-14)$$

Using (A-4) and the fact that $\mu_1 = \mu_0$ allows (A-14) to be placed in the form of

$$\Gamma_h = \frac{\sqrt{\dfrac{1}{\epsilon_1}} \cos\emptyset - \sqrt{\dfrac{1}{\epsilon_0}} \sqrt{1 - \dfrac{\epsilon_0}{\epsilon_1} \sin^2\emptyset}}{\sqrt{\dfrac{1}{\epsilon_1}} \cos\emptyset + \sqrt{\dfrac{1}{\epsilon_0}} \sqrt{1 - \dfrac{\epsilon_0}{\epsilon_1} \sin^2\emptyset}} \qquad (A-15)$$

which reduces to

$$\Gamma_h = \frac{\cos\emptyset - \sqrt{\dot{\epsilon}-\sin^2\emptyset}}{\cos\emptyset + \sqrt{\dot{\epsilon}-\sin^2\emptyset}} \qquad (A-16)$$

where $\dot{\epsilon}$ is given by (A-7). Using (A-8), equation (A-16) takes the form of

$$\Gamma_h = \frac{\cos\emptyset - p+jq}{\cos\emptyset + p-jq} \qquad (A-17)$$

where p and q are given in (A-9). Making the denominator of (A-17) real gives

$$\Gamma_h = \frac{\cos^2\emptyset - r + j2q\cos\emptyset}{(\cos\emptyset + p)^2 + q^2} \qquad \text{(A-18)}$$

Taking the square of the magnitude of (A-18) results in

$$|\Gamma_h|^2 = \frac{(\cos^2\emptyset - r)^2 + 4q\cos^2\emptyset}{[(\cos\emptyset + p)^2 + q^2]^2} \qquad \text{(A-19)}$$

The horizontally polarized emissivity can be written from (A-1) and (A-19) as

$$\epsilon_h = \frac{4p\cos^3\emptyset + 4r\cos^2\emptyset + 4pr\cos\emptyset + 4\cos^2\emptyset(p^2 - q^2)}{[(\cos\emptyset + p)^2 + q^2]^2} \qquad \text{(A-20)}$$

which reduces to the final form

$$\epsilon_h = \frac{4p\cos\emptyset}{(\cos\emptyset + p)^2 + q^2} \qquad \text{(A-21)}$$

Appendix II. Integration with High Frequency Integrands

If $K(x,y)$ is a piecewise continuous function for $a \leq x \leq b$, then

$$\lim_{R \to \infty} \int_a^b K(x,y)\sin Rx \, dx = 0 \qquad (A-22)$$

To prove (A-22), it can be assumed without loss of generality that $K(x,y)$ is continuous. The interval of integration can always be broken up into a finite number of subintervals and proved for each of the subintervals where the function $K(x,y)$ is continuous. The y variable in $K(x,y)$ will be dropped since it is a constant with respect to the integration variable x.

To begin the proof a change of variables is performed. Replacing x with $t + \frac{\pi}{R}$, results in

$$\int_a^b K(x)\sin Rx \, dx = -\int_a^{b-\frac{\pi}{R}} K(t + \frac{\pi}{R})\sin Rt \, dt \qquad (A-23)$$

Doubling(A-23) gives

$$2\int_a^b K(x)\sin Rx \, dx = \int_a^b K(t)\sin Rt \, dt - \int_{a-\frac{\pi}{R}}^{b-\frac{\pi}{R}} K(t + \frac{\pi}{R})\sin Rt \, dt \qquad (A-24)$$

Equation (A-24) can be exapnded as

$$2\int_a^b K(x)\sin Rx \, dx = -\int_a^{b-\frac{\pi}{R}} [K(t + \frac{\pi}{R})-K(t)]\sin Rt \, dt$$

$$+ \int_{b-\frac{\pi}{R}}^{b} K(t)\sin Rt\, dt - \int_{a-\frac{\pi}{R}}^{a} K(t+\tfrac{\pi}{R})\sin Rt\, dt \quad \text{(A-25)}$$

If $K(x)$ is continuous for $a \leq x \leq b$, then R can be chosen sufficiently large so that $|K(t + \frac{\pi}{R})-K(t)| < \delta/(b-a)$ for all t in the interval. Also, R can be picked large enough so that $\frac{\pi}{R} < \delta/2M$, where $|K(t)|<M$ in the interval. Rewriting (A-25) gives

$$2\left| \int_{a}^{b} K(x)\sin Rx\, dx \right| < \left| - \int_{a}^{b-\frac{\pi}{R}} [K(t + \tfrac{\pi}{R})-K(t)]\sin Rt\, dt \right|$$

$$+ \left| \int_{b-\frac{\pi}{R}}^{b} K(t)\sin Rt\, dt \right| + \left| - \int_{a-\frac{\pi}{R}}^{a} K(t + \tfrac{\pi}{R})\sin Rt\, dt \right| \quad \text{(A-26)}$$

Substituting into the right side of (A-26) and simplifying gives

$$2\left| \int_{a}^{b} K(x)\sin Rx\, dx \right| < \frac{\delta}{(b-a)} [b-a] + \frac{\delta}{2} + \frac{\delta}{2} \quad \text{(A-27)}$$

which reduces to

$$\left| \int_{a}^{b} K(x)\sin Rx\, dx \right| < \delta \quad \text{(A-28)}$$

Since δ is arbitrary, it can be set equal to zero in (A-28) forcing $R \rightarrow \infty$.

Appendix III. Program to Restore Finite Wave
Tank Measurements

```
0001          SUBROUTINE INVERT (TAM,RHO,PCL,TBW,GXS,ANGL,NPT)
        C
        C   ***********************************************************86
        C   * THIS SUBROUTINE REQUIRES A NORMALIZED ANTENNA PATTERN    *
        C   * IN DB FOR 0.0 TO 180.0 DEGREES SAMPLED AT BIN/2+1        *
        C   * POINTS                                                   *
        C   * TAM=9 ALPHA ANTENNA TEMPERATURE PROFILES (0-80 DEGREES   *
        C   * IN 10 DEGREE STEPS)                                      *
        C   * RHO=ANTENNA HEIGHT IN FEET                               *
        C   * POL=1.0 FOR VERTICAL POLARIZATION, 2.0 FOR HORIZONTAL    *
        C   * POLARIZATION                                             *
        C   * TBW=WATER BRIGHTNESS TEMPERATURE PROFILE CALCULATED      *
        C   * FROM THE 9 TAM CURVES                                    *
        C   * GXS=THE GAIN PATTERN IN DB (-180 TO +180 DEGREES)        *
        C   * ANGL=INCIDENCE ANGLE OF THE BRIGHTNESS TEMPERATURE       *
        C   * PROFILE                                                  *
        C   * NPT=NUMBER OF POINTS IN THE TBW ARRAY                    *
        C   ***********************************************************
        C
0002          REAL*8 DPI,DTT,DDEL,ANG,DCOS,DSIN,DDEL2,DABS
0003          INTEGER BIN,BIN2,BIN4,BIN8,BIN21,BIN41,SCR,STAR,STP,TM
0004          COMPLEX FGXS(256),FFX(256),BX(256)
0005          COMMON SCR,C
0006          DIMENSION GXS(256),SCR(256),C(129),TA(256),FX(256)
0007          DIMENSION AX(256),CX(256),DX(256),TBW(100),TBES(256)
0008          DIMENSION TAM(9,256),ALPD(9),ANGL(100)
0009          DATA ALPD/0.,10.,20.,30.,40.,50.,60.,70.,80./
0010          INTEGER*4 INDEL(9)/128,121,114,107,100,92,85,78,71/
0011          INTEGER*4 NLST(9)/1,8,13,22,28,33,39,43,53/
0012          INTEGER*4 NLFN(9)/7,12,21,27,32,38,42,50,58/
0013          INTEGER*4 INDEH(9)/128,121,114,107,100,93,86,79,72/
0014          INTEGER*4 NHST(9)/1,6,13,18,26,33,40,49,55/
0015          INTEGER*4 NHFN(9)/5,12,17,24,30,35,42,49,56/
0016    370 FORMAT (2F10.4)
        C   ***********************************************************
        C   * PROGRAM SETUP                                            *
        C   ***********************************************************
0017          BIN=256
0018          BIN2=BIN/2
0019          BIN4=BIN/4
0020          BIN8=BIN/8
0021          BIN21=BIN2+1
0022          BIN41=BIN4+1
0023          DPI=3.14159265358979
0024          PI=DPI
0025          PII=PI
0026          DTT=2.*DPI
0027          DDEL=DTT/FLOAT(BIN)
0028          TT=DTT
0029          DEL=DDEL
0030          RAD=PI/180.
0031          DEG=180./PI
0032          NRUN=1
0033          DO 703 I=1,100
0034          ANGL(I)=0.0
0035    703 TBW(I)=0.0
        C   ***********************************************************
        C   * COSINE TABLE FOR FFT SUBROUTINE                          *
        C   ***********************************************************
0036          C(1)=1.0
0037          C(BIN4+1)=0.0
0038          CS=DCOS(DDEL)
0039          SS=DSIN(DDEL)
0040          DO 1 J=1,BIN8
0041          C(J+1)=C(J)*CS-C(BIN4+2-J)*SS
0042      1 C(BIN4+1-J)=C(J)*SS+C(BIN4+2-J)*CS
        C   ***********************************************************
        C   * ROUTINE TO UNSCRAMBLE FFT COEFICIENTS                    *
        C   ***********************************************************
0043          SCR(1)=1
0044          M=1
0045          N=1
0046          TM=BIN2
0047      2 DO 3 J=1,M
0048          N=N+1
0049      3 SCR(N)=TM+SCR(J)
```

```
0050              IF(BIN-SCR(N))5,5,4
0051          4 M=M+M
0052            TM=TM/2                                               87
0053            GO TO 2
0054          5 CONTINUE
      C    *****************************************************************
      C    * ROUTINE TO CALCULATE THE FOURIER TRANSFORM OF THE           *
      C    * GAIN PATTERN                                                *
      C    *****************************************************************
0055            DO 371 I=1,BIN21
0056        371 READ (1,370) AX(I),CX(I)
0057            DO 372 I=1,BIN21
0058            IF (AX(I).GT.0.0) AX(I)=-AX(I)
0059            IF (CX(I).GT.0.0) CX(I)=-CX(I)
0060            AX(I)=10.0**(AX(I)/10.0)
0061        372 CX(I)=10.0**(CX(I)/10.0)
0062            DO 374 I=1,BIN41
0063            IF (POL.EQ.1.0) GXS(I)=AX(I)
0064        374 IF (POL.EQ.2.0) GXS(I)=CX(I)
0065            DO 375 I=BIN41,BIN21
0066            IF (POL.EQ.1.0) DX(I)=AX(I)
0067        375 IF (POL.EQ.2.0) DX(I)=CX(I)
0068            DO 376 I=1,BIN4
0069            FX(I)=DX(2*BIN4-I+2)
0070            FX(I+BIN4)=GXS(BIN4-I+2)
0071            FX(I+BIN2)=GXS(I)
0072        376 FX(I+3*BIN4)=DX(I+BIN4)
0073            DO 377 I=1,BIN
0074            GXS(I)=FX(I)
0075            IF (I.LE.BIN2) DX(I)=FX(I+BIN2)
0076        377 IF (I.GT.BIN2) DX(I)=FX(I-BIN2)
0077            CALL FOUR (DX,FGXS,BIN)
0078            DO 378 I=1,BIN
0079        378 FX(I)=1.0
0080            CALL FOUR (FX,BX,BIN)
0081            DO 379 I=1,BIN
0082        379 BX(I)=TT*BX(I)*CONJG(FGXS(I))
0083            CALL REVFUR (BX,BIN)
0084            DO 400 I=1,BIN
0085        400 FGXS(I)=FGXS(I)/REAL(BX(I))
      C    *****************************************************************
      C    * LIMITS OF THE WATER TANK                                    *
      C    *****************************************************************
0086          6 IF (NRUN.GE.10) GO TO 600
0087            ALP=ALPD(NRUN)*RAD
0088            TH1=ATAN2(7.-RHO*SIN(ALP),RHO*COS(ALP))+ALP+DEL
0089            TH2=ATAN2(7.+RHO*SIN(ALP),RHO*COS(ALP))-ALP+DEL
      C    *****************************************************************
      C    * ROUTINE TO EXPAND THE DATA POINTS                           *
      C    *****************************************************************
0090            DO 900 I=1,78
0091        900 TA(I)=TAM(NRUN,I)
0092            AX(1)=TA(1)
0093            DO 450 I=1,25
0094            N=I*4+1.001
0095            TMP=TA(I)
0096            DIFF=TA(I+1)-TA(I)
0097            AX(N-3)=TMP+DIFF/4.
0098            AX(N-2)=TMP+DIFF/2.
0099            AX(N-1)=TMP+3.*DIFF/4.
0100        450 AX(N)=TA(I+1)
0101            DO 451 I=1,27
0102            U=N+I*2+.001
0103            AX(U-1)=(TA(I+26)+TA(I+25))/2.
0104        451 AX(U)=TA(I+26)
0105            DO 452 I=1,25
0106            N=I*4+U+.001
0107            TMP=TA(I+52)
0108            DIFF=TA(I+53)-TA(I+52)
0109            AX(N-3)=TMP+DIFF/4.
0110            AX(N-2)=TMP+DIFF/2.
0111            AX(N-1)=TMP+3.*DIFF/4.
0112        452 AX(N)=TA(I+53)
0113            AX(256)=(AX(255)+AX(1))/2.
0114            DO 453 I=1,BIN
0115            TAM(NRUN,I)=AX(I)
```

```
0115          453 TA(I)=AX(I)
      C     *********************************************************
      C     * ROUTINE TO CALCULATE THE ANTENNA TEMPERATURE DUE TO    *88
      C     * THE WATER FROM THE TOTAL ANTENNA TEMPERATURE
      C     *********************************************************
0117              IF (PUL.EQ.2.) GO TO 92
0118              GO TO 93
0119           92 X=PI/2.0-ALP+DEL
0120              I=1
0121           80 IF ((BIN4-I+1)*DEL.LT.(TH1+12.0*RAD)) GO TO 81
0122              I=I+1
0123              GO TO 80
0124           81 DO 82 J=1,BIN4
0125              TBES(J)=TA(J)
0126              TBES(J+BIN4)=TA(J+BIN4)
0127              IF ((BIN4-J+1)*DEL.LT.(TH1+12.0*RAD)) TBES(J+BIN4)=TA(I+BIN4)
0128              IF ((BIN4-J+1)*DEL.LT.TH1) TBES(J+BIN4)=0.0
0129              TBES(J+BIN2)=TA(J+BIN2)
0130              IF (J*DEL.LT.(TH2+12.0*RAD)) TBES(J+BIN2)=TA(I+BIN4)
0131              IF (J*DEL.LT.TH2) TBES(J+BIN2)=0.0
0132              IF (J*DEL.GT.X) TBES(J+BIN2)=TA(J+BIN2)
0133           82 TBES(J+3*BIN4)=TA(J+3*BIN4)
0134              CALL FOUR (TBES,FFX,BIN)
0135              DO 701 I=1,BIN
0136          701 FFX(I)=TT*CONJG(FGXS(I))*FFX(I)
0137              CALL REVFOR (FFX,BIN)
0138              DO 702 I=1,BIN
0139          702 TA(I)=TA(I)-REAL(FFX(I))
      C     *********************************************************
      C     * ROUTINE TO CALCULATE THE WATER BRIGHTNESS TEMPERATURE  *
      C     * BY THE METHOD OF SUCCESSIVE RESTORATIONS               *
      C     *********************************************************
0140           93 CALL FOUR (TA,FFX,BIN)
0141              DO 500 I=1,BIN
0142          500 BX(I)=FFX(I)
0143              DO 501 N=1,3
0144              DO 501 I=1,BIN
0145          501 FFX(I)=FFX(I)+(1.0-TT*CONJG(FGXS(I)))**N*BX(I)
0146              CALL REVFOR (FFX,BIN)
      C     *********************************************************
      C     * FORMS CONTINUOUS TBW CURVE FROM 9 ALPHA CURVES         *
      C     *********************************************************
0147              IF (RHO.LE.13.1) IND=INDEL(NRUN)
0148              IF (RHO.LE.13.1) STAR=NLST(NRUN)
0149              IF (RHO.LE.13.1) STP=NLFN(NRUN)
0150              IF (RHO.GT.13.1) STAR=NHST(NRUN)
0151              IF (RHO.GT.13.1) STP=NHFN(NRUN)
0152              IF (RHO.GT.13.1) IND=INDEH(NRUN)
0153              J=1
0154              DO 800 I=STAR,STP
0155              ANGL(I)=(IND+STAR-130+J)*DEL*DEG+ALPD(NRUN)
0156              J=J+1
0157          800 TBW(I)=REAL(FFX(IND+1))
0158              NRUN=NRUN+1
0159              GO TO 6
0160          800 J=1
0161              DO 801 I=1,STP
0162              IF (TBW(I).NE.0.0) TBW(J)=TBW(I)
0163              IF (TBW(I).NE.0.0) ANGL(J)=ANGL(I)
0164          801 IF (TBW(I).NE.0.0) J=J+1
0165              NPT=J-1
0166              RETURN
0167              END
```

```
       C
.0001         SUBROUTINE FOUR(FUN,COMP,NUM)
       C
       C  *************************************************** 89
       C  * COMP= FFT OF THE GIVRN REAL FUNCTICN, FUN           *
       C  ***************************************************
       C
0002          INTEGER SCR
0003          COMMON SCR,C
0004          COMPLEX E,COMP(256),CC(256)
0005          DIMENSION FUN(256),C(129),REALL(512),SCR(256)
0006          EQUIVALENCE (CC(1),REALL(1))
0007          NUM2=2*NUM
0008          DO 1 K=2,NUM2,2
0009        1 REALL(K)=0.0
0010          KJ=1
0011          DO 2 K=1,NUM2,2
0012          REALL(K)=FUN(KJ)
0013        2 KJ=KJ+1
0014          DO 3 J=1,NUM
0015        3 COMP(J)=CC(J)
0016          CALL FFOUR(NUM,COMP,NUM)
0017          DO 4 I=1,NUM
0018        4 COMP(I)=CCMP(I)/FLOAT(NUM)
0019          RETURN
       C
       C  ***************************************************
       C  * COMP= INVERSE FFT OF THE GIVEN COMPLEX FUNCTION, COMP  *
       C  ***************************************************
       C
0020          ENTRY REVFCR (COMP,NUM)
0021          CALL FFOUR (NUM,COMP,NUM)
0022          NN=NUM/2
0023          COMP(1)=COMP(NUM)
0024          DO 5 L=1,NN
0025          E=COMP(NUM-L+1)
0026          COMP(NUM-L+1)=COMP(L+1)
0027        5 COMP(L+1)=E
0028          RETURN
0029          END
```

```
                C
    0001              SUBROUTINE FFOUR(T,X,BIN)
                C
                C     **************************************************************90
                C     * FAST FOURIER TRANSFORM (FFT) SUBROUTINE                     *
                C     * BY J. R. FISHER, NRL REPORT 7041                            *
                C     **************************************************************
                C
    0002              REAL CSE,C
    0003              INTEGER T,TINC,THTA,BIN,SCR
    0004              COMMON SCR,C
    0005              COMPLEX E,F,X(256)
    0006              DIMENSION SCR(256),CSE(2),C(129)
    0007              EQUIVALENCE (E,CSE(1))
    0008              TINC=BIN/T
    0009              LINC=T/2
    0010         10   LOC=LINC
    0011         40   THTA=0
    0012         80   CSE(1)=C(THTA+1)
    0013              CSE(2)=-C(BIN/4+1-THTA)
    0014         60   LOC=LOC+1
    0015              LOC1=LOC-LINC
    0016              E=E*(X(LOC1)-X(LOC))
    0017              X(LOC1)=X(LOC1)+X(LOC)
    0018              X(LOC)=E
    0019              THTA=THTA+TINC
    0020              IF(THTA-BIN/2)20,30,30
    0021         20   IF(THTA-BIN/4)80,50,50
    0022         50   CSE(1)=-C(BIN/2+1-THTA)
    0023              CSE(2)=-C(THTA-(BIN/4-1))
    0024              GO TO 60
    0025         30   IF(LOC-T)90,91,91
    0026         90   LOC=LOC+LINC
    0027              GO TO 40
    0028         91   IF(2-LINC)92,93,94
    0029         92   LINC=LINC/2
    0030              TINC=TINC+TINC
    0031              GO TO 10
    0032         93   DO 100 LOC=2,T,2
    0033              LOC1=LOC-1
    0034              E=X(LOC1)-X(LOC)
    0035              X(LOC1)=X(LOC1)+X(LOC)
    0036        100   X(LOC)=E
    0037         94   CONTINUE
    0038              DO 9 J=1,T
    0039              I=SCR(J)
    0040              IF(J-I)9,9,11
    0041         11   F=X(J)
    0042              X(J)=X(I)
    0043              X(I)=F
    0044          9   CONTINUE
    0045              RETURN
    0046              END
```

C-2

ABSTRACT

Existing microwave radiometer technology now provides a suitable method for remote determination of the ocean surface's absolute brightness temperature. To extract the brightness temperature of the water from the antenna temperature equation, an unstable Fredholm integral equation of the first kind is solved. Fast Fourier Transform techniques are used to invert the integral after it is placed into a crosscorrelation form. Application and verification of the methods to a two-dimensional modeling of a laboratory wave tank system are included. The instability of the Fredholm equation is then demonstrated and a restoration procedure is included which smooths the resulting oscillations. With the recent availability and advances of Fast Fourier Transform techniques, the method presented becomes very attractive in the evaluation of large quantities of data. Actual radiometric measurements of sea water are inverted using the restoration method, incorporating the advantages of the Fast Fourier Transform algorithm for computations.